8-2016

A novel mode-switching hydraulic hybrid for an on-highway vehicle: A study of architecture and control

Hiral Jayantilal Haria
Purdue University

PURDUE UNIVERSITY
GRADUATE SCHOOL
Thesis/Dissertation Acceptance

This is to certify that the thesis/dissertation prepared

By HIRAL JAYANTILAL HARIA

Entitled

A NOVEL MODE-SWITCHING HYDRAULIC HYBRID FOR AN ON-HIGHWAY VEHICLE: A STUDY OF ARCHITECTURE AND CONTROL

For the degree of Master of Science in Mechanical Engineering

Is approved by the final examining committee:

MONIKA IVANTYSYNOVA	
Chair	
ANDREA VACCA	
JOHN M. STARKEY	

To the best of my knowledge and as understood by the student in the Thesis/Dissertation Agreement, Publication Delay, and Certification Disclaimer (Graduate School Form 32), this thesis/dissertation adheres to the provisions of Purdue University's "Policy of Integrity in Research" and the use of copyright material.

Approved by Major Professor(s): MONIKA IVANTYSYNOVA

Approved by: JAY P. GORE 5/20/2016

Head of the Departmental Graduate Program Date

A NOVEL MODE-SWITCHING HYDRAULIC HYBRID FOR AN ON-HIGHWAY VEHICLE: A STUDY OF ARCHITECTURE AND CONTROL

A Thesis

Submitted to the Faculty

of

Purdue University

by

Hiral Jayantilal Haria

In Partial Fulfillment of the

Requirements for the Degree

of

Master of Science in Mechanical Engineering

August 2016

Purdue University

West Lafayette, Indiana

For my family.

ACKNOWLEDGMENTS

Firstly, I would like to thank Dr. Monika Ivantysynova for giving me an opportunity to work in her research team at Maha Fluid Power Research Center. Her constant support, guidance and expertise have played a vital role in successful completion of my work. I would also like to thank my committee members, Dr. Andrea Vacca and Dr. John Starkey for kindly agreeing to be a part of my advisory committee.

I would like to thank my parents for their unconditional love, trust and guidance throughout my life. I am grateful to them for always being my inspiration and making this journey possible. I would like to extend my gratitude to Prof. Suresh Nakhare who has been a guru to me. I am thankful to Amir and Sharanya for their support. I am grateful to my close friends: Mrudula, Ninad, Pulkit, Ram, Divya, Matteo and Pramod for being my family away from home and making my stay at Purdue unforgettable.

This research could not have been possible without the resources and members at Maha. I would like to thank Enrique Busquets and Mike Sprengel for all the advice and help that they provided me with and for being great mentors. I would also like to thank Tyler Bleazard for his contribution on the hybrid vehicle project and working with me. I would always cherish the interesting discussions I had with them. I would also like to thank Anthony for all his help on the manufacturing side. I would specially like to thank Susan whose warmth and cheerfulness spread a positive attitude in the lab. Finally, I would like to thank all my lab-mates for all the good times we spent in the lab.

TABLE OF CONTENTS

Page

LIST OF TABLES

LIST OF FIGURES

NOMENCLATURE

$C_{H,HP}$	Capacitance of high pressure accumulator
A_f	Frontal Area
C_d	Coefficient of Drag
C_H	Hydraulic Capacitance
C_r	Coefficient of Rolling Resistance
C_v	Coefficient of flow through the valve
D	Diameter of hydraulic transmission line
E	Energy
$E_{1\rightarrow 2}$	Energy stored in accumulator
F_x	Force in x Direction
F_{xf}	Resultant Force on Front Axle
F_{xr}	Resultant Force on Rear Axle
F_g	Force Due to Gravity
F_D	Force Due to Drag
F_g	Force due to grade in the road
F_{rf}	Force due to Rolling Resistance on Front Axle
F_{rr}	Force due to Rolling Resistance on Rear Axle
i_1	Gear Ratio between engine and Unit 1
i_axle	Gear Ratio between Units 2, 3 and the wheels
J_{eng}	Engine inertia
J_w	Vehicle inertia
K_{oil}	Bulk modulus of hydraulic oil
K_Q	Volumetric flow loss coefficient
K_T	Torque loss coefficient
L	Length of hydraulic transmission line
M_{comb}	Combustion torque of engine
M_e	Effective Torque

M_f	Frictional torque in engine
M_L	Load torque on the engine
M_s	Torque Losses
M_{th}	Theoretical Torque
M_{WOT}	Engine brake torque at Wide open throttle
n	Rotational speed in rpm / polytropic constant
N	Normal Force
p	Pressure
p_A	Pressure in Line A
p_B	Pressure in Line B
p_{HP}	Pressure of High Pressure Accumulator
p_{in}	Pressure at inlet of valve
p_{out}	Pressure at outlet of valve
p_{set}	Set Pressure of relief valve
p_0	Pre-charge pressure of the high pressure accumulator
Q_e	Effective Flow
Q_{check}	Flow through check valve
Q_{relief}	Flow through relief valve
Q_s	Flow Losses
Q_{th}	Theoretical Flow
Re	Reynolds Number
T_{in}	Temperature at the inlet of hydraulic unit
u	Control input
u_{CE}	Throttle input to the engine
V	Unit displacement
V_d	Derived displacement volume of hydrauic unit
v_{veh}	Vehicle Velocity
V_0	Volume of accumulator when at Pre-charge pressure
W	Vehicle Weight
x	State
β	Percent Displacement

ω	Rotational Speed in rad/s
ρ	Density of hydraulic fluid
λ	Linear Scaling term
ν	kinematic viscosity
Δp	Pressure differential across a hydraulic unit
θ	Angle of Incline

ABBREVIATIONS

BSFC	Brake Specific Fuel Consumption
CE	Combustion Engine
CVT	Continuously Variable Transmission
DP	Dynamic Programming
EPA	Environmental Protection Agency
FUDS	Federal Urban Driving Schedule
HP	High Pressure
HST	Hydrostatic Transmission
LP	Low Pressure
MAN	Maschinenfabrik Augsburg-Nurnberg
mpg	Miles per Gallon
MSH	Mode-Switching Hybrid
PGT	Planetary Gear Train
UDDS	Urban Dynamometer Drive Schedule

ABSTRACT

Haria, Hiral Jayantilal M.S.M.E, Purdue University, August 2016. A Novel Mode-Switching Hydraulic Hybrid for an On-Highway Vehicle: A Study of Architecture and Control. Major Professor: Monika Invantysynova, School of Mechanical Engineering.

Increasing demand for fossil fuels, their limited reserves and the environmental effects resulting from the transportation sector has raised severe concerns to government agencies, transportation industry as well as the end-users. This has raised interests in improving the fuel economy of road vehicles. One of the promising technologies in this regard is hybridization of vehicle transmission. Hydraulic hybrids have progressively gained acceptance due to their high power density and low component costs relative to their electric counterpart.

Many different hydraulic hybrid architectures have been developed to achieve better power management and regenerative braking and have been tested for performance and efficiency on transmission test rigs and off-highway vehicles. The most commonly used architecture is the series hybrid which offers great flexibility for implementation of power management strategies. But the direct connection of the high pressure accumulator to the system often results in operation of the hydraulic units in high pressure and low displacement mode. However, in this operating mode the hydraulic units are highly inefficient. Also, the accumulator renders the system highly compliant and makes the response of the transmission sluggish. In contrast, a hydrostatic transmission has a very stiff response which ensures a good drivability. However, it lacks energy storage. Keeping these in mind, a blended hybrid architecture was recently developed. However, the complexity of the architecture results in difficulties while developing control strategies and results in poor drivability while mode switching. Drivability is a major concern along with performance in an on-highway vehicle. This work focuses on the development of a new hydraulic hybrid architecture called the "Mode-Switching Hybrid". This novel architecture combines the merits of a hydrostatic transmission as well as a series hybrid and separates the power transmission and energy recovery function to achieve better drivability. The hydrostatic mode facilitates stiff response and hence, a good driving experience. On the other hand

the energy recovered through regenerative braking can be used at a later time to boost the performance of the vehicle by operating it in secondary control mode. The aim of this work is to design the mode switching hybrid for an on-highway vehicle and implement it on a prototype and develop control strategies to improve its drivability.

For this work, a non linear system model was developed and the operating modes like acceleration, deceleration and braking along with energy recovery were simulated. The model was linearized and control strategies were developed to improve the drivability of the vehicle. A 1999 Range Rover 4.0 was selected as the prototype vehicle to test the new transmission. A packaging architecture was designed using 3D modeling and implemented on the prototype vehicle. A data acquisition system was designed to record different parameters while conducting the experiments. Different control strategies were implemented and the performance of these control strategies was demonstrated.

1. INTRODUCTION

The boom in the different industrial sectors over the last two decades has resulted in increase in the consumption of crude oil. This increase in the use of oil has resulted in the increased dependency of U.S. on foreign oil with output falling each year. After 1970, when U.S. petroleum production reached its all time maximum, there has been a decrease in the output till the recent boom in the oil industry. Even though the use of advanced technologies like hydraulic fracturing have opened new gates for petroleum production, the projections in Figure 1.1 show that U.S. will be unable to get rid of its dependency on foreign oil. The sector-wise consumption of petroleum shows that the transportation sector is one of the key contributors to the consumption of petroleum in the U.S. and consumed 68.9% of the total petroleum products from 2008 - 2014 (Davis et al. 2014). Figure 1.2 clearly indicates that highway vehicles like cars and light trucks consumed nearly 86.4% of all the transportation petroleum in 2013 (Davis et al. 2014). Figure 1.3 shows that 58% and 23.5% was consumed by light vehicles and medium-heavy trucks and buses respectively in 2013 (Davis et al. 2014).

Along with the diminishing oil reserves, the emissions from the vehicles have an adverse effect on health and environment. The emissions release various harmful gases like carbon dioxide, carbon monoxide and nitrogen oxides. These gases are a cause of many health issues related to respiratory and cardiovascular systems. Also, carbon dioxide is considered to be the largest contributor to green house effect.

These statics make it evident that in order to increase the supply of crude oil in U.S. and decrease the emission level, it is important to reduce the fuel consumed by highway vehicles. Keeping this in mind, government agencies, academic researchers and automotive manufactures are actively working towards enhancing the fuel economy of on and off-highway vehicles.

One of the components that substantially affects the performance of the entire powertrain and consecutively the fuel economy is the transmission. A transmission's primary task is to transmit power from the engine to the wheels of the vehicle while converting the

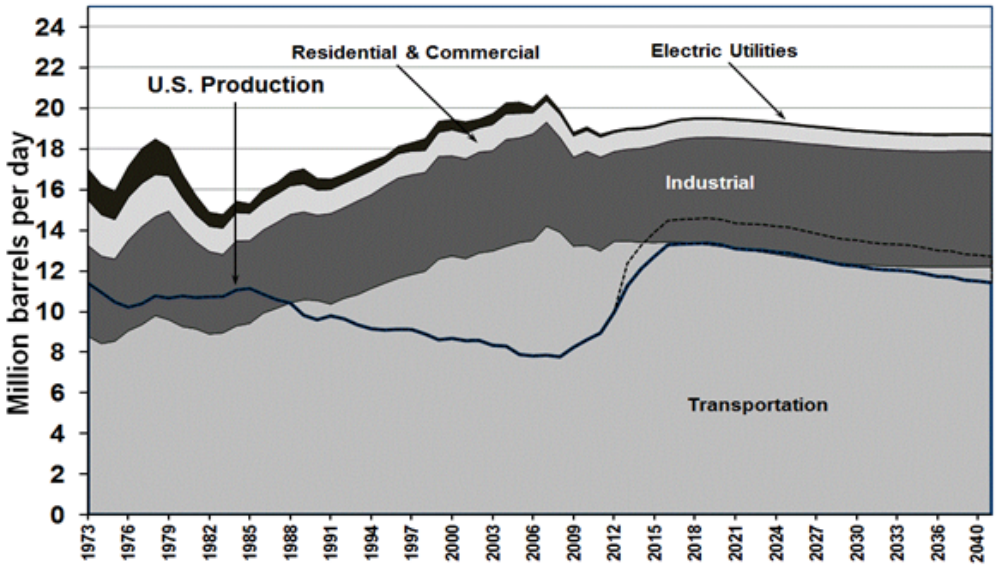

Figure 1.1. : United States Petroleum Production and Consumption - All Sectors, 1973-2040 (Davis et al. 2014).

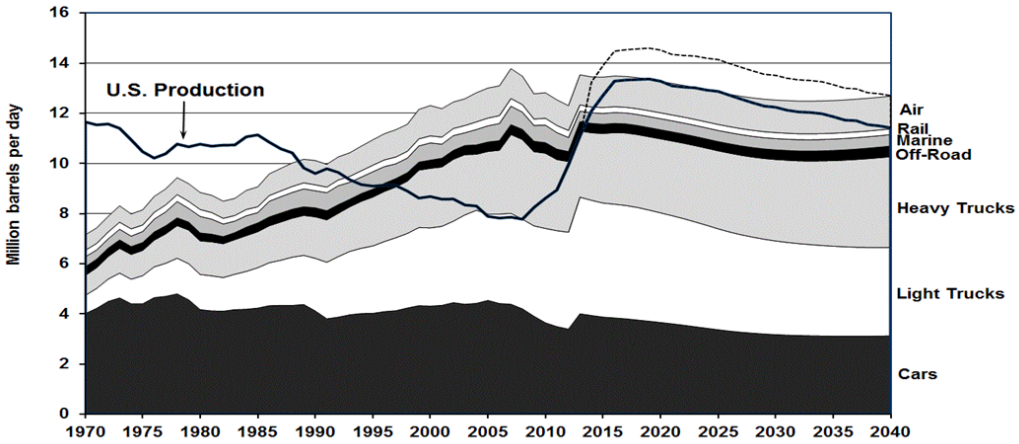

Figure 1.2. : United States Petroleum Production and Transportation Consumption, 1970-2040 (Davis et al. 2014).

low torque/ high speed input from the engine to high torque/ low speed output required at the wheels. There are many different architectures for transmission in the market. Currently, the conventional transmissions mainly include manual and automatic transmission. However, with the use of conventional transmissions, there has been a little improvement in the fuel mileage of cars and light trucks in the last 15 years. The average miles per

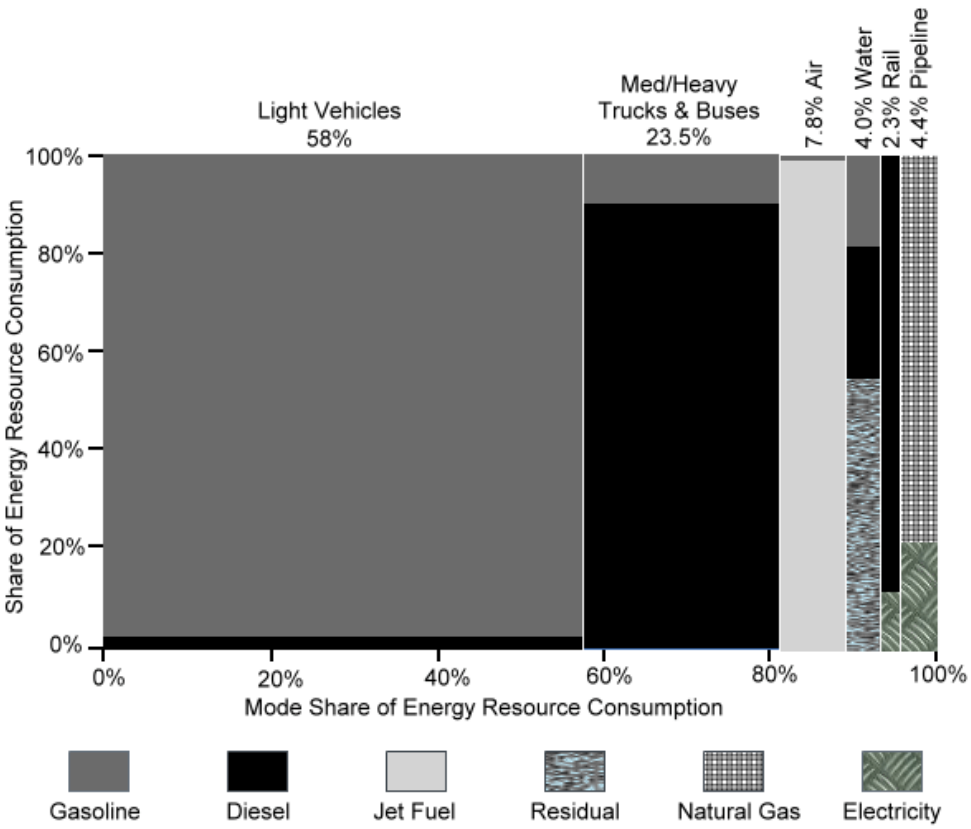

Figure 1.3. : United States Consumption of Transportation Energy Use by Mode and Fuel Type, 2013 (Davis et al. 2014).

gallon achieved by trucks has remained the same for the last 30 years at approximately 5.5 miles per gallon (Wargo et al. 2006). Thus, there is a need to move away from conventional transmissions and develop new technologies to improve fuel economy. Hybrid transmission is one such technology which has shown great potential.

1.1 Hybrid Vehicles

Wouk defined an on-road hybrid vehicle as one in which propulsion energy, during specified operational missions, is available from two or more kinds or types of energy stores, sources, or converters, Wouk (1995). Electric and hydraulic hybrid vehicles are the two main types of hybrids available today. Electric hybrids use electric motors and generators as energy converters and batteries or electric capacitors as storage devices as opposed to hydraulic hybrids that use hydraulic pumps and motors as converters and hydro-pneumatic

accumulators as energy storage devices. These hybrids facilitate improvement in the fuel economy of the vehicles by means of power management strategies. Power management in hybrids is a combination of regenerative braking and engine management.

1.1.1 Engine Management

Engine management refers to operating the engine in its most efficient operating point. Transmission indirectly affects the engine efficiency by influencing the operating region of the engine. In a conventional transmission, the engine speed is defined by the wheel speed and the gear ratio as the engine is mechanically coupled to the wheel. Therefore, for a given wheel speed and torque demand, the engine operating point will be fixed based on the gear ratio. Hence, the engine may not always operate at its most efficient point. This affects its fuel economy. The fuel consumption can be quantified using brake specific fuel consumption (bsfc). A bsfc map represents the fuel consumed by the engine to generate the required energy and defines the most efficient region for engine operation. This map is represented by Figure 1.4. Along with this, the other limitation is that the entire energy generated by the engine has to be utilized immediately and cannot be stored for later use.

Unlike the conventional transmissions, continuously variable transmission (CVT), which have recently become famous in the market, offer the advantage of infinite gear ratios that can be selected based on the speed and torque demand. This helps in decreasing the fuel consumption by operating the engine at the speed with lowest fuel consumption for the current power demand. But, this transmission, like the conventional power-trains, cannot store the excess engine energy.

On the other hand, the simplest of hybrid power-trains facilitate storage of excess engine energy or brake energy and use it at a later stage in case of high loads. This energy is stored in the form of potential energy. Therefore, when stored energy is available, all the power requirement need not be satisfied by the engine alone. This offers a great flexibility in system operation. But, the discrete gears may still not result in the operation of engine in its most efficient zone.

The recent developments in hybrid vehicle technology incorporate the advantage of energy storage as well as a CVT. Thus, a given vehicle speed can be attained either by using

the stored potential energy recovered during braking or operating the engine at the point of lowest fuel consumption or a combination of both and still meet the power requirements.

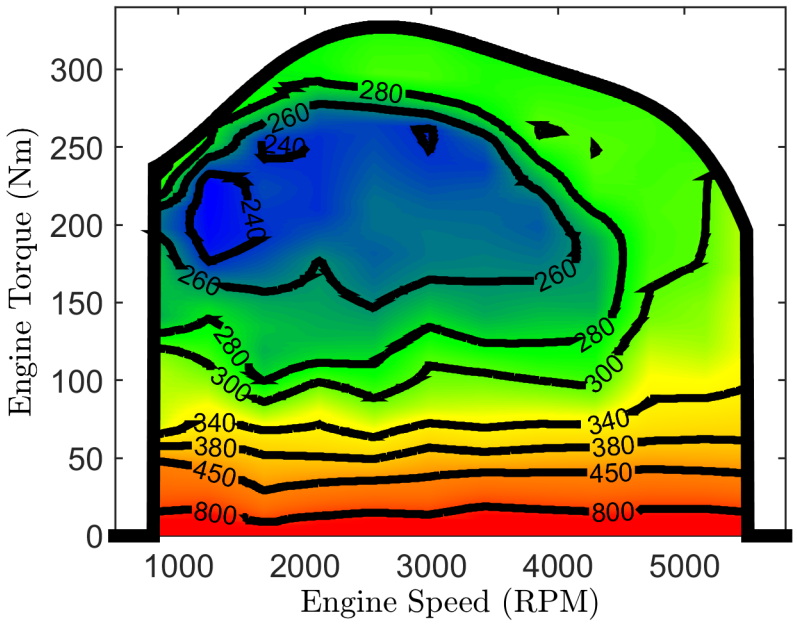

Figure 1.4. : BSFC Map (kW-h/g).

1.1.2 Regenerative braking

Regenerative braking is a technology which is used to convert the kinetic energy of the vehicle during a braking event into another form which can either be used immediately or stored for later time to aid the engine as opposed to conventional transmissions in which the entire energy is dissipated in the form of heat through friction brakes. There are many systems that are used to convert the braking energy and store them in different storage media. Figure 1.5 represents a Ragone Diagram which categorizes these different energy storage media based on their energy density and power density. Higher the energy density, the higher is the total energy that can be stored during braking whereas higher the power density, faster is the energy storage. Electric hybrids are more energy dense and can store energy for a longer time period as compared to hydraulic hybrids which are more power dense and can recover energy at a faster rate. The advantage of regenerative braking can be

achieved by using a power dense system which can recover maximum amount of energy in relatively short time intervals. This makes the hydraulic hybrids a very attractive alternative to the electric ones even though the electric hybrids currently dominate the hybrid vehicle market. This work will be focused on hydraulic hybrid transmissions.

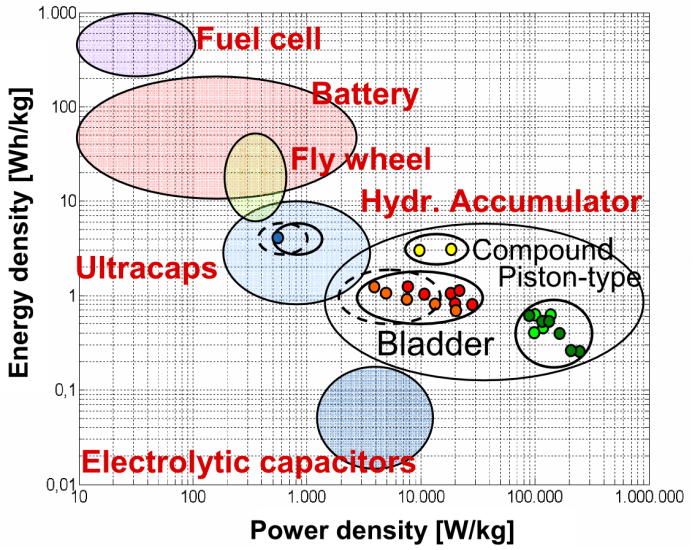

Figure 1.5. : Ragone Diagram (Baseley et al. 2007).

1.2 Hydraulic Transmissions

Hydraulic transmissions make use of positive displacement machines to convert the rotational energy into hydraulic pressure and vice versa. Different combinations of these components have resulted in many different architectures. They can be classified as non hybrid and hybrid architectures.

1.2.1 Non Hybrid Hydraulic Transmission

Non hybrid hydraulic transmission transmits input power from the engine to the wheels by converting rotational power into hydraulic pressure and back to mechanical energy without storage of energy. Hydrostatic transmission is an example of a non hybrid hydraulic transmission.

1.2.1.1 Hydrostatic Transmission

A hydrostatic transmission consists of at least two hydraulic units. One of the units is coupled to the engine shaft and the other to the wheels. These hydraulic units may either be fixed or variable displacement units. Using at least one variable displacement unit results in a continuously variable transmission. Figure 1.6 represents a hydrostatic transmission.

Hydrostatic transmission is a closed circuit architecture with the flow recirculating between the hydraulic units and both the lines can act as high pressure lines. Unit 1 acts as a pump during acceleration and pressurizes line A. Unit 2 acts as a motor to convert the hydraulic power into rotational power and transmits it to the wheels. During braking, the pressure lines switch causing line B to become the high pressure line, unit 1 goes to zero displacement and unit 2 acts as a pump. In this transmission, whatever flow leaves one unit must pass through the other. Hence, this transmission acts as a flow control system. This results in the wheel speed which is a function of the flow rate and unit 2 displacement along with losses. The torque at the wheels is a function of vehicle speed, grade and acceleration which is propagated back in the form of system pressure. Hence, the pressure in the system is load dependent. The flow control and load dependent pressure make the system response stiff while meeting the torque demand at the wheels. This results in a good driver feel.

One of the first works on HST was done for off-highway vehicles by Institute of Agricultural Engineering in Silsoe, UK with development in tractor research (Hamblin,1952). Later, many manufacturers conducted research on HSTs without developing any significant products (Meile,1961). In 1956, one of the first commercially available HST was introduced by Linde (Linde,2015). In 1967, the joint venture by International Harvester and Sunstrand Corporation resulted in commercial production of HST for agricultural tractors (Morris, 1967). However, after its initial success, the design was discontinued due to inefficiencies and high production cost as compared to the mechanical transmission (Renius and Resch, 2005). Eventually, HSTs gained popularity in low power ($\sim$ 30kW) off-highway applications (Renius and Resch,2005).

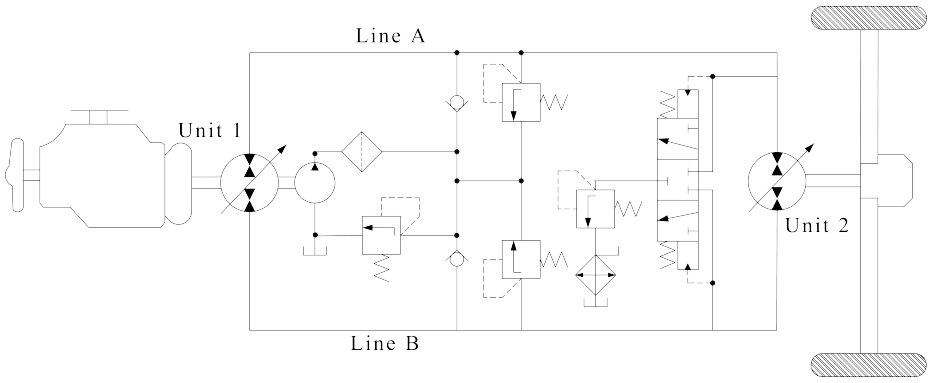

Figure 1.6. : Hydrostatic Transmission Layout.

1.2.2 Hybrid Hydraulic Transmissions

Hybrid transmissions, along with transmitting power from the engine to the wheels, store the kinetic energy available during braking using hydro-pneumatic accumulators in the form of potential energy which can be used at a later time. Almost all the hybrids can be broadly classified into one of the three architectures: parallel, series and series-parallel hybrids.

1.2.2.1 Parallel Hybrid

A parallel hybrid consists of an energy converter and energy storage media as a part of the hydraulic system which acts as an auxiliary drive-train that is mechanically coupled to the traditional transmission as shown in Figure 1.7. The hydraulic system consists of a hydraulic unit (pump/motor) as the energy converter and hydro-pneumatic accumulator that acts as the storage media. The hydraulic unit is often mechanically coupled to the drive shaft of the existing transmission and either absorbs the excess power and stores it in the accumulator or releases accumulator energy to propel the vehicle. One of the biggest advantage of this type of architecture is simplicity of its design which makes it easy to be retrofitted in conventional transmissions

The operation of this system is very simple. The presence of discrete gears results in excess torque supply from the engine than required. The hydraulic unit acts as a pump and stores the excess energy generated by the engine or the kinetic energy available during

regenerative braking in the accumulator. This accumulator energy is released to propel the vehicle by running the hydraulic units as a motor. Different power management techniques have been developed which strategically operate the hydraulic unit in pumping or motoring mode to efficiently transmit power to the wheels and improve the fuel economy. However, this architecture suffers from the losses of the conventional transmission due to the mechanical coupling between the two. Also, discrete gears limit engine management as compared to the modern hybrids.

Research on parallel hybrids was first published by Dunn & Wojcienchowski (1972). They experimentally measured the round trip efficiency of a hydraulic system comprising of a 79cc/rev hydraulic unit, a 19 litre accumulator and a 907 kg flywheel was used to store the energy in flywheel into the accumulator. This energy was then released to the flywheel. The effective energy conversion occuring in the process of charging and discharging the accumulators was used to calculate the round trip efficiency of the hydraulic unit. They measured the round trip efficiency to be 50%. However, on conducting further measurements, they found the efficiency to be 66%. Thus, they concluded that the 24% of the lost energy was as a result of losses in the hydraulic units. Further studies were conducted by Dewey et al. (1974) where they incorporated the effect of the aerodynamic drag of the flywheel. They achieved a round trip efficiency of 75%.

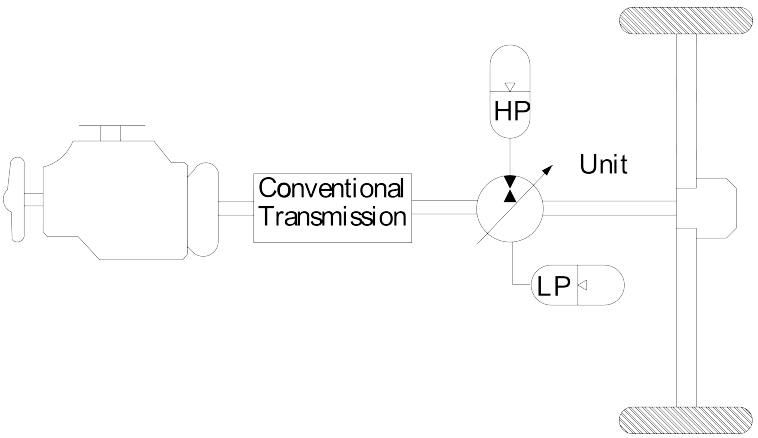

Figure 1.7. : Parallel Hybrid Layout.

The simplicity of its design and the possibility to install it as an addition to an existing transmission resulted in its use in many prototype vehicles. In the 1984, Maschinenfabrik

Augsburg-Nurnberg (MAN) in Berlin, Germany demonstrated 25% reduction in fuel consumption on a bus (Martini 1984). In 1987, Mitsubishi Motors Corp. developed a prototype bus and demonstrated 30% improvement in fuel economy (Nakzawa et al. 1987). In 2002, Ford Motor Company along with Eaton and Environmental Protection Agency (EPA) invented the Hydraulic Power Assist. The transmission was implemented on a 7500 lbs SUV. They demonstrated a reduction in acceleration time for 0-30 mph from 5.4 seconds to 3.5 seconds along with 23.6% gain in fuel economy on Federal Test Procedure (FTP) cycle. Apart from these, many manufacturers and government agencies have implemented this architecture on buses, trucks and military vehicles.

1.2.2.2 Series Hybrid

A series hybrid consists of two energy converters and an energy storage media such that the energy storage is in series with the engine. For a hydraulic transmission, the energy converters are the hydraulic units and the energy storage device is a hydro-pneumatic accumulator. A series hybrid architecture is shown in Figure 1.8. Unit 1 converts the rotational energy of the engine into fluid power which is either stored in the accumulator or sent to unit 2 to provide rotational power at the wheels. Hence, there is no mechanical coupling between the engine and wheels.

The biggest advantage of this transmission is that the two hydraulic units form a CVT. This facilitates complete decoupling of engine operating point from wheel speed. This results in a greater potential of this architecture for power management as compared to a parallel hybrid. Also, the high compliance of the accumulator has a huge impact on system operation. It results in two possible paths for the flow from unit 1. The flow can either go to the accumulator and the energy be stored for later use or to unit 2 in case the accumulator is already at reference pressure and be used immediately. As a result, there is a greater flexibility in power management independent of the torque demand at the wheels.

Series hybrid operates in a secondary control mode. The measured speed or torque is compared to the required quantities and unit 2 is adjusted to meet this demand. On the other hand, unit 1 provides flow to maintain a reference pressure in the lines which is governed by the compliance of the lines and the accumulator. While braking, unit 2 goes

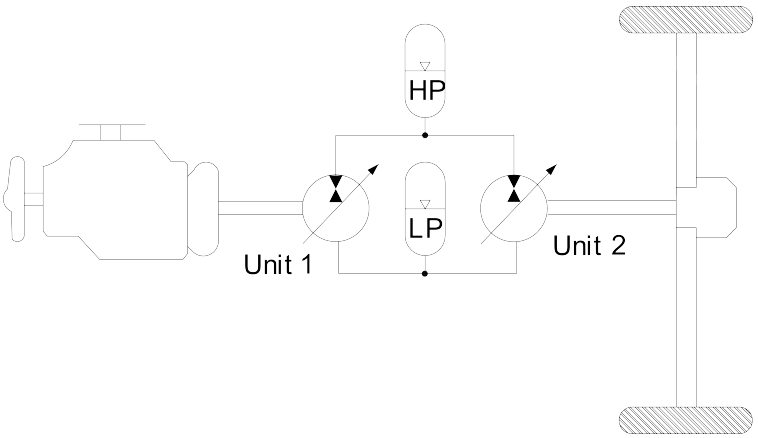

Figure 1.8. : Series Hybrid Layout.

over-center without changing the direction of rotation and acts as a pump directing flow into the accumulator. This results in energy storage.

The series hybrid, along with the benefits with respect to power management, also suffers from some drawbacks. Sizing of the units is very crucial in order to absorb the full power from the engine while providing the power required at the wheels. As all the power at the wheels is provided by unit 2, it is often large in size. This may restrict the top speed of the vehicle. Also, the units are most efficient when operated at high displacement and low pressure. But the pressure in this system is predefined. This results in a high pressure difference across the units which can cause the units to run at low displacements when the torque demand is not high. Hence, the efficiency of the units is compromised.

Elder & Otis (1973), were one of the first to study the series hybrid architecture. They conducted simulations on a passenger vehicle using the Federal Urban Driving Schedule (FUDS) and showed the feasibility of series hybrid along with substantial fuel savings. Later, in 1979, Heggie & Sandri investigated the concept of declutching, called the "mechanical bypass", on a series hybrid and demonstrated the fuel savings of 17% and 22%. In 1985, Wu et al. simulated a series hybrid passenger vehicle on FUDS cycle along with engine shut off capability and showed a fuel consumption of 60 mpg.

In 1990's, nearly two decades after the parallel hybrids, the industrial counterparts started showing interest in series hybrids and developed prototype vehicles. The Cumulo Hydrostatic Drive which was a secondary controlled series hybrid was applied to a bus and

demonstrated 48% savings on trapezoidal start-stop drive cycle (Hugosson 1993). In 2006, a Class 5 UPS delivery truck was developed under the partnership of Eaton Corporation, United Postal Service and other industries. On field testing in Detroit, MI, the vehicle showed fuel savings of 60% to 70% (Wendel et al. 2007). Later, in 2012, a series hydraulic hybrid was designed, built and tested by the U.S. Federal Transit Authority on a transit bus called Altair Bus. This bus was designed from scratch instead of retrofitting an already existing vehicle. A more advanced engine, a lighter frame and materials, advanced HVAC system and many other advanced features resulted in a more efficient and cost effective transit bus with 29% improvement in fuel economy over the most efficient electric hybrid and 47% increase over identical non hybrid one. It showed an overwhelming 109% increase over the conventional Altair Bus (Heskitt et al. 2012).

1.2.2.3 Series-parallel Hybrid

The series-parallel hybrids, often known as the power split transmissions, are a combination of series and parallel hybrids. They are considered to be the most efficient of all the hybrid architectures. A planetary gear train (PGT) is the most important part of the power split transmission. Based on the location of the PGT, the power split architectures are classified as output-coupled, input coupled or more complex architectures with multiple PGTs. There are also architectures which incorporate clutches like dual stage and also, compound power split transmission. An output coupled power split transmission is shown in Figure 1.9.

Power split transmission is so named as the PGT splits the input power from the engine onto a continuously variable hydraulic path and a more efficient mechanical path. This power from the two paths is then added together before the wheels. When all the power is transmitted through the hydraulic path, the transmission acts like a series hybrid whereas it acts like a parallel hybrid when the power is combined. Initially when the vehicle is at rest, all the engine power is transmitted through the hydraulic path. As the speed of the vehicle increases, the PGT causes unit 1 to slow down. Thus, the amount of power transmitted through the hydraulic path decreases with an increase in the power through mechanical path. At a designed velocity, unit 1 stops rotating and power is no longer transmitted

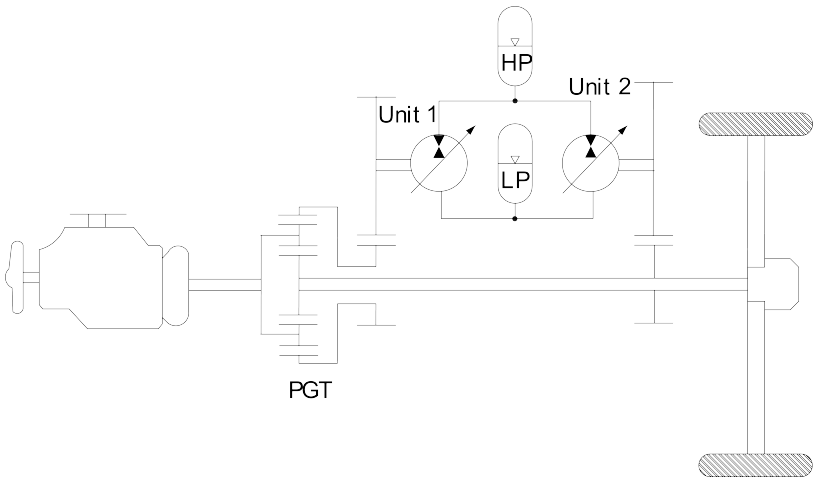

Figure 1.9. : Series-Parallel Hybrid Layout.

through the hydraulic path with only mechanical path being used. The mechanical path is highly efficient in operation and this makes the power split transmission very efficient. During braking, the unit goes over-center and the kinetic energy is stored in the accumulator through the hydraulic path. Also, unit 1 is capable of storing excess engine energy in the accumulator.

Shiber (1980) was the first to patent the power split hydraulic hybrid when he implemented this architecture on a VW Jetta. The data showed doubling of fuel economy compared to a non hybrid vehicle (1979). In Germany, MAN continued their development on the hybrid bus and prototyped the second phase called Hydrous II incorporating a power split transmission. They measured 18% to 33% increase in fuel economy as compared to the conventional bus (Martini 1984). In 2012, 20 power split transmissions, developed by Parker Hannifin were installed by United Postal Service into gasoline powered delivery trucks in Baltimore MD area. They also incorporated engine shut off strategy during idle. For better representation of performance, a drive cycle was developed based on the GPS data that was recorded on these 20 vehicles. The vehicle, when tested on the drive cycle using a chassis dynamometer, observed 19-52% improvement in fuel economy than the traditional diesel vehicle and 30-56% than gasoline vehicle (Lammert et al. 2014). The latest development in power-split transmission is Air Hybrid, a passenger vehicle, developed by PSA-Peugeot-Citroen which demonstrated 45% reduction in fuel consumption in city driving and 35%

overall (PSA-Peugeot-Citroen 2014). Other developments by companies is limited due to high costs.

1.2.2.4 Blended Hybrid Transmission

The blended hybrid architecture is a combination of a hydrostatic and a parallel hybrid transmission. It consists of hydraulic units that are coupled to the engine shaft and also the wheels and transmit power from engine to the wheels. It also consists of a High Pressure accumulator which can be connected or disconnected from the circuit with the use of different actively and passively controlled valves. Figure 1.10 shows the layout of this architecture.

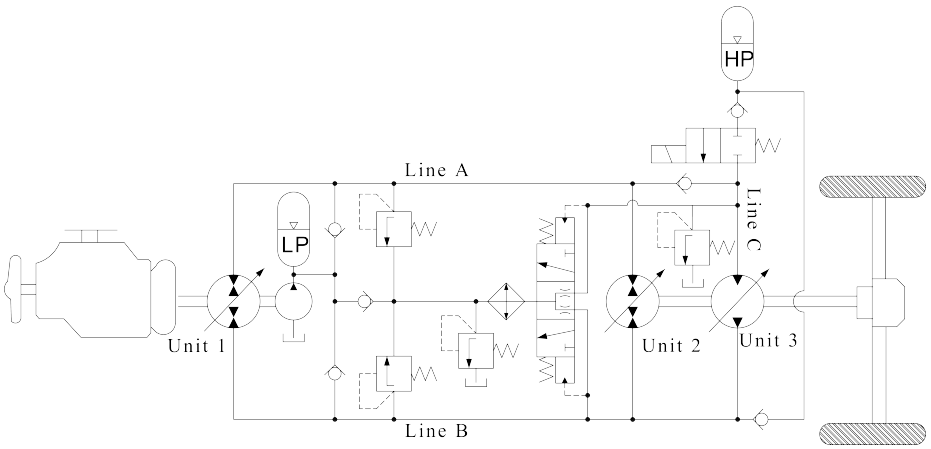

Figure 1.10. : Blended Hydraulic Hybrid Circuit (Sprengel & Ivantysynova 2014*b*).

The blended hybrid can be operated in various modes to achieve higher efficiency as compared to the conventional transmission. During acceleration, it can either be operated in hydrostatic mode where unit 1 powers units 2 and 3 or it can use the energy storage in the accumulator to power unit 3 and operate as a pure hybrid or blend the two modes. Thus, based on the torque requirements at the wheels and current state of the accumulator, control strategies can be developed to operate the system as hydrostatic, pure hybrid or blended hybrid. During braking, unit 1 goes to zero displacement and the pressure switches lines like in HST. This causes line B to operate as a high pressure line. When the pressure in line B rises above that of the accumulator, the accumulator is charged allowing regenerative

braking. The brake energy recovery and operating the vehicle in pure hybrid or blended mode helps in better fuel economy.

This transmission was first introduced by Sprengel & Ivantysynova (2012). It was developed at the Maha Fluid Power Research Center. The researchers compared the fuel consumption of the blended hybrid with different architectures (Sprengel & Ivantysynova 2013). This was done using dynamic programming to optimally control each transmission on a UDDS cycle with the objective function to minimize the fuel consumption. The blended hybrid demonstrated 37% improvement in fuel economy over automatic transmission with fuel economy of 21.1 mpg (Sprengel & Ivantysynova 2013). Later, an energetic analysis of power-split transmission with blended hybrid as hydraulic was performed on UDDS cycle to compare it with different transmissions (Sprengel & Ivantysynova 2014*a*). It showed 0.8% and 7.7% improvement in fuel economy over series hybrid power-split and manual transmission respectively (Sprengel & Ivantysynova 2014*a*). Later, a Hardware-In-The-Loop test rig was developed to simulate the potential of blended hybrid on a passenger vehicle (Sprengel & Ivantysynova 2014*b*) and implemented on an SUV, (Sprengel et al. 2015). Thus, the blended hybrid has been the most recent development in the hydraulic hybrid transmission.

Apart from these architectures, closed loop hydraulic energy regenerative system was developed by Ho & Kyoung. This architecture was based on a closed loop hydrostatic system and used a hydraulic accumulator as energy storage system to recover brake energy without flow reversion, Ho & Kyoung (2012). The architecture was implemented on a test rig. However, the results were presented for the series and the hydrostatic mode separately and in secondary control, the system was maintained at a constant pressure.

The existing architectures, were mainly applied to heavy vehicles like trucks, buses and off-highway vehicle. These architectures have a small range of speed operations and the acceleration rates are limited. Also, the architectures evaluated to be applied to on-highway vehicles have been implemented mainly on hardware in loop test rigs. The blended hybrid architecture that was implemented on an SUV uses conventional control techniques which are more suited for different applications and the driver feel was compromised. Along with this, while implementing hydraulic hybrid transmission, the main focus has been on power management and economy and not much research has been directed towards the drivability aspect of the on-highway vehicles.

1.3 Thesis Statement

The aim of this thesis is to implement the novel "Mode-Switching Hybrid" transmission in an all time four wheel drive on-highway SUV and develop control strategies to achieve improved drivability of the vehicle. More specifically these include:

- Propose a new hydraulic hybrid architecture called the "Mode-Switching Hybrid" to achieve smoother operation of the vehicle and develop a simulation model to validate different operating modes like acceleration, braking and coasting.
- Design a packaging architecture using 3D modeling and implement the assembly of the transmission on a prototype vehicle.
- Design and manufacture custom parts.
- Design and implement a new braking system to achieve regenerative braking by modifying the existing brake pedal and allows the use of hydraulic friction brakes in extreme braking conditions.
- Develop and implement a throttle actuation system to control engine speed.
- Design different control strategies to demonstrate different modes of operation, to achieve improved drivability and check the stability of the controllers.
- Implement the controllers on the prototype vehicle and test their performance.

2. THE PROPOSED ARCHITECTURE

This thesis focuses on the design and implementation of a new hydraulic hybrid architecture called the "Mode-Switching Hybrid" and development of control strategies to achieve better drivability. This transmission was proposed to overcome the weaknesses of the conventional architectures in terms of drivability.

This chapter discusses the deficiencies in the conventional transmissions and the way the mode-switching hybrid overcomes them. It also discusses the new architecture in detail along with its different modes of operation.

Series Hybrid: Series hybrid is one of the most common type of hybrid transmission available in the market. Its working has been described in Section 1.2.2.2. The advantages of series hybrid have been evident with respect to improvement in fuel economy over the conventional transmission due to storage of energy in the accumulator and a greater flexibility for implementing power management strategies. However, these advantages come along with certain drawbacks. The biggest drawback of the series hybrid is the direct connection of the high pressure accumulator to the system which influences the hydraulic units and subjects them to the high pressure of the accumulator. Due to this, often, the hydraulic units are operated in high pressure and low displacement mode. However, the hydraulic units are the most efficient in high displacement and low pressure mode. Hence, the efficiency of the hydraulic units is compromised. The next disadvantage is the need for over-center units. In series hybrid, the pressure cannot switch lines due to the presence of the high pressure accumulator. This necessitates the use of over-center units. While braking, unit 2 goes over-center and pumps fluid in line A creating a resistive torque to slow down the vehicle. The problem lies in the fact that only a limited number of hydraulic units in the market allow this functionality.

The last drawback is related to driver feel. The torque at the wheels is a function of system pressure and the displacement of unit 2. Hence, in the case when the required torque at the wheel is high and accumulator pressure is low, the system pressure must first

be raised by pumping fluid into the accumulator through unit 1. This makes the system highly complaint and slows down the response resulting in a poor driving feel.

Even after all these deficiencies, the series hybrid has a major advantage when it comes to brake energy recovery. Also, the accumulator energy can be used as boost at later stage to achieve higher acceleration.

Hydrostatic Transmission: The hydrostatic transmission is another such transmission which is popular in the market. It is shown in Figure 1.6. The biggest disadvantage of HST is the absence of a high pressure accumulator. Hence, the brake energy can be converted to mechanical energy and used at the same time but cannot be stored for later use. Also, all the torque required at the wheels has to be supplied by the hydraulic units. This may result in situations where the units are maxed out and cannot provide the required torque. Hence, sizing of units is critical. The last drawback is that the larger size of units in order to meet higher torque demands may result in operation of the units at low displacement. This affects the efficiency of the units.

Although these demerits exist, the HST has a great advantage in terms of drivability. The torque at the wheels (the load) define the system pressure which varying the displacements of the units. Hence, due to the system being flow controlled, the flow displaced by the pump has to pass through the motor which results in a stiff response to any input given by the driver. This results in a superior driving experience. Apart from driver feel, this architectures allows switching of pressure lines. Therefore, over-center units are not a necessity for its operation.

2.1 The Mode-Switching Hybrid

To overcome the shortcomings of the conventional transmissions as well as make full use of their merits, the mode-switching hybrid was developed at the Maha Fluid Power Research Center. This transmission is called mode-switching hybrid as it is a combination of a series hybrid and a hydrostatic transmission and involves switching between the two types based on the operating conditions. The mode-switching hybrid is shown in Figure 2.1.

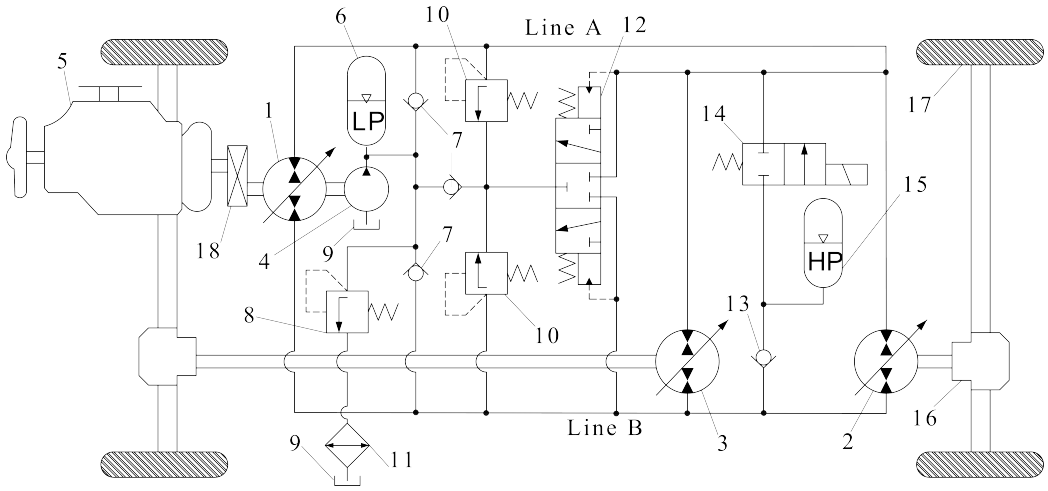

1. Unit 1
2. Unit 2
3. Unit 3
4. Charge Pump
5. Combustion Engine
6. LP Accumulator
7. Check Valve
8. LP Relief Valve
9. Reservoir
10. HP Relief Valve
11. Oil Cooler
12. Flushing Valve
13. Check Valve
14. Enabling Valve
15. HP Accumulator
16. Axle
17. Wheels
18. Gear Box

Figure 2.1. : Mode-Switching Hybrid.

As seen in the figure, the mode-switching hybrid acts as a hydrostatic transmission when the enabling valve (14) is closed and there is no flow from the accumulator to line A. However, compared to the hydrostatic transmission shown in Figure 1.6, this transmission has two hydraulic motors (2) and (3). These hydraulic motors are connected to different axles; unit (2) being coupled to the rear and unit (3) to the front axle. The use of two motors of comparatively smaller sizes to provide the same amount of torque, results higher output speeds. Apart from this, a series of check valves is used to connect and disconnect the high pressure (HP) accumulator (15) from the circuit. The enabling valve (14), when in open position, switches the transmission from hydrostatic to series hybrid enabling secondary control. Also, while braking, the pressure switches lines and line B pressure increases which makes it a high pressure and line A, a low pressure line. The check valve (13) then connects the HP accumulator to line B and allows regenerative braking.

Additionally, the low pressure charge pump (4) uses the oil from the reservoir (9) to provide for the control pressure for the hydraulic units as well as pressurizes the low pressure line by supplying flow to the lines through the check valve (7). The charge pump along

with the low pressure (LP) accumulator (6) provides flow needed by units (2) and (3) while storing the braking energy into the accumulator. The presence of flushing valve (12) helps in connecting either one of the lines to the low pressure system and charging the LP Accumulator. It also enables cooling and filtering of oil when the flow goes through the LP relief valve (8) to the oil cooler (11) and finally into the reservoir. Additional components like the gear box (18) and differential (16) help in scaling the torques from engine to the transmission.

The following sections describe the different modes of operation of the mode-switching hybrid in detail.

2.1.1 Hydrostatic Driving Mode

As mentioned previously, when the enabling valve (14) is closed, the mode-switching hybrid operates as a hydrostatic transmission. Initially, when the vehicle is at rest, unit 1 is at zero displacement and units 2 and 3 are at full displacement. As displacement of unit 1 is increased, it starts providing flow to line A and the pressure in the line increases. This pressure is built to provide for the torque required at the wheels as the units 2 and 3 absorb the flow from unit 1. Thus, pressure in the system depends on the load and speed of the units on the flow. At the beginning, unit 1 acts as a variable displacement pump till it reaches full displacement and units 2 and 3 act as fixed displacement motors. For further increase in speed of the vehicle, unit 1 is maintained at full displacement and the displacements of units 2 and 3 are decreased.

2.1.2 Driving in Secondary Control Mode

When the enabling valve (14) is opened, the HP accumulator is connected to line A and the transmission becomes a series hybrid. The accumulator provides flow to line A if the pressure of the accumulator is higher than the line. Hence, the accumulator energy is used to provide for the demanded torque at the wheels through units 2 and 3. This results in secondary control mode. When the accumulator energy falls below the required system pressure, unit 1 provides flow to the accumulator and either the system can be operated in

secondary control mode or the accumulator can be disconnected from the circuit by closing the enabling valve and converting the transmission back to hydrostatic mode.

2.1.3 Regenerative Braking

During braking, the pressure switches lines as in hydrostatic mode with line B acting as a high pressure and line A as low pressure line. units 2 and 3 act as pumps with their flow directed in two different ways. Firstly, unit 1 can act as a motor and provide power to overcome parasitic losses. Secondly, as the pressure in line B becomes higher than the pressure in the HP Accumulator, flow is directed to the HP accumulator through the check valve (13). Thus, braking energy is stored in the accumulator and can be used as a later stage to provide boost power. The inlet flow to units 2 and 3 while pumping is provided by the charge pump (4) and the LP accumulator (6). Excess flow from the units that does not go to the accumulator or unit 1 is drained out using the high pressure relief valve (10).

2.1.4 Reverse Operation

For reverse operation, unit 1 goes over-center and starts pumping flow into line B. line B becomes the high pressure line and provides torque to units 2 and 3 to drive the wheels backwards. While doing so, if the pressure in the line exceeds the pressure in the HP accumulator, the oil flows into the accumulator through the check valve (13). While braking in reverse mode, similar to the forward driving, pressure switches lines making line A a high pressure line. However, unlike regenerative braking, the flow from units 2 and 3 now is absorbed by unit 1 to compensate for parasitic losses or goes over the HP relief valve (10) and charge the LP accumulator (6) or to the reservoir (9) through the LP relief valve (10) and oil cooler (11).

Another alternative to the above method for reverse operation is to switch units 2 and 3 over-center. Apart from this change in displacements of units 2 and 3, the rest of the system works like in forward driving mode. line A acts as high pressure line. However, this approach has an advantage over the previous once during braking. While braking, energy storage is possible due to pressure switching and line B being under high pressure facilitating

flow into the accumulator. Having mentioned this fact, this advantage is noticeable only in case of heavy or off-highway vehicles.

3. SYSTEM MODELING

The mode-switching hybrid has been studied for an on-highway application in this thesis. To explore system architecture, study system behavior and develop control strategies, an accurate system model was a necessity. A mathematical model provides the ease of modifying the system level components and operating parameters to study the behavior of the system. The principal components of this architecture include the engine, the hydraulic transmission and the mechanical system. The physics behind each system and its components is used to generate a dynamic model to simulate and understand the behavior of mode-switching hybrid for an on-highway application. When there is a lack of understanding of physics behind working of certain systems, an empirical model was used. High-fidelity models were developed in MATLAB-Simulink Environment. The hydraulic system model was developed to calculate the torque generated by the hydraulic system which was coupled to the mechanical model which calculated the system parameters like vehicle velocity. Hence, this chapter focuses on the dynamic models of the individual components and their integration as tools to study the control strategies on mode-switching hybrid.

3.1 Mathematical Models for Hydraulic System

The mode switching hybrid forms the hydraulic system of the on highway vehicle. The main components of the system include hydraulic units, hydraulic transmission lines, hydropneumatic accumulators, check valves, relief valves and the low pressure system. This section describes the modeling of each of these components.

3.1.1 Hydraulic Units

The hydraulic units in this architecture are axial piston machines which are capable of operating as a pump as well as a motor based on the loading conditions. The hydraulic units are responsible for circulating the flow of the hydraulic fluid in the system in order to provide

the torque required by the mechanical system i.e the vehicle. The hydraulic units act as control elements in case of DC actuation which makes the accuracy of the model of utmost importance. Hence, even the losses in the units are crucial. These losses are a function of unit speed, differential pressure and the derived displacement volumes of the units. The derived displacement, V_d, which is more accurate than the geometric displacement volume, is determined using the Toet method. This procedure involves a linear extrapolation of the data at multiple differential pressures to calculate the volumetric displacement at zero differential pressure.

$$V_d = \frac{1}{n} \cdot \frac{\sum_{j=1}^{k} Q_{ej} \cdot \sum_{j=1}^{k} \Delta p_j^2 - \sum_{j=1}^{k} \Delta p_j \cdot \sum_{j=1}^{k} \Delta p_j \cdot Q_{ej}}{k \cdot \sum_{j=1}^{k} \Delta p_j^2 - \left(\sum_{j=1}^{k} \Delta p_j\right)^2} \tag{3.1}$$

where Q_e represents the effective flow rate of the hydraulic units, n stands for the unit speed and Δp for the differential pressure across the hydraulic unit. A polynomial fit is obtained for the steady state measurements performed for various speeds, displacements and differential pressures of the unit under the condition of constant inlet temperature.

Using this derived displacement volume, the theoretical flow rate and the torque produced by the hydraulic unit can be calculated as a function of swash plate angle, β.

$$Q_{th} = \beta \cdot V_d \cdot n \tag{3.2}$$

$$M_{th} = \beta \frac{\Delta p \cdot V_d}{2\pi} \tag{3.3}$$

Then, the unit volumetric loss, Q_s, is obtained based on derived displacement and is a function of the swash plate angle, β using the Equation (3.4). This loss is a summation of different loss components like internal losses, external losses, compressibility losses and losses due to incomplete filling of the displacement chamber. However, calculating these losses individually isn't possible and empirical relation is obtained from measured data.

$$Q_s(V_d, n, \Delta p)_{T_{in}=constant} = \sum_{i_1=0}^{I_1} \sum_{i_2=0}^{I_2} \sum_{i_3=0}^{I_3} K_Q(i_1, i_2, i_3) V_d^{i_1} n^{i_2} \Delta p^{i_3} \tag{3.4}$$

where K_Q stands for the volumetric flow loss coefficient.

Along with volumetric loss flow rate, the torque loss, M_s is calculated by fitting a curve using the measured data and is expressed as in Equation (3.5). The torque losses are a result of the friction occurring between sliding surfaces, movable parts and flow of viscous fluid and pressure drops in the displacement chamber. Other losses depend on operational parameters like manufacturing tolerances, stresses on seals, preloaded springs, etc.

$$M_s(V_d, n, \Delta p)_{T_{in}=constant} = \sum_{i_1=0}^{I_1} \sum_{i_2=0}^{I_2} \sum_{i_3=0}^{I_3} K_T(i_1, i_2, i_3) V_d^{i_1} n^{i_2} \Delta p^{i_3} \tag{3.5}$$

where K_T stands for the torque loss coefficient.

However, evaluating these losses through accurate and time consuming measurements for each unit size is a tedious process. Hence, the geometry is scaled to determine the losses based on the data available for a single unit. Thus, scaling laws, known as linear scaling laws, are simple relationships used to predict operational parameters of a unit based on measured data available for a unit of different size. These laws use a linear scaling term, λ, which is a function of the displacements of desired as well as reference units and is defined as in Equation (3.6).

$$\lambda = \sqrt[3]{\frac{V_{scaled}}{V_{ref}}} \tag{3.6}$$

The scaling term is used to determine scaled losses as described in Equation (3.7) and Equation (3.8).

$$Q_{s,scaled} = Q_s \cdot \lambda^2 \tag{3.7}$$

$$M_{s,scaled} = M_s \cdot \lambda^3 \tag{3.8}$$

These losses are then used to calculate the effective flow rate and torque generated by the hydraulic unit. The expressions for effective flow and torque can be derived based on the operating mode of the hydraulic unit. The unit can be operated in eight modes based on different combinations of the direction of rotation, pressure differential and swash plate position. These eight quadrants include four modes of pumping and four of motoring. Figure 3.1 shows the hydraulic unit as a pump and a motor when $p_A > p_B$.

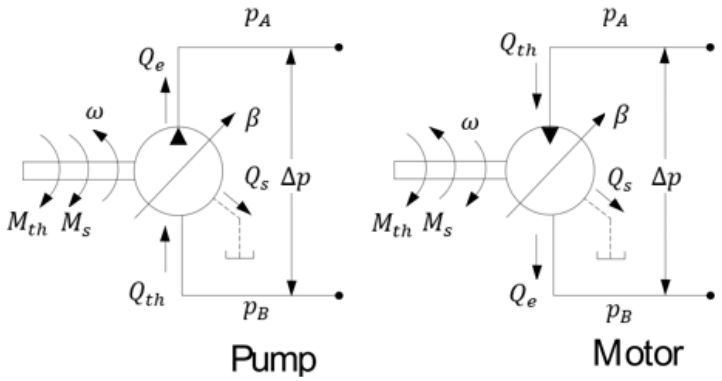

Figure 3.1. : Pump and Motor Schematic.

The effective flow rate and torque can be calculated for the two different modes of operation of the hydraulic units can be expressed as in Equation (3.9) - Equation (3.12).

- Pumping Mode:

$$Q_e = Q_{th} - Q_s = \beta \cdot V_d \cdot n - Q_s \tag{3.9}$$

Where Q_e is the effective flow rate, Q_{th} is the theoretical flow rate as defined in Equation (3.2) and Q_s are the volumetric flow losses as defined in Equation (3.4).

$$M_e = M_{th} + M_s = \beta \frac{\Delta p \cdot V_d}{2\pi} + M_s \tag{3.10}$$

Where M_e is the effective torque, M_{th} is the theoretical torque as defined in Equation (3.3) and M_s are the torque losses as defined in Equation (3.5).

- Motoring Mode:

  Similar to the pumping mode, the effective quantities for the motoring mode are as in Equation (3.11) and Equation (3.12).

$$Q_e = Q_{th} + Q_s = \beta \cdot V_d \cdot n + Q_s \tag{3.11}$$

$$M_e = M_{th} - M_s = \beta \frac{\Delta p \cdot V_d}{2\pi} - M_s \tag{3.12}$$

The effective flow rates and torque for the eight different modes of operation based on the rotation, pressure differential and swash plate position are defined in Table 3.1.

Table 3.1. : Effective Flow Rate and Torque for Eight Quadrant Operation.

Rotation	**Pressure**	**Swash Plate**	**Flow**	**Mode**	$\mathbf{Q_A}$	$\mathbf{Q_B}$	$\mathbf{M_e}$
$+\omega$	$+\Delta p$	$+\beta$	B to A	Pump	$Q_{th} - Q_s$	$-Q_{th}$	$-M_{th} - M_s$
		$-\beta$	A to B	Motor	$-Q_{th} - Q_s$	Q_{th}	$M_{th} - M_s$
	$-\Delta p$	$+\beta$	B to A	Motor	Q_{th}	$-Q_{th} - Q_s$	$M_{th} - M_s$
		$-\beta$	A to B	Pump	$-Q_{th}$	$Q_{th} - Q_s$	$-M_{th} - M_s$
$-\omega$	$+\Delta p$	$+\beta$	A to B	Motor	$-Q_{th} - Q_s$	Q_{th}	$-M_{th} - M_s$
		$-\beta$	B to A	Pump	$Q_{th} - Q_s$	$-Q_{th}$	$M_{th} - M_s$
	$-\Delta p$	$+\beta$	A to B	Pump	$-Q_{th}$	$Q_{th} - Q_s$	$M_{th} - M_s$
		$-\beta$	B to A	Motor	Q_{th}	$-Q_{th} - Q_s$	$-M_{th} - M_s$

3.1.2 Hydro-Pneumatic Accumulator

A hydro-pneumatic accumulator as shown in Figure 3.2 is a hydraulic energy storage device that is used to convert a hydraulic transmission into a hybrid. The braking energy can be stored into the accumulator and used at a later stage to aid the engine for propulsion as well as power auxiliary systems. This is done by converting the kinetic energy of the vehicle into pressurized fluid using units 2 and 3 which then is stored in the HP accumulator. The accumulator can either have a direct connection to the hydraulic system or it can be separated using enabling valve. When it is in direct connection with the system like in series hybrid, the accumulator increases the capacitance of the high pressure line and gives

a flexibilty to implement power management strategies. When in indirect connection, the capacitance of the line does not increase till the accumulator is connected to the system.

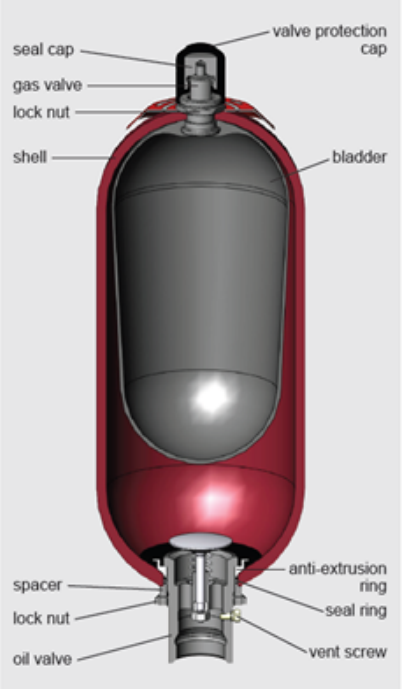

Figure 3.2. : Bladder Type Hydro-Pneumatic Accumulator.

The accumulator stores the energy using the compressibility of the nitrogen gas present in it. The gas and the fluid are separated using elastic membrane or a piston depending on the type of accumulator. The bladder type uses the elastic membrane and the piston type uses the piston as the separating device. The accumulator encloses the fluid, gas and separating device in a pressure vessel which is a steel housing or more advanced low weight carbon fiber.

The energy storage in the accumulator is achieved by pumping pressurized fluid into the oil side of the accumulator. As the oil is pumped, the nitrogen gas starts compressing due to the force acting on the separating device. This results in energy storage in the accumulator due to the compressibility of the nitrogen gas. The accumulator is modeled using the polytropic process as the nitrogen is assumed to be an ideal gas and hence, follows the ideal gas laws. Equation (3.13) describes the accumulator model.

$$p \cdot V^n = c \tag{3.13}$$

Thus,

$$p_0 \cdot V_0^n = p \cdot V^n \tag{3.14}$$

Where p and V are the pressure and volume of gas in the accumulator respectively, n is the polytropic index which is taken as 1.3 and c is a constant. p_0 is the initial precharge pressure of the accumulator and V_0 is the volume of the initial accumulator volume. The initial case is the one when the accumulator is completely empty. However, to increase the life of the accumulator, a minimum pressure is defined. The precharge pressure is defined as 0.9 times the minimum pressure. The change in the accumulator volume is given by Equation (3.15). Based on the above model, the energy stored in the accumulator can be calculated using Equation (3.19).

$$\Delta V = V_0 \left[\left(\frac{p_0}{p_1} \right)^{\frac{1}{n}} - \left(\frac{p_0}{p_2} \right)^{\frac{1}{n}} \right] \tag{3.15}$$

$$E_{1\to 2} = \int_{V_1}^{V_2} p dV \tag{3.16}$$

$$= \int_{V_1}^{V_2} \frac{c}{V} dV \tag{3.17}$$

$$= \int_{V_1}^{V_2} \frac{p_0 \cdot V_0}{V^n} dV \tag{3.18}$$

$$= \frac{p_0 \cdot V_0^n}{1-n} (V_2^{1-n} - V_1^{1-n}) \tag{3.19}$$

Where V_1 and V_2 are the volumes when the pressures are p_1 and p_2 and $E_{1\to 2}$ describes the energy change in the accumulator while going from state 1 to 2.

3.1.3 Check Valves

Check valves are hydraulic components that allow flow only in one direction. The flow through the check valve is derived using the orifice flow equation. The check valve is modeled as in Equation (3.20).

$$Q_{check} = \begin{cases} C_v \cdot \sqrt{\frac{2 \cdot (p_{in} - p_{out})}{\rho}}; & p_{in} > p_{out} \\ 0; & p_{in} \leq p_{out} \end{cases} \tag{3.20}$$

Where Q_{check} is the flow through the check valve, p_{in} and p_{out} are the pressure values at the inlet and the exit of the check valve respectively and ρ is the density of fluid in the line.

3.1.4 Relief Valves

Relief valve is used to define a limit on the maximum allowable pressure of the system. It acts as the safety device for a hydraulic system. When the pressure in the system exceeds this limit, the oil flows over the pressure relief valve and the system pressure is controlled. The flow from the pressure relief valve is modeled as flow from the orifice as in Equation (3.21).

$$Q_{relief} = \begin{cases} C_v \cdot \sqrt{\frac{2 \cdot (p_{in} - p_{set})}{\rho}}; & p_{in} > p_{set} \\ 0; & p_{in} \leq p_{set} \end{cases} \tag{3.21}$$

Where Q_{relief} is the flow through the relief valve, p_{in} and p_{set} are the pressure values at the inlet and of the relief valve and p_{set} is the set maximum allowable pressure in the system.

3.1.5 Low Pressure System

The low pressure system is designed to compensate for the volumetric flow losses occurring in the system. It also helps in controlling the swash plate of the hydraulic units and cooling of the oil in the system by providing the control pressure. Also, while braking the additional flow to charge the HP accumulator is provided to units 2 and 3 by the LP accumulator and the charge pump. The low pressure system in this architecture consists of an external gear pump, LP Accumulator, relief valve to set the pressure of the low pressure system at a desired value, flushing valve, cooler and reservoir.

Similar to the hydraulic units, a scaled loss model is used for the gear pump and the LP accumulator is modeled similar to the HP accumulator. The flow from the low pressure

system to any of the lines occurs through the check valves when the line pressure falls below the low pressure system. Also, the flushing valve directs the excess flow to the cooler before draining it to the reservoir.

3.1.6 Hydraulic Transmission Lines

All the individual components in the hydraulic system are connected to each other by the transmission lines. The flow between these components occurs through these lines and undergoes laminar and turbulent losses. These losses result in a pressure drop across the lines. These losses are modeled using a lumped parameter approach and derived from Navier-Stokes equations by balancing the load forces against the viscous forces. The expressions for the laminar and turbulent losses are shown in Equation (3.22) and Equation (3.23) respectively.

$$\Delta p_{lam,loss} = \frac{512 \rho L Q^2}{Re \cdot \pi^2 D^5} \tag{3.22}$$

$$\Delta p_{turb,loss} = 8 \rho L \frac{0.316 Q^2}{Re^{0.25} \pi^2 D^5} \tag{3.23}$$

Where L is the transmission line length, D is the diameter of the line, Q is the volumetric flow rate in the line, Re is the Reynold's number which is defined in Equation (3.24) and ρ is the density of the hydraulic fluid. $\Delta p_{lamloss}$ and $\Delta p_{turbloss}$ are the pressure drops due to laminar and turbulent flow in the lines. If the $Re < 2300$, the flow is considered to be laminar else the flow is turbulent and pressure drop is calculated accordingly. The expression for Re is defined in Equation (3.24).

$$Re = \frac{Q D_H}{\nu A} \tag{3.24}$$

Where ν is the kinematic viscosity, D_H is the hydraulic diameter of the line and A, the cross sectional area.

Now, the flow in the lines results in pressure generation which is given by the pressure build up equation. These equations form the final part of the hydraulic system.

3.1.7 Pressure Build Up

The entire system operates based on the pressure developed in the lines. This pressure is resultant of the inflow and outflow of hydraulic oil in the lines from the hydraulic components. The generalized form of pressure built up equation is as given in Equation (3.25).

$$\dot{p_{Line}} = \frac{1}{C_H} \sum Q \tag{3.25}$$

Where p_{Line} is the pressure in the hydraulic line, C_H is the hydraulic capacitance of the line which is defined as in Equation (3.26) and $\sum Q$ is the net flow in and out of the line.

$$C_H = \frac{V}{K_{oil}} \tag{3.26}$$

Where K_{oil} is the bulk Modulus of the oil and is given by Equation (3.27).

$$K_{oil}(p) = (p + b) \left[\frac{1}{a} - \ln \left(1 + \frac{p}{b} \right) \right] \tag{3.27}$$

Where p is the pressure and a and b are constants. $a = 0.0733$ and $b = 999.93$ bar (for HLP32 at 52^o C (20cSt)).

However, the hydraulic capacitance of the accumulator is different as compared to that of lines and is defined as in Equation (3.28).

$$C_{H,HP} = \frac{V_0}{n} \cdot \left(\frac{p_0^n}{p_{HP}^{(n+1)/n}} \right) \tag{3.28}$$

3.2 Mathematical Models for Mechanical Systems

The hydraulic system is coupled to two mechanical systems. The first being the wheels and the second being the engine. The hydraulic transmission transmits the power from engine to the wheels.

3.2.1 Vehicle Model

The hydraulic units 2 and 3 are coupled to the wheels. The torque is transmitted from the units to the wheels of the vehicle through the axle and differential. The torque at the wheel is applied through the units and has to overcome the resistances in order to propel the vehicle. The resistances consist of aerodynamic drag F_D, rolling resistance F_r and grading force F_g as in Figure 3.3. The expressions for these components of resistances are as given by Equation (3.29), Equation (3.30) and Equation (3.31).

$$F_D = \frac{1}{2}\rho A_f C_d v_{veh}^2 \tag{3.29}$$

$$F_r = W C_r \cos(\theta) \tag{3.30}$$

$$F_g = W \sin(\theta) \tag{3.31}$$

Where A_f is the frontal area of the vehicle, C_d is the coefficient of drag, v_{veh} is the vehicle velocity, $W = m_{veh} \cdot g$ is the gravity force due to the mass of the vehicle and C_r is the coefficient of rolling resistance.

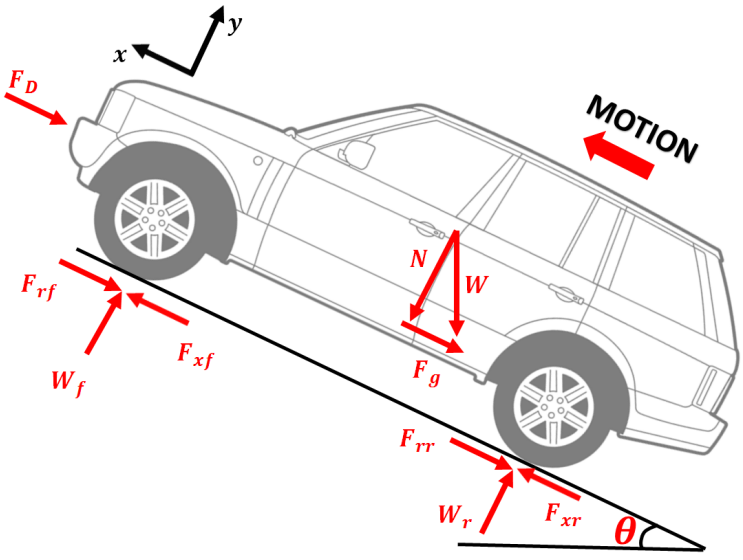

Figure 3.3. : Forces Acting on a Vehicle.

The balance of the forces on the vehicle based on the free body diagram shown in Figure 3.3 in the x-direction gives the resultant propulsive force on the vehicle. The resultant force is given by Equation (3.32).

$$F_x = F_{xf} + F_{xr} + F_g + F_D + F_{rf} + F_{rr} \tag{3.32}$$

Where F_{xf} and F_{xr} are the forces acting on front and the rear wheels respectively in x-direction due to the torque supplied by the engine. F_{rf} and F_{rr} are the rolling resistances on the front and the rear wheels respectively.

Using the force balance, the speed of the vehicle can be calculated as in Equation (3.33).

$$\dot{\omega_{wheel}} = \frac{1}{J_w}\left(T_{app} + (F_D + F_g + F_r r) \cdot r_{dyn}\right) \tag{3.33}$$

where $T_{app} = (F_{xf} + F_{xr}).r_{dyn}$ is the torque applied by the transmission on the wheels and $J_w = m_{veh} \cdot r_{dyn}^2$ represents the inertia of the vehicle. While deriving wheel speed from the vehicle speed, wheel slipping is neglected.

3.2.2 Engine Model

The engine dynamics are modeled using Equation (3.34).

$$\dot{\omega_{CE}} = \frac{1}{J_{eng}}\left[\frac{u_{CE}}{100} \cdot M_{comb} - M_f - M_L\right] \tag{3.34}$$

Where ω_{CE} is the angular velocity of the engine, J_{eng} is the rotational inertia of the engine, u_{CE} is the throttle command to the engine, M_{comb} is the combustion torque of the engine, M_f is the frictional torque and M_L is the load on the engine. The combustion torque is obtained using Equation (3.35).

$$M_{comb} = M_{WOT} + M_f \tag{3.35}$$

Where M_{WOT} is the torque under wide open throttle condition and is determined experimentally. The frictional torque for a gasoline engine is given by the empirical relation

shown in Equation (3.36) as it is more difficult to measure than WOT torque. This empirical formula is based on published data, (Heywood 1988).

$$M_f = \frac{V_{eng}}{4 \cdot \pi}(0.05 \cdot n_{eng}^2 + 0.15 \cdot n_{eng} + 0.97) \cdot 10^5 \tag{3.36}$$

Where V_{eng} is the displacement volume of the combustion chamber and n_{eng} is the angular velocity of the engine (rpm).

The combustion torque generated by the engine is dependent on the accelerator pedal input given by the driver. The accelerator pedal input is translated to the throttle body which results in air flow to the engine.

3.3 State Space Equations

The system model of the mode-switching hybrid can be summarized as in this section and the Simulink model is as in Appendix A.

$$\dot{\omega_{CE}} = \frac{1}{J_{eng}}\left[\frac{u_{CE}}{100} \cdot M_{comb} - M_f - M_L\right] \tag{3.37}$$

$$\dot{p_A} = \frac{1}{C_{H,A}}\left[Q_{1,A} + Q_{A,LP,check} - Q_{A,relief} - Q_{2,A} - Q_{3,A} + Q_{enab} - Q_{A,flushing}\right] \tag{3.38}$$

$$\dot{p_B} = \frac{1}{C_{H,B}}\left[-Q_{1,B} + Q_{B,LP,check} - Q_{B,relief} + Q_{2,B} + Q_{3,B} - Q_{HP,check} - Q_{B,flushing}\right] \tag{3.39}$$

$$\dot{p_{HP}} = \frac{1}{C_{H,HP}}\left[Q_{HP,check} - Q_{enab}\right] \tag{3.40}$$

$$\dot{p_{LP}} = \frac{1}{C_{H,LP}}\left[Q_{CP} - Q_{CP,relief} + Q_{cooler,check} - Q_{LP,check} + Q_{A,relief} + Q_{B,relief}\right] \tag{3.41}$$

$$\dot{p_{flushing}} = \frac{1}{C_{H,LP}} \left[Q_{A,flushing} + Q_{B,flushing} - Q_{cooler,check} - Q_{cooler,relief} \right] \tag{3.42}$$

$$\dot{\omega_{wheel}} = \frac{1}{J_w} \left(T_{app} + (F_D + F_g + F_r r) \cdot r_{dyn} \right) \tag{3.43}$$

Where Q_i represents the inflow and outflow from various components into the hydraulic lines, p_i is the pressure in the lines due to the flows and C_H is the capacitance in the lines. $Q_{1,A}$, $Q_{A,LP,check}$, Q_{enab} are the flows between the line A from unit 1, LP system and HP accumulator through the enabling valve respectively. $Q_{A,relief}$, $Q_{2,A}$, $Q_{3,A}$ and $Q_{A,flushing}$ are the flow interactions between line A through the relief valve, units 2 and 3 and through flushing valve respectively. Similarly, $Q_{2,B}$, $Q_{3,B}$, $Q_{B,LP,check}$ are the flows between line B from units 2 and 3 and the LP system through the check valve. $Q_{1,B}$, $Q_{B,relief}$, $Q_{HP,check}$ and $Q_{B,flushing}$ are the flows between line B to unit 1, relief valve, HP accumulator through the check valve and the flushing valve. Q_{CP} $Q_{cooler,check}$ are the flow interactions of charge pump and cooler with LP system.

These equations were used to formulate the state space model of the system. The state space is a mathematical representation of the system. The general form of the state space is given in Equation (3.45).

$$\dot{\mathbf{x}} = A\mathbf{x} + B\mathbf{u} \tag{3.44}$$

$$\mathbf{y} = C\mathbf{x} + D\mathbf{u} \tag{3.45}$$

where $\mathbf{x}$ is a state vector, $\mathbf{u}$ is the input vector, $\mathbf{y}$ is the output vector A is the state or system matrix, B is the input matrix, C is the output matrix and D is the feedforward matrix. For the mode switching hybrid, the state and input vectors are as in Equation (3.46) and Equation (3.47).

$$\mathbf{x(t)} = \begin{pmatrix} \omega_{eng} & p_A & p_B & p_{HP} & p_{LP} & p_{flushing} & \omega_{wheel} \end{pmatrix}^T \tag{3.46}$$

$$\mathbf{u(t)} = \begin{pmatrix} u_{eng} & \beta_1 & \beta_2 & \beta_3 & u_{enab} \end{pmatrix}^T \tag{3.47}$$

The full scale non linear model was formulated based on state space. However, the state space was linearized in order to implement linear control theory while developing control strategies for the hybrid.

3.3.1 Linear System Model

There are certain assumptions that can be made in order to linearize the system. The linear model facilitates simplification of the nonlinear systems and enables the implementation of control strategies designed for linear systems.

The non linear model is first simplified to determine simple non linear equations to describe the system. While doing so, it was realized that the behavior of the HP accumulator was extremely nonlinear. Hence, the system was simplified only for the hydrostatic case in which the HP accumulator is disconnected from the system. The following are the assumptions made while simplifying the equations.

- The engine is operated at a constant speed and hence, eliminated from the state space.
- The LP system is assumed to deliver a constant pressure of 30 bar due to the presence of the LP accumulator and the charge pump.
- The LP system compensates for any loss of flow from the flushing valve. Thus, $Q_{LP,check}$ is taken equivalent to $Q_{flushing}$ for both lines A and B. Hence, the two flows in the pressure build up can be canceled out. Also, the flushing valve is connected to the LP system through a check valve. Any rise in pressure of flushing valve due to inflow results in flow transfer from the flushing line to the LP system. Hence, the flushing valve line is also maintained at a pressure of 30 bar.
- The flow from accumulator to line A is zero as the enabling valve is closed but there is flow into the accumulator from line B through the check valve during braking. Also, the enabling valve is always in closed position and hence, enabling valve input is deterministic.

- The relief valves act only as safety devices and during normal operation have no flow passing through them.
- The flow is equally distributed between units 2 and 3 and they are of equal sizes. The displacement of the two units is equal and hence, the flow from the two units is equal. Thus, the flows from units 2 and 3 can be combined into one flow term. Hence, $Q_{2,A} = Q_{3,A}$.
- The losses in the hydraulic units are only pressure dependent.
- The capacitance in the lines are considered as constants.
- The aerodynamic drag is derived as a function of wheel speed whereas the rolling resistance is accounted applying a factor to the applied torque at the wheels.

The simplified Equations are state as Equation (3.48).

$$\begin{pmatrix} \dot{p_A} \\ \dot{p_B} \\ \dot{p_{HP}} \\ \dot{\omega_{wheel}} \end{pmatrix} = \begin{pmatrix} \frac{1}{C_{H,A}} \left[Q_{1,A} - 2 \cdot Q_{2,A} \right] \\ \frac{1}{C_{H,B}} \left[-Q_{1,B} + 2 \cdot Q_{2,B} - Q_{HP,check} \right] \\ \frac{1}{C_{H,HP}} \cdot Q_{HP,check} \\ \frac{1}{J_w} \cdot T_{net} \end{pmatrix} \tag{3.48}$$

Based on the Equation (3.9), Equation (3.11), Equation (3.12), Equation (3.33), terms of Equation (3.48) can be written as follows:

$$Q_{1,A} = \frac{\beta_1 \cdot n_e \cdot V_1}{i_1} - (p_A - p_B) \cdot k_1 \tag{3.49}$$

$$Q_{2,A} = \beta_2 \cdot \omega_{wheel} \cdot V_2 \cdot i_{axle} + (p_A - p_B) \cdot k_2 \tag{3.50}$$

$$Q_{1,B} = \frac{\beta_1 \cdot n_e \cdot V_1}{i_1} + (p_A - p_B) \cdot k_1 \tag{3.51}$$

$$Q_{2,B} = \beta_2 \cdot \omega_{wheel} \cdot V_2 \cdot i_{axle} - (p_A - p_B) \cdot k_2 \tag{3.52}$$

$$Q_{HP,check} = (p_B - p_{HP}) \cdot k_{HP} \tag{3.53}$$

$$T_{net} = 2 \cdot \frac{\beta_2 \cdot (p_A - p_B) \cdot V_2}{2\pi \cdot i_{axle}} \cdot k_{rr} - \omega_{wheel} \cdot k_f - \omega_{wheel} \cdot k_d \cdot r_{dyn}^2 \tag{3.54}$$

where k_1 and k_2 are the coefficient of loss in units 1 and 2. i_1 is the gear ratio between the engine and unit 1 and and i_{axle} is that between unit 2,3 and wheels. k_{rr}, k_f and k_d are the coefficients to account for rolling resistance, frictional losses between units 2 and 3 and wheels and aerodynamic drag.

Using the simplified nonlinear state space, the model is linearized as in Equation (3.55). While doing so, the pressure terms were combined to form one pressure differential term.

$$\begin{pmatrix} \dot{\Delta p} \\ \dot{p_{HP}} \\ \dot{\omega_{wheel}} \end{pmatrix} = A \cdot \begin{pmatrix} \Delta p \\ p_{HP} \\ \omega_{wheel} \end{pmatrix} + B \cdot \begin{pmatrix} \beta_1 \\ \beta_2 \end{pmatrix} \tag{3.55}$$

These equations can be further simplified based on the mode of operation.

The matrices A and B can be determined by taking the Jacobian of the non linear equations. The details are mentioned in the appendix A.

3.4 Simulation Results

Using the models of the individual components and the state space of the system, a high fidelity model was developed in Matlab-Simulink environment. In reality, the inputs are in terms of accelerator pedal and brake pedal positions which are translated to displacement of the units using control strategies. However, without developing control strategies, the only way to test the model was to define the inputs in terms of displacements of the units. A profile was generated for the displacements of the hydraulic units to simulate acceleration, deceleration and braking scenario. The displacements inputs were as defined in Figure 3.4.

As seen in Figure 3.4, the block labeled (1) represents acceleration, (2) shows constant speed, (3) shows deceleration and (4) shows braking. In acceleration, the part (A) represents acceleration case with variable displacement unit 1 and fixed displacement units 2 and 3

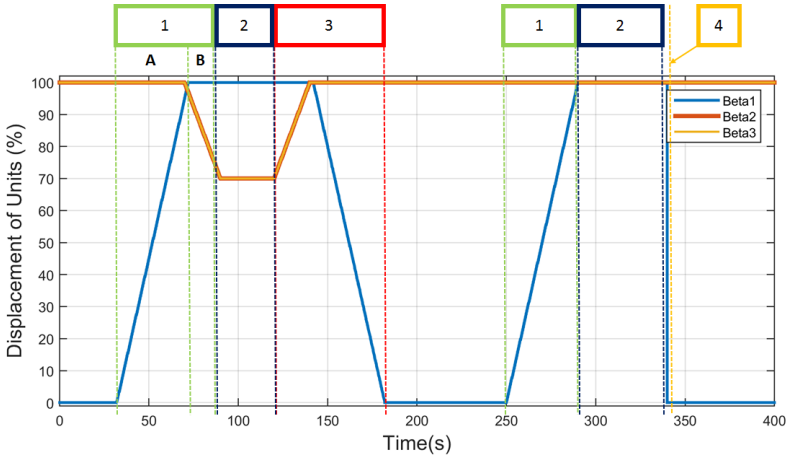

Figure 3.4. : Simulation Results: Predefined Inputs as Displacement of Hydraulic Units.

while part (B) demonstrates a fixed displacement unit 1 and variable displacement units 2 and 3. The engine was maintained at a constant speed of 2500 rpm. The results of these inputs are shown in terms of pressures in the different lines and vehicle velocity in Figure 3.5 and 3.6.

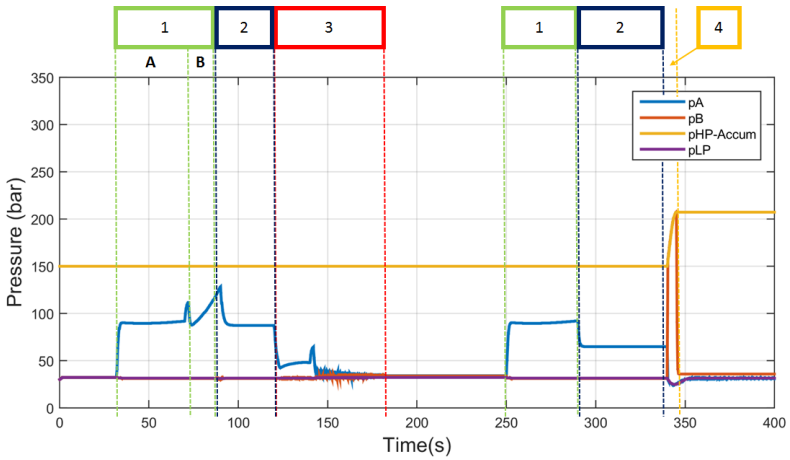

Figure 3.5. : Simulation Results: Pressures.

As shown in the figures, acceleration, deceleration and braking events are simulated. Initially, the displacement of units 2 and 3 is 100% and that of unit 1 is zero which indicates that the vehicle is at rest. as unit 1 displacement is increased, the pressure in line A increases and the vehicle starts moving. This is the case for a variable displacement pump and fixed displacement motors. When unit 1 reaches 100%, further increase in speed is obtained by

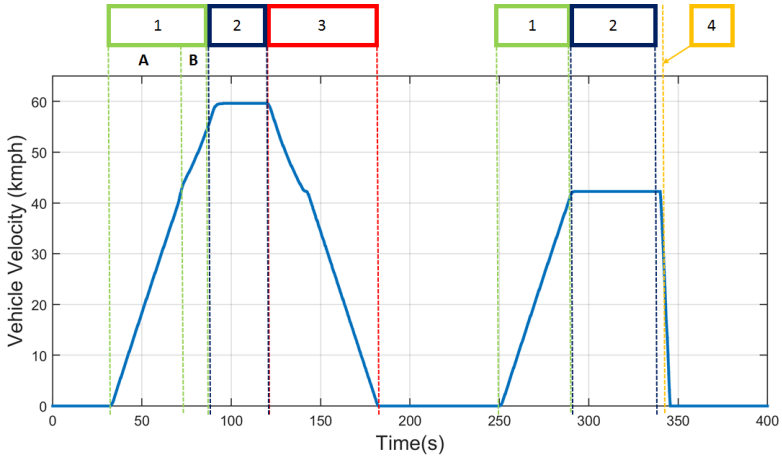

Figure 3.6. : Simulated Results: Vehicle Velocity.

decreasing the displacement of units 2 and 3. In this case, the pump displacement is kept at 100 % and motor displacements are varied. Next, the unit 2 and 3 is brought back to 100% and the unit 1 displacement is decreased to reduce the vehicle speed. In the second part of the cycle, after accelerating the vehicle using just unit 1, braking is achieved by commanding unit 1 to be zero. During braking, the pressure switches sides with increase in line B pressure. As the line B pressure exceeds the pressure in HP accumulator, hydraulic fluid flows into the accumulator. Thus, brake energy is stored and the pressure of the accumulator rises. Thus, the simulations demonstrate the working of the mode-switching hybrid. The results with the inputs as accelerator and brake pedal position would be discussed in Chapter 6 after developing control strategies.

Thus, this chapter summarizes the system modeling of the mode-switching hybrid. The models for each of the components are integrated in a high fidelity system model using Matlab-Simulink. The results of the simulation model for pressures and vehicle velocity have been discussed for predefined inputs for displacements of hydraulic units.

4. VEHICLE PROTOTYPE IMPLEMENTATION

The focus of this thesis was to test the drivability of the mode-switching hybrid. With this in mind, it was necessary to develop a working prototype of this transmission and implement it on an on-road vehicle.

4.1 Prototype Vehicle

A 1999 Range Rover 4.0 SE by Land Rover was selected as a prototype vehicle. Figure 4.1 shows the vehicle donated to the Maha Fluid Power Research Center. This prototype vehicle has a 4.0 liter V-8 engine with an automatic transmission and an all time four wheel drive functionality. The automatic transmission in the conventional design of this vehicle has four gear ratios and a lock-up clutch on the torque converter. The fuel consumption on this vehicle has been recorded to be 12 mpg and 15 mpg for city and on-highway driving respectively, U.S. Department of Energy (2015). Some of the important parameters of the vehicle are shown in Table 4.1.

Figure 4.1. : Vehicle Prototype: 1999 Range Rover 4.0 SE.

Table 4.1. : Range Rover 4.0 SE Parameters.

Parameter	**Value**	**Parameter**	**Value**
Max Power	142 kW @ 4750 RPM	**Max Torque**	320 Nm @ 2600 RPM
Gross Vehicle Mass	2780 kg	**Axle Ratio**	3.54:1
Rolling Radius	0.358 m	**Frontal Area**	2.78 m^2
Drag Coefficient	0.4	**Fuel**	Gasoline

Some of the parameters like rolling resistance, aerodynamic drag and engine torque curve were not known and were derived either empirically or experimentally, (Bleazard 2015).

4.2 Sizing of the Components

The sizing of the transmission plays a crucial role for ensuring good fuel economy as well as drivability in terms of performance. Initially the sizing of the components while implementing the transmission on prototype was done for the blended hybrid transmission. However, due to practicality and based on the operating conditions, the same sizing is used for mode-switching hybrid. While sizing the transmission, it was observed that the transmission that was designed for maximizing the fuel economy of the vehicle, did not necessarily perform well under all driving conditions. Hence, it was evident that the transmission had to be sized keeping in mind the fuel economy as well as the performance of the vehicle. Before sizing the components, baseline measurements were determined on the existing vehicle for fuel consumption and performance in terms of acceleration of the vehicle, (Bleazard 2015).

A new sizing methodology that combines the optimal sizing for efficiency obtained using dynamic programming and sizing for maximum performance obtained from dynamic simulations was used, (Bleazard et al. 2015). However, static sizing is initially performed in order to get an estimate on the size of the components. Based on static sizing, a range of sizes of different components was established and a parametric study was conducted for 735 designs. Firstly, dynamic programming was used to eliminate the effect of the controller in order to analyze the transmission for efficiency. For this study, the designs were evaluated using a UDDS cycle. Next, all the 735 designs were evaluated for performance

using dynamic simulations. In this case, the designs were evaluated based on a 20 second acceleration cycle with the engine running at its maximum power point and accumulator fully charged. All the designs with performance below the baseline were discarded.

The results from the two methods were plotted using a pareto front which is a graphical representation for optimizing quantities with opposing objective functions. The scaled performance was plotted on the x-axis and the scaled efficiency on y-axis. The scaled efficiency was calculated by setting the least efficient design to a value of zero and most efficient to one. The acceleration performance was scaled based on the baseline performance. The performance results for each run were integrated to the total distance traveled in 20 seconds and the baseline measured distance was subtracted from this value. It was then scaled such that one indicated the best performing transmission, zero was performance equivalent to the baseline and a negative value indicated performance lower than the baseline. Thus, the actual sizing was the product of the combination of the results obtained from the dynamic programming and the dynamic simulations. The blending of the results for efficiency and performance resulted in a design that was highly efficient and met the performance criteria under all conditions, (Bleazard et al. 2015).

4.2.1 Combined Results for Different Unit 1 Sizes

Figure 4.2 shows the pareto distribution of the efficiency against performance for different unit 1 sizes. The distribution clearly indicates that the size of the unit largely influences the performance of the transmission. The smaller units accelerate the vehicle slower than the larger units. There is no significant trend in the efficiency and it is influenced by other factors of the transmission. However, an increase in the performance results in a decrease in the efficiency.

4.2.2 Combined Results for Different Unit 2 and 3 Sizes

Figure 4.3 shows the pareto front for different unit 2 and 3 sizes. As seen in the graph, there is a significant contribution of the units to efficiency. Smaller units result in a higher system efficiency. But the smaller units are not able to meet the performance requirements.

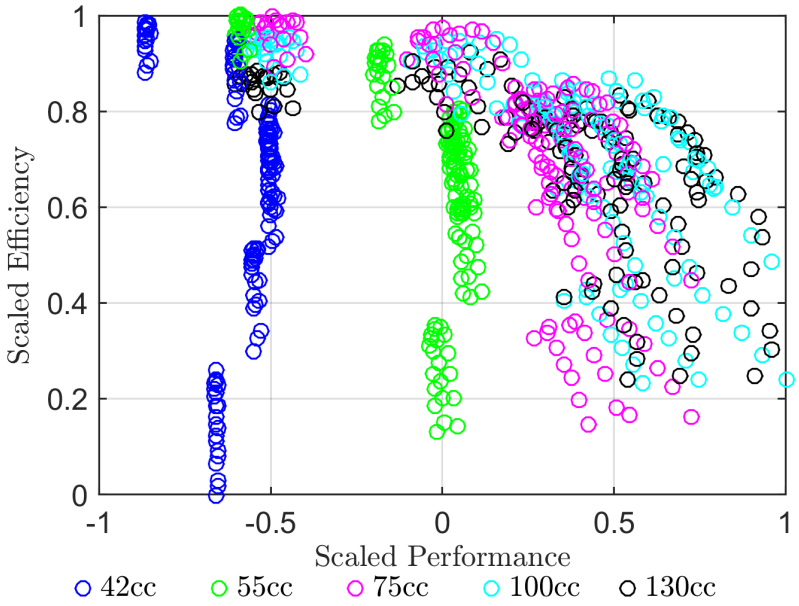

Figure 4.2. : Combined Efficiency and Performance Showing Unit 1 Trends, (Bleazard et al. 2015).

The performance criteria is met only using larger unit 2 and 3 with a larger unit 1. Also, from the graph it is seen that 55 cc/rev units are highly efficient and meet the performance of the base vehicle. However, this is misleading. The 55 cc/rev units accelerate slower than the measured acceleration at the beginning of the cycle and at a later stage accelerate faster. Thus, they average out to give the same performance as the base. Also, while selecting the components, it is important to make sure that the transmission is able to accelerate faster at low speeds too.

4.2.3 Combined Results for Different HP Accumulator Sizes

Figure 4.4 shows the pareto front for different HP accumulator sizes. The figure clearly indicates that the accumulator size has no significant effect on the efficiency but a larger accumulator increases the performance due to larger amounts of energy stored in it. It is to be noted that the increase in the weight on using a larger accumulator has not been incorporated in the model. Also, for transmissions with low performance, the accumulator size does not influence the performance and efficiency. This is because the size of unit 1

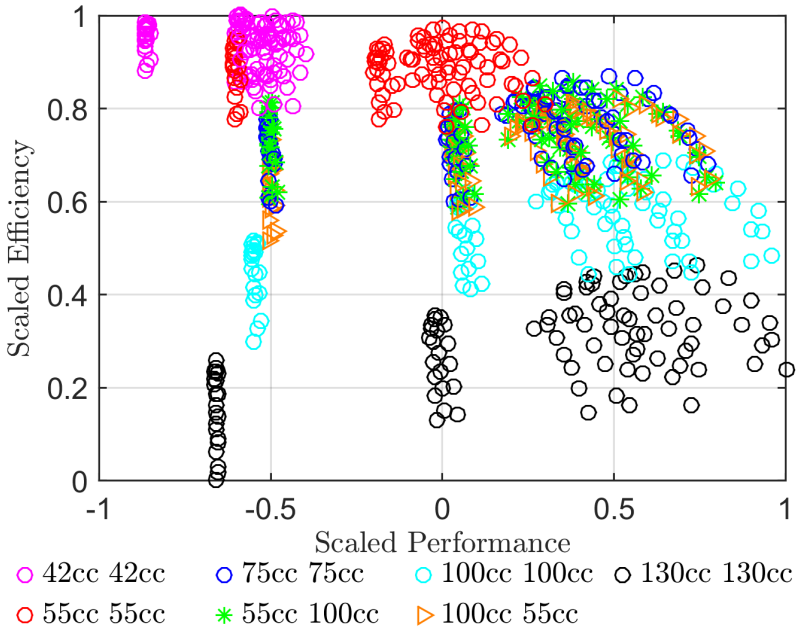

Figure 4.3. : Combined Efficiency and Performance showing Unit 2 and 3 Trends, (Bleazard et al. 2015).

is small and cannot extract all the power available from the engine. Thus, units 2 and 3 operate at high pressures (nearly 450 bar) to extract as much power from the engine as possible to meet the torque demand at the wheels and the accumulator remains unused.

4.2.4 Combined Results for Different Minimum Pressure of the HP Accumulator

Figure 4.5 shows the pareto front for different minimum pressures of HP accumulator. The trend showed that for a given size of the hydraulic units, higher efficiency is obtained at 120 and 90 bar. For lower performing transmission, the accumulator minimum pressure is insignificant as the accumulator remains unused. However, it has been shown by Bleazard that 144 bar is the minimum pressure that yields maximum energy density, (Bleazard 2015). However, in the dynamic simulations, the accumulator never falls upto the minimum pressure and hence is unable to release all the stored energy. Thus, the minimum pressure of the accumulator should be based on the minimum pressure that would fully load the engine. This enables the transmission to extract all the engine power as well as use the

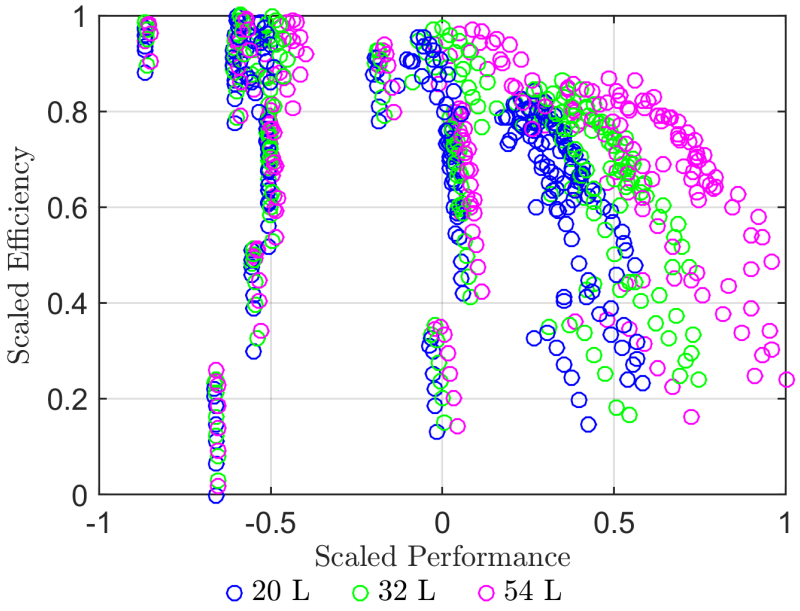

Figure 4.4. : Combined Efficiency and Performance Showing Trends in Accumulator Size, (Bleazard et al. 2015).

accumulator energy. But the performance will still be compromised as a higher minimum pressure will result in less energy being stored in the accumulator.

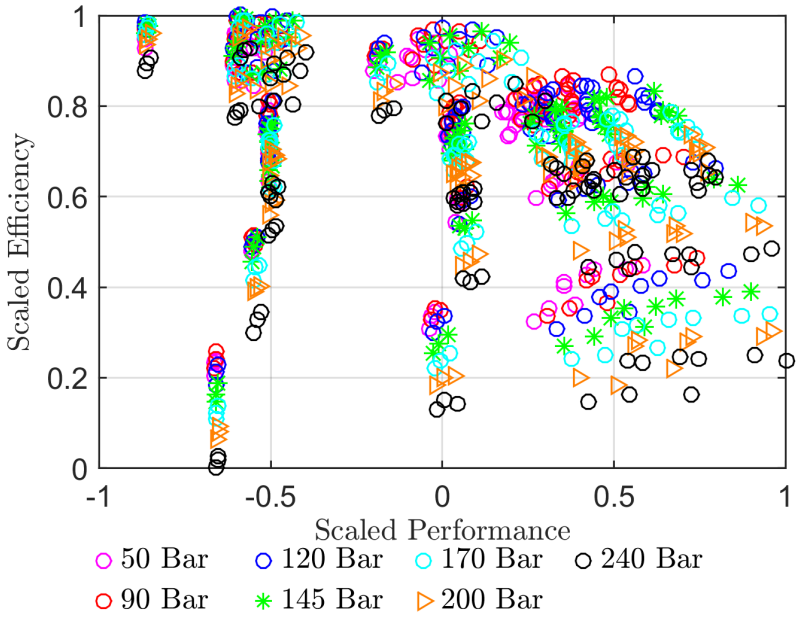

Figure 4.5. : Combined Efficiency and Performance Showing Accumulator Minimum Pressure Trends, (Bleazard et al. 2015).

The effect of the accumulator minimum pressure and unit 1 size on the performance is reflected in Figure 4.6. Each simulation ensured a constant unit 2 and 3 size of 75 cc/rev and HP accumulator of 32 liter. The figure plots the minimum pressure needed to load unit 1 on x-axis and the scaled performance on y-axis for different unit 1 sizes. From the figure it is clear that the smaller units resulted in high system pressure to attain maximum performance which consequently resulted in the HP accumulator being unused. Hence, minimum pressure of the accumulator did not have any impact on the performance. Larger the unit 1, the performance shows a peak at the pressure needed to load the engine fully. Thus, the peak is at a higher pressure for 75 cc/rev than 130 cc/rev unit. After a limit, the unit sizes are largely affected by losses and the minimum pressure falls below that corresponding to the pressure that attained maximum energy density. This is due to lower amount of energy stored in the accumulator if the minimum pressure is lowered. This is reflected in the curves for 100 cc/rev and 130 cc/rev. The 100 cc/rev shows higher performance than 130 cc/rev as the losses are greater in the later. Thus, performance is highly influenced by the minimum pressure of the accumulator.

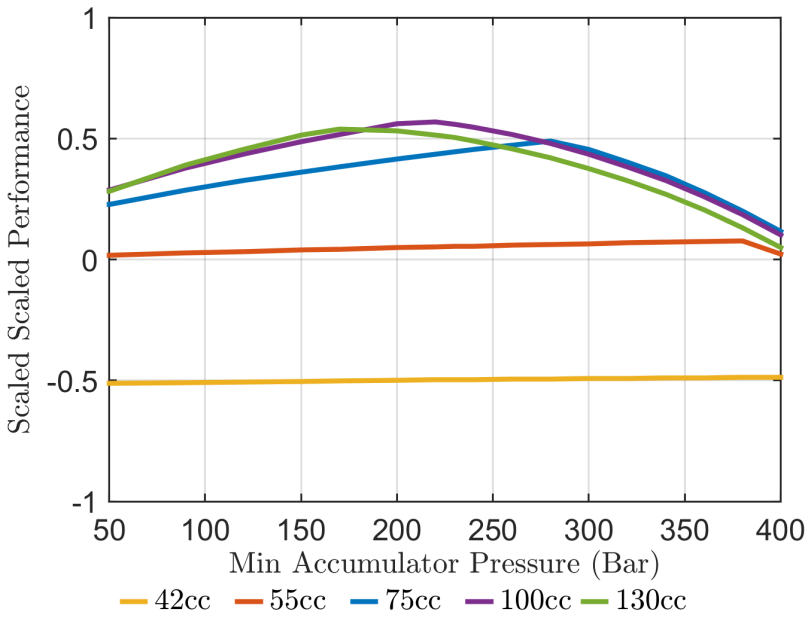

Figure 4.6. : Scaled Performance according to Minimum Pressure and Unit 1 Size.

From the results, it can be concluded that units 2 and 3 play a significant role in the efficiency of the transmission while unit 1 interacts with units 2 and 3 to optimize the

efficiency. The 100 cc/rev unit shows better efficiency on an average but the efficiency is the highest with smaller units. The accumulator size is not very influential but the efficiency is slightly better with a larger accumulator. Though the size of accumulator doesn't affect the performance, the minimum pressure does. The lower the minimum pressure, the higher is the efficiency except at the pressure that were below the pressure required for braking. This was due to the loss of energy from the friction brakes.

The performance of the transmission is greatly influenced by unit 1 size which should be large enough to extract all the power available at the engine. The other two units are influential at lower speeds when the engine is capable of providing more power than units 2 and 3 can convert to provide to the wheels. The size of the HP accumulator affects the performance due to the amount of energy that it can store. Also, its minimum pressure has an impact on the performance. It should be greater than the pressure needed to fully load the engine.

Thus, the component selection based on the new sizing methodology has been summarized in Table 4.2.

Table 4.2. : Component Sizes Using New Sizing Methodology.

Component	**Size**
Unit 1	100 cc/rev
Unit 2 and 3	75 cc/rev
HP Accumulator Volume	32 liter

4.3 Selection of Components

Based on the results obtained using the new methodology for sizing of components, the components were selected for the hybrid. Also, along with the major components like hydraulic units and HP accumulator as described in the previous section, many other secondary components were to be designed or customized in order to build a fully functional prototype.

4.3.1 Hydraulic Units

Based on the results of the sizing, the hydraulic units were selected for higher efficiency and performance. The details of the units are mentioned in Table 4.3.

Table 4.3. : Hydraulic Units Selected For Range Rover.

Unit	**Model**	**Size**	**Max Pressure**	**Max Speed**
Unit 1	Danfoss S90	100 cc/rev	450 bar	3650 rpm
Unit 2	Danfoss S90	75 cc/rev	450 bar	3950 rpm
Unit 3	Danfoss S90	75 cc/rev	450 bar	3950 rpm

4.3.2 Gear Box

A gear box is used between the engine and unit 1. This is to enable unit 1 to operate at a lower speed. Though this resulted in a larger unit, operating at lower speeds reduces the noise from the unit. The gear box used in the Range Rover was donated by Durst with specifications as shown in Table 4.4.

Table 4.4. : Gear Box Selected for Range Rover.

Manufacturer	**Model**	**Ratio**	**Max Power**	**Max Input Torque**
Durst	1PD06	1.48	396 kW	1414 Nm

4.3.3 HP and LP Accumulators

A 32 liter HP accumulator was donated by Hydac. The weight of the accumulator was a major concern. Thus, a light weight accumulator which was wrapped in kevlar was selected for the Range Rover. The accumulator gas volume was filled with foam. This was to avoid the transfer of heat from the gas to the accumulator shell and finally to the atmosphere when the accumulator pressure increases. An accumulator without the foam can also experience

a drop in pressure as the gas cools down due to this heat transfer. Thus, the foam acts as an insulator and prevents the pressure and temperature drop in the accumulator. Table 4.5 gives the specifications of the HP accumulator chosen for the Range Rover.

Table 4.5. : High Pressure Accumulator Specifications.

Nominal Volume	**Dry Weight**	**Maximum Pressure**	**Pre-charge Pressure**	**Length**	**Diameter**
32 L	71 kg	500 bar	150 bar	1422 mm	227 mm

During the braking event, the pressure switches line and the units 2 and 3 operate as pumps. In this process, they pump fluid into line B. However, unit 1 is at zero displacement. The flow required by units 2 and 3 is provided by the low pressure system. Thus, an LP accumulator is designed accordingly. The size of LP accumulator is different from that of HP accumulator as the size and the minimum pressure of the accumulator affect the amount of energy stored and the performance of the accumulator. Using Equation (3.15) with a precharge pressure of 14.5 bar and maximum pressure of 30 bar, the LP accumulator volume can be evaluated. Thus, a 38 liter accumulator is needed to store 16.3 liters of hydraulic fluid. Hence, a 42 liter accumulator manufactured by Hexagon Lincoln and made of carbon fiber is selected. The specifications of the LP accumulator are mentioned in Table 4.6.

Table 4.6. : Low Pressure Accumulator Specifications.

Nominal Volume	**Dry Weight**	**Maximum Pressure**	**Pre-charge Pressure**	**Length**	**Diameter**
42 L	– kg	350 bar	14.5 bar	880 mm	274 mm

4.3.4 Charge Pump

The charge pump is a part of the LP system. It provides flow in order to compensate for the losses occurring in the hydraulic units as well as provide flow to the control system.

The charge pump was sized based on the dynamic simulations of the mode switching hybrid for an aggressive cycle. The size was selected such that LP system does not drop below 15 bar and does not cavitate. The maximum demand for the charge pump is during braking as the charge pump along with the LP accumulator supply flow to units 2 and 3. The specifications for the charge pump are as in Table 4.7.

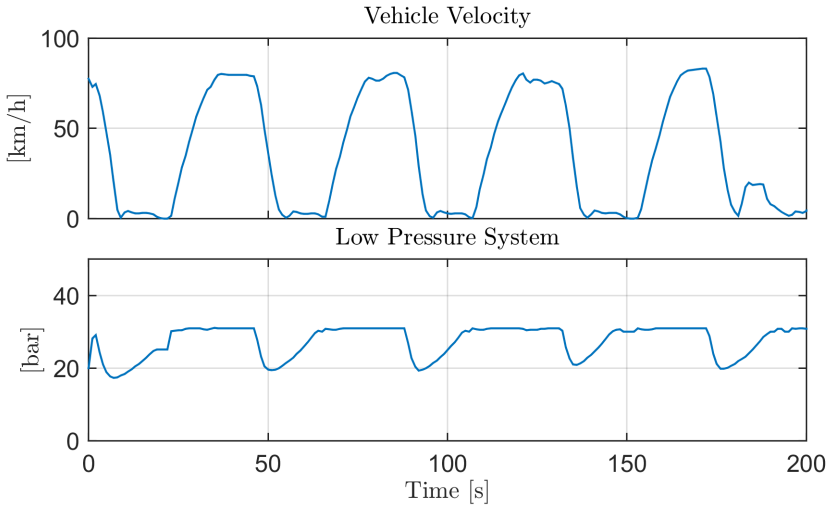

Figure 4.7. : Pressure of LP system with 26.4 cc/rev Charge Pump, (Bleazard 2015).

Table 4.7. : Charge Pump Specifications.

Manufacturer	**Model**	**Displacement**	**Max Pressure**	**Max Speed**
Casappa	Polaris 20-25	26.4 cc/rev	210 bar	2500 rpm

4.3.5 Reservoir

The purpose of the reservoir is to release entrained air in the hydraulic oil, help in cooling the oil, hold the oil that is drained from the accumulator and provide flow to the charge pump. Equation (4.1) is used to calculate the size of the reservoir.

$$\text{Res}_{vol} = \sum V_i \tag{4.1}$$

Where V_i represents the volume of each component. Using the equation, the size of the reservoir was evaluated to be 70 liters and hence, considering a safety factor, 80 liter tank was selected.

4.3.6 Cooler

All the components in the system like hydraulic units, hoses, valves, etc. are subject to losses which get converted to heat. It is necessary to dissipate this heat. The cooler was selected based on the power loss calculated using dynamic simulation, (Bleazard 2015). The specifications of the cooler are as in Table 4.8.

Table 4.8. : Oil Cooler Specifications.

Manufacturer	**Model**	**Heat Rejection @ 37.8 °C ETD**	**Max Pressure**	**Max Temperature**
AKG	D20-12	15 kW @ 100 l/min	26 bar	121 °C

The cooler as installed in the Range Rover is shown in Figure 4.8.

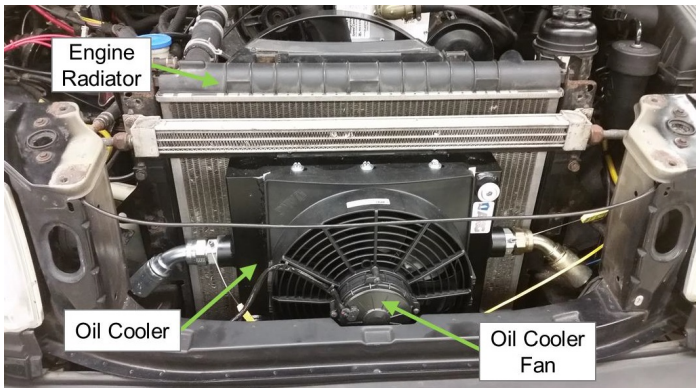

Figure 4.8. : Packaging of Cooler in Range Rover.

4.3.7 Filter

The filter was installed in order to prevent any contamination from damaging hydraulic units and valves. The charge pump is the source of flow into the system. Thus, the filter was placed after the charge pump to ensure that only clean fluid enters the system. The specifications of the filter are shown in Figure 4.9.

Table 4.9. : Filter Specifications.

Manufacturer	**Flow Rate**	**Filter Size**	**Max Pressure**
Parker	75 l/min	10 micron	34 bar

4.4 Packaging Architecture and Design

Before implementing the transmission on the Range Rover, a packaging architecture was designed using 3D CAD modeling. This was initiated in order to optimize the limited space available in the under body of the vehicle to fit all the components of the new architecture as shown in Figure 4.9.

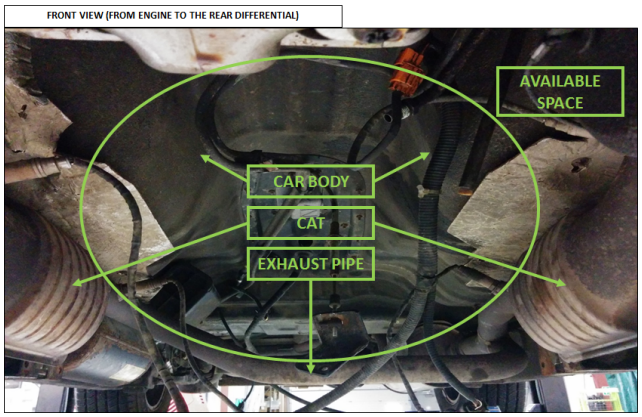

Figure 4.9. : Limited Space Available in the Under Body of Range Rover.

4.4.1 Subassembly: Gear Box, Unit 1 and Charge Pump

Packaging and designing the coupling of engine to unit 1 and charge pump was a major challenge. In the original automatic transmission, the engine flywheel was coupled to a flex plate and torque converter to which the transmission is mechanically coupled. The engine block was coupled to automatic transmission through bell housing. In the mode-switching hybrid, this bell housing was modified so that engine output could be coupled to the gear box and unit 1 and the charge pump. The CAD as well as the custom manufactured bell housing are shown in Figure 4.10.

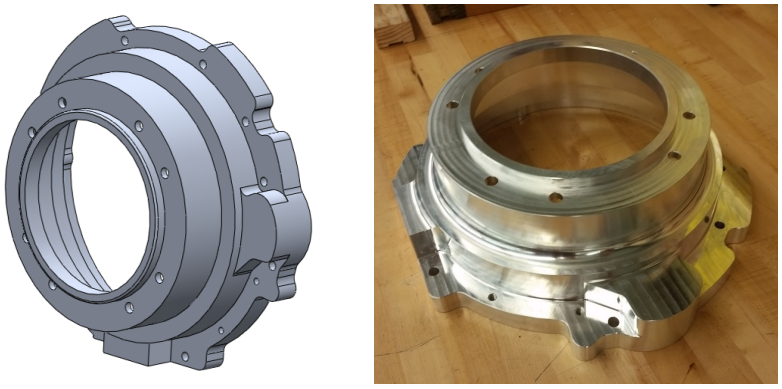

(a) Bell Housing Design.

(b) Manufactured Custom Bell Housing.

Figure 4.10. : Bell Housing Design.

The next portion of the subassembly was to couple the gear box to engine output. A custom adapter plate and pre-manufactured flex plate were used to couple the flywheel to the splined shaft of gear box. In order to utilize the adapter as a speed feedback to engine, 60 teeth were machined on its perimeter and used a pick-up by hall effect sensor. The plate was dynamically balanced for safety reasons. Next, unit 1 was connected to the gear box using the exiting pump mounting pad. However, to mount the charge pump on to unit 1, a custom adapter plate is designed. The custom mounting has slots for O-ring on both sides to prevent leakage and also align the components. Figure 4.11 shows the exploded view of the subassembly.

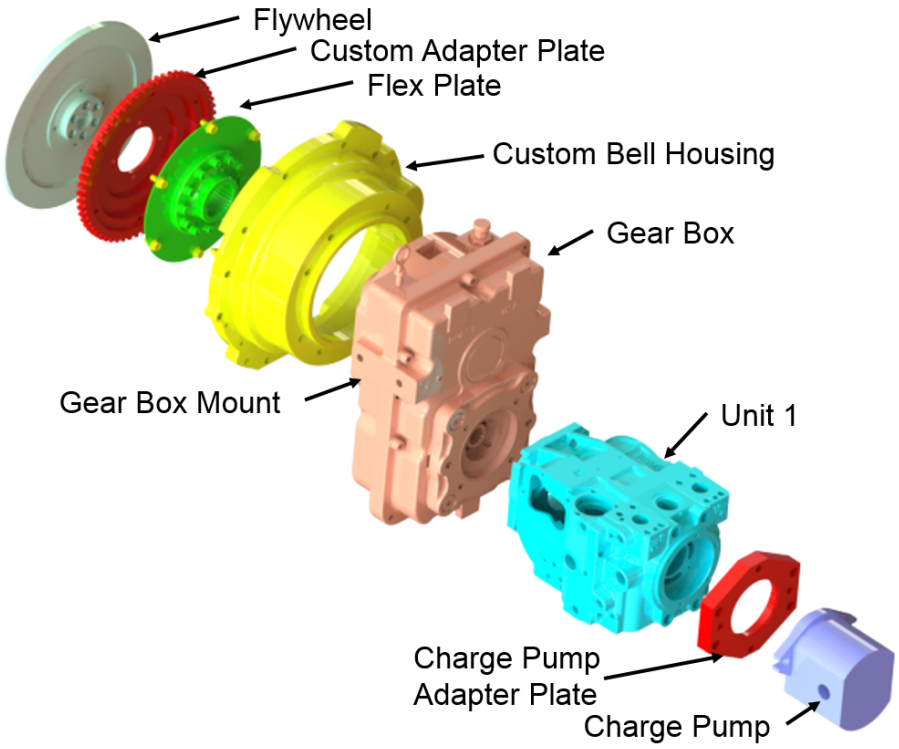

Figure 4.11. : Exploded View of Engine Flywheel to Unit 1 Subassembly.

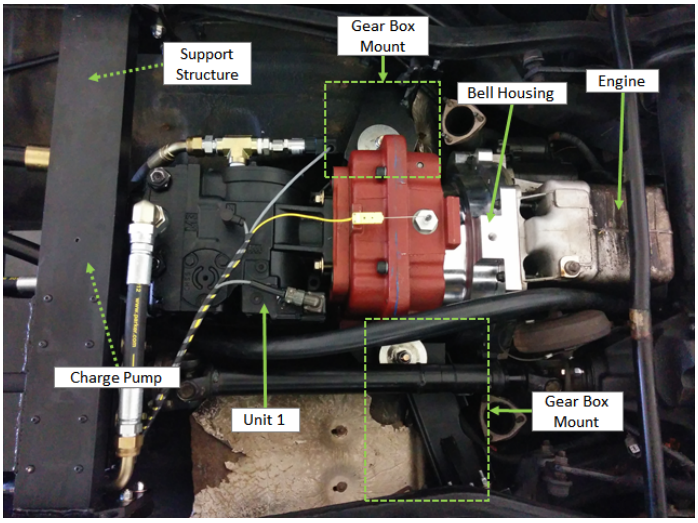

Figure 4.12. : Install of Unit 1 Assembly.

Table 4.10. : Unit 2 and Unit 3 Vibration Isolator Specifications.

Manufacturer	**Model**	**Type**	**Max Load**	**Spring Rate**
LORD	LM-CB-1180-1	Center Bonded	400 lbs	2963 lbs/in

The engine is mounted in the vehicle using two in-line mounts. These mounts hold the engine but do not restrict its rotation. Hence, unit 1 had to be mounted to the vehicle frame and engine face. For this, gear box mounts and vibration isolators were used to mount the subassembly. Figure 4.12 shows the way in which the subassembly is mounted to the frame. The charge pump is not visible in the figure due to tight packaging. Also, Table 4.10 gives the type of vibration isolators selected. The isolators help in reducing the vibrations that are transfered from the components to the vehicle frame.

4.4.2 Subassembly: Unit 2, Unit 3 and HP Accumulator

Installing unit 2 and 3 was a major challenge due to the space available and mounting constraints. A new frame was designed which consisted of C-channel to mount the units to the vehicle frame based on stress calculations. The C-channel facilitated a stiff structure and also helped in achieving a compact design to hold the units. The units were mounted on this

frame using custom designed adapter mounts. These two mounts were specially designed and manufactured. Vibration isolators were used to mount the units on to the C-channel and these isolators fit inside the C-channel mount without occupying extra vertical space. These isolators were different from the ones used to mount the first subassembly. This is due to the fact that at high pressures, the units can emit harsh vibrations. The specifications for the isolators are provided in Table 4.11. Also, the HP accumulator was mounted longitudinally to a structural member on the under side of the vehicle and frame for valve block using accumulator straps. This was the only possible option for accumulator mounting due to space constraints. Figure 4.13 shows the packaging design of this subassembly whereas Figure 4.14 shows the subassembly in the Range Rover.

Table 4.11. : Unit 2 and Unit 3 Vibration Isolator Specifications.

Manufacturer	**Model**	**Type**	**Max Load**	**Material**
ACE Controls	CM-US2-25-S	Cup Mount	250 *lbs*	Silicon

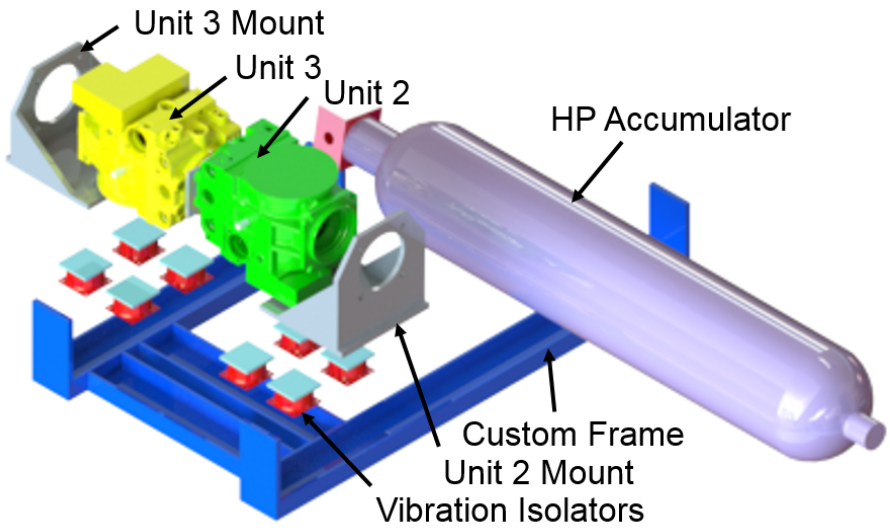

Figure 4.13. : Unit 2, Unit 3 and HP Accumulator Exploded View.

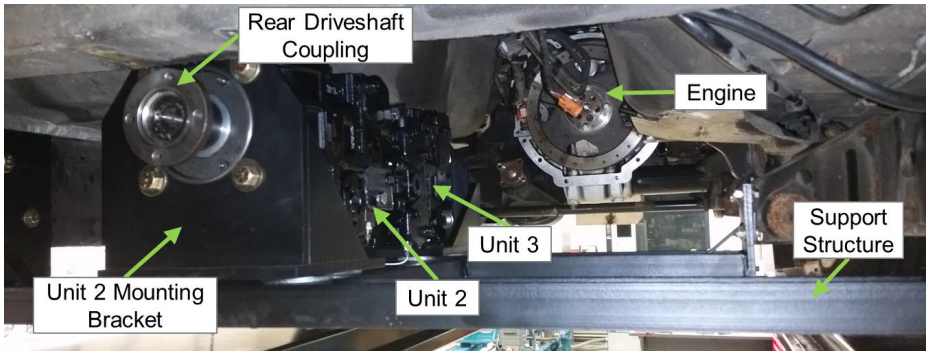

Figure 4.14. : Unit 2 and Unit 3 Installation.

4.4.3 Valve Block

The valve block was used to incorporate the check valves, the flushing valve and the enabling valve in a single unit. It resulted in a compact design, saved space, minimized complexity and probability of failure. It was donated by Sun Hydraulics. Figure 4.15 shows the valve block design as well as its position in the vehicle. As seen in the figure, the block was suspended on a frame mounted below the rear seats of the vehicle and vibration dampers were used to isolate the block and frame to prevent the transmission of pressure pulsations. While deciding the position of valve block, routing of hoses was considered in detail.

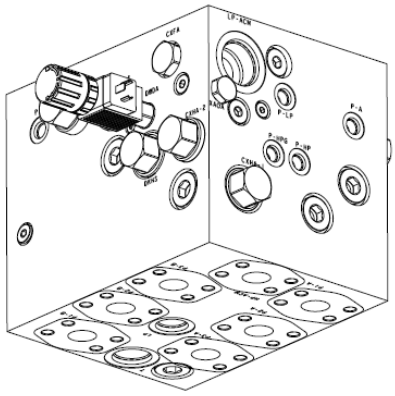

(a) Valve block design.

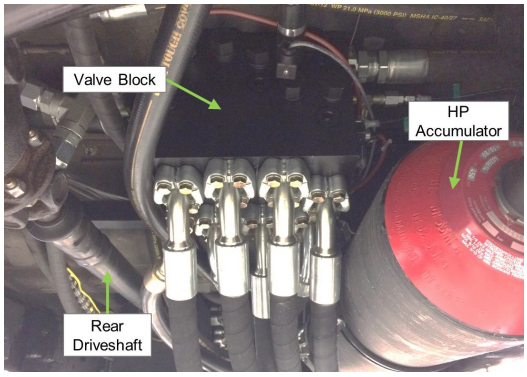

(b) Valve block installed in vehicle.

Figure 4.15. : Valve block design and installation in vehicle.

4.4.4 LP Accumulator

This was the only component that was not placed in the under body but in the boot of the vehicle behind the rear seats. Figure 4.16 shows the LP accumulator installed on the vehicle.

Figure 4.16. : Low pressure accumulator packaging.

4.4.5 Drive Shafts

Originally, the drive shafts coupled the output of the transfer case to the differentials. The length of the drive shafts was variable in order to account for the vertical motion caused by the suspension. The length of the drive shafts was redesigned in order to incorporate the mode switching hybrid in the Range Rover. unit 2 couples to the rear differential and unit 3 to the front. While doing so, the length of the drive shafts was modified. Also, a sliding mechanism was necessary to allow contraction and extension of the drive shaft in order to account for the vertical travel due to the suspension. This mechanism is well represented by Figure 4.17.

The new drive shafts were designed such that the front drive shaft had a minimum and maximum length of 25.5 inches and 27.5 inches respectively while the rear had 31 inches and 33 inches respectively. These lengths were smaller than the original ones. Thus, the new drive shafts were made by shortening the original shafts and were rebalanced. The modified drive shaft are in Figure 4.17(b) and 4.17(c).

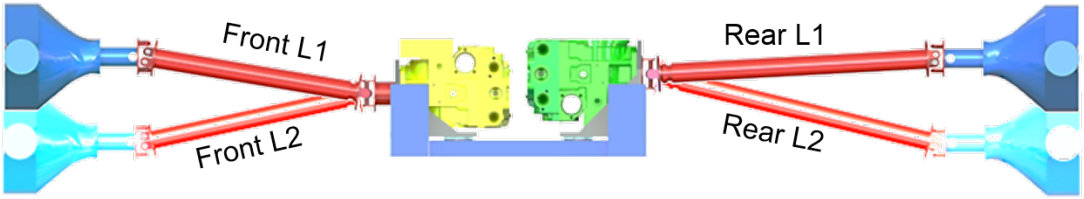

(a) Drive Shaft Packaging and Design.

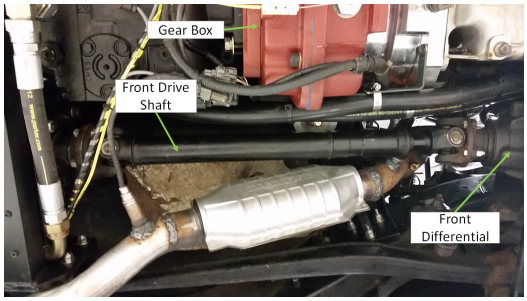

(b) Front Drive Shaft Installed in Vehicle.

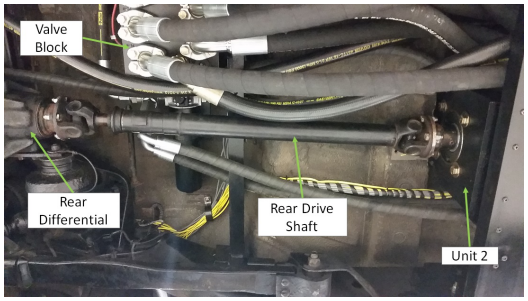

(c) Rear Drive Shaft Installed In Vehicle.

Figure 4.17. : Design and Installation of Drive Shafts.

4.4.6 Hydraulic Reservoir and Fuel Tank

According to the sizing calculations, an 80 liter reservoir was selected. A 5 gallon fuel tank was manufactured keeping in mind fuel measurements.The fuel tank used the original fuel pump and a no-drip quick disconnect fitting in order to minimize the loss of fuel while removing the tank for fuel consumption measurements. A special frame was manufactured to mount these two components below the car boot in space originally used for spare tire. Figure 4.18 these components outside the vehicle and after installation.

(a) Resevoir and Fuel Tank on Cradle. (b) Installed Resevoir and Fuel Tank.

Figure 4.18. : Oil Reservoir and Fuel Tank Assembly.

4.4.7 Final Assembly

The integration of all the components described in this chapter into a full scale CAD model helped in tackling the space constraints and in precise design of the components. Figure 4.19 shows the final CAD of the packaging architecture of the mode-switching hybrid. Figure 4.20 is the final architecture of the prototype.

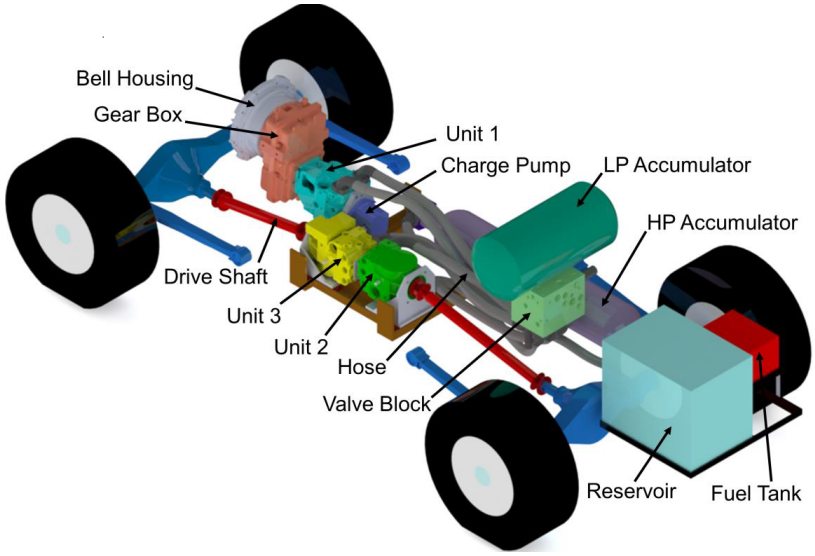

Figure 4.19. : Final Packaging Design of Mode-Switching Hybrid.

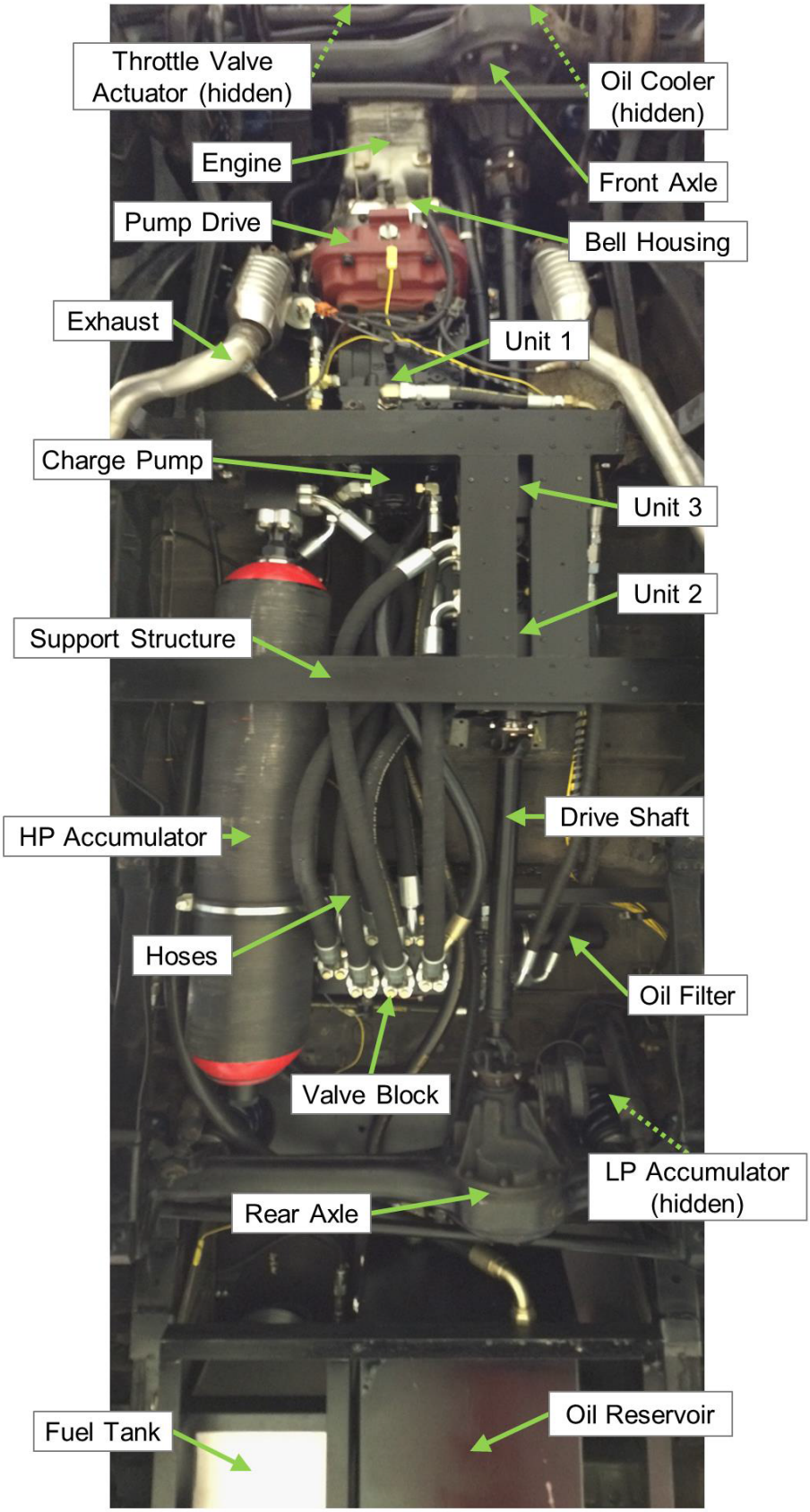

Figure 4.20. : Final Installation of Mode-Switching Hybrid.

4.5 Instrumentation

Once the packaging architecture was finalized, the next step was to install the different sensors in the vehicle. Some of these sensors are necessary in order to obtain feedback from the system and are to be included even in a production vehicle. However, some of the other sensors were installed just for academic purpose. The description of these sensors is given in Figures B.1 and B.2 in Appendix B.

4.5.1 Accelerator and Brake Pedal Inputs

The accelerator and brake pedal form the only two inputs that are controlled by the user. Based on the accelerator and brake pedal input, the behavior of the system is controlled. In the conventional system, the accelerator pedal is directly connected through a cable to the throttle body in the air intake system. Hence, the accelerator pedal controls the amount of air supplied to the engine and hence, the engine torque. Similarly, the brake pedal is also mechanically connected to the master cylinder. Thus, the accelerator and brake inputs result in acceleration and deceleration commands to the vehicle respectively.

However, in the mode-switching hybrid, no direct coupling of the accelerator and brake pedal to the system exists. The pedals inputs control the displacements of the units, enabling valve position, engine throttle and the original friction brakes to cause the required acceleration or deceleration. To sense the position of the accelerator and brake pedals, linear potentiometers were installed. The potentiometers are as shown in Figure 4.21 and their specifications are as in Table 4.12. Thus, there is no hard wire connection between the accelerator and engine throttle anymore. The brake pedal mechanism was redesigned to incorporate the regenerative braking.

Table 4.12. : Linear Potentiometer Specifications.

Manufacturer	**Model**	**Measurement Range**	**Resolution**	**Non-Linearity**
Sensor Connection	LPPS-100	100 mm	infinite	±0.08%

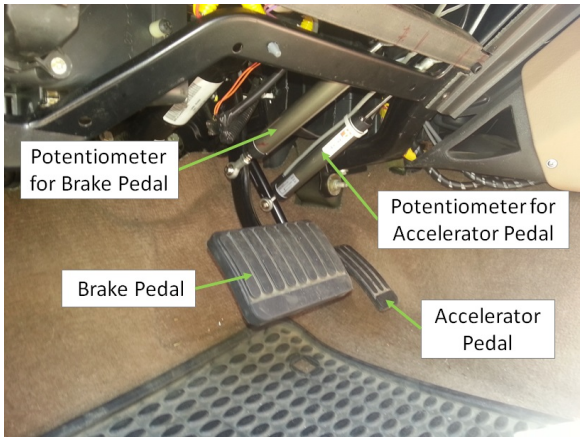

Figure 4.21. : Accelerator and Brake Pedal Assembly.

The brake system was redesigned to achieve regenerative braking during the initial pedal travel and later actuate the master cylinder to activate the friction brakes in case of aggressive braking. Thus, the braking is regenerative under most of the operating conditions and friction brakes act only when braking torque from regenerative braking is insufficient during extreme braking events. Friction brakes act as safety brakes in this case or when control pressure is lost and units no longer generate torque. In order to achieve this, the mechanical linkage connecting brake pedal to the master cylinder was modified. The original design as in Figure 4.22(a) consisted of a revolute joint. This was modified to a sliding joint in the new design as in Figure 4.22(b). Thus, when the brakes are applied using the new joint, the pedal travels through the slot. In this case, regenerative brakes are active and master cylinder is not actuated. As the brakes are applied further, the pedal reaches the end of slot and then actuates the master cylinder. Thus, now the braking action is due to regenerative as well as friction brakes. Figure 4.23 shows the old and the new braking mechanisms. The slot is designed such that the first 35 % of the brake pedal travel is purely regenerative. In case additional braking torque is required, the brake pedal needs to be pressed more than 35 %. The relationship between brake pedal position and master cylinder pressure is as shown in Figure 4.24.

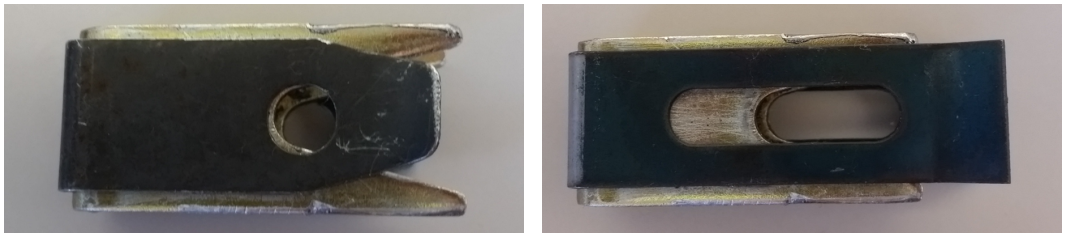

(a) Old linkage with revolute joint. (b) New linkage with sliding joint.

Figure 4.22. : Brake Pedal linkage Modification.

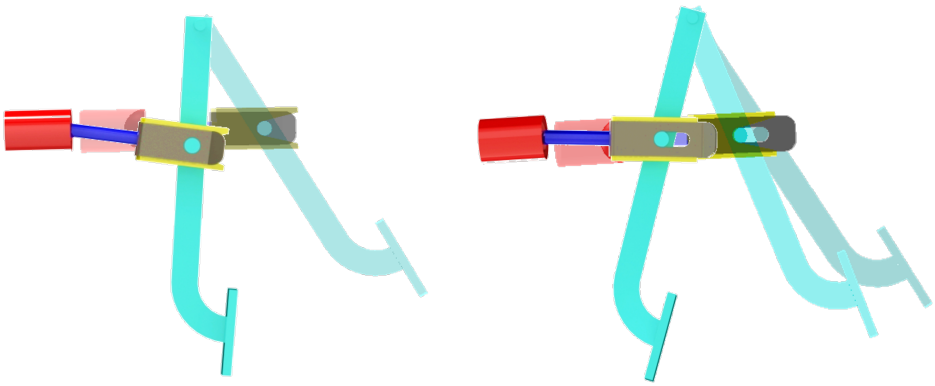

(a) Old Brake Pedal Operation. (b) New Brake Pedal Operation.

Figure 4.23. : Old and New Brake Pedal Assemblies and Operation.

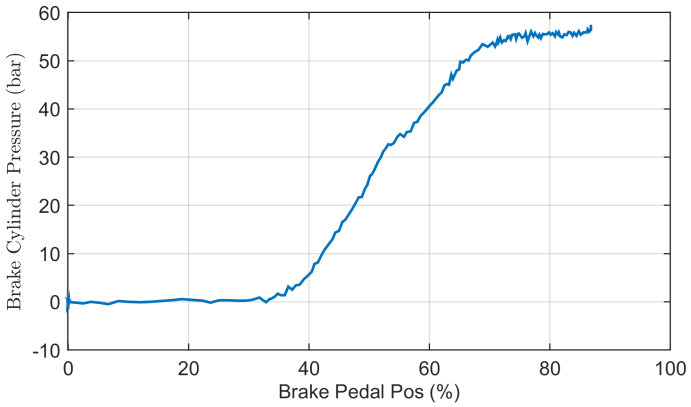

Figure 4.24. : Brake Pedal Position vs. Brake Cylinder Pressure.

4.5.2 Engine Speed Controller

In the conventional transmission, the engine speed is the result of the net torque generated by the engine after it overcomes the load and resistive torques at the wheel, the

transmission and the torque converter. The engine speed increases if the torque generated is higher than the load and resistive torques and decreases if the torque generated is lower than those torques. The torque generated depends on the driver input. The driver acts as a feedback and presses the accelerator pedal to increases the engine torque. But for continuously variable transmission, an engine speed can be selected based on a supervisory controller because the engine speed is now independent on the wheel speeds. This enables the implementation of power management strategies. Apart from this fact, the hybrid transmission not only supplies torque to the wheels from the engine but also from the accumulator. Hence, instead of controlling the engine torque with the accelerator pedal, a separate actuator is necessary which controls the engine speed.

The engine speed in mode-switching hybrid is controlled using a throttle actuator manufactured by Woodward as in Figure 4.25. The throttle actuator is an electric actuator with an integrated speed control and features like configurable start and stop behavior and integrated frequency counter that calculates the engine speed based on the flywheel position. Along with speed control, it has an option to control angular throttle position. The specifications of the actuator are as in Table 4.13.

Figure 4.25. : Engine Speed Controller and Actuator.

Table 4.13. : Engine Controller Specifications.

Manufacturer	Woodward
Model	ProAct ISC Model II
Voltage	18-32 V
Max Transient Power	251 W
Slew Rate	1000 deg/sec
Steady State Speed Band	0.5 % of rated

The engine speed controller was placed near the engine throttle and has a linkage between the shaft of the actuator and the throttle. This linkage extends the range of the actuator shaft from 0-75 deg to 0-90 deg of the engine throttle. Also, the pump for the AC unit had to be removed to fit the actuator. Figure 4.26 shows the block diagram of air intake system with the new actuator and Figure 4.27 shows the engine speed controller and the engine speed feedback sensor.

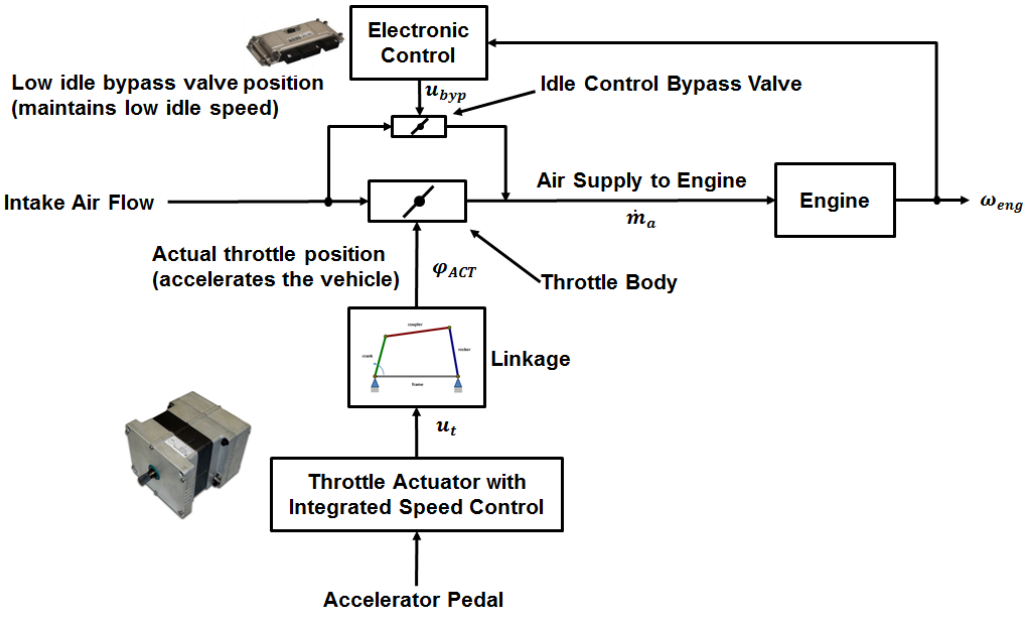

Figure 4.26. : Block diagram of Air Intake System.

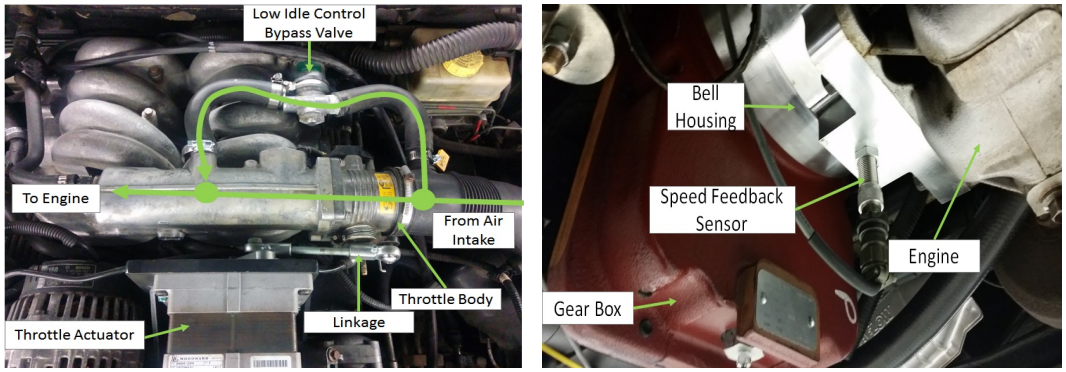

(a) Engine Speed Controller and Actuator. (b) Engine Speed Sensor Used for Feedback.

Figure 4.27. : Installed Engine Speed Controller and Speed Feedback Sensor.

A feedback sensor was used to feedback the actual engine speed to the controller. This was achieved using a magnetic pick up sensor which is installed at the bottom of the bell housing. The sensor outputs pulse every time a teeth of the custom adapter plate passes the sensor. Based on the error between the desired engine speed and the actual engine speed, a simple PI control strategy was used to control the engine speed. The control strategy in speed control mode is shown in Figure 4.28 whereas in throttle control mode is shown in Figure 4.29. Advance control strategies can be used to control the engine speed.

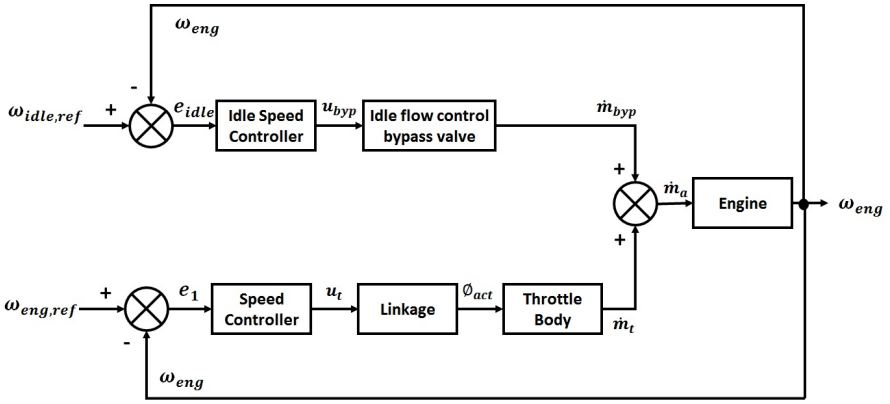

Figure 4.28. : Engine Speed Control Block Diagram.

Where $\omega_{eng,ref}$ is the reference engine speed which can be commanded using a supervisory control, $\omega_{idle,ref}$ is the reference speed of engine during idling and ω_{eng} is the actual engine speed. e_{idle}, e_1 are the errors between the actual engine speed and the idle engine

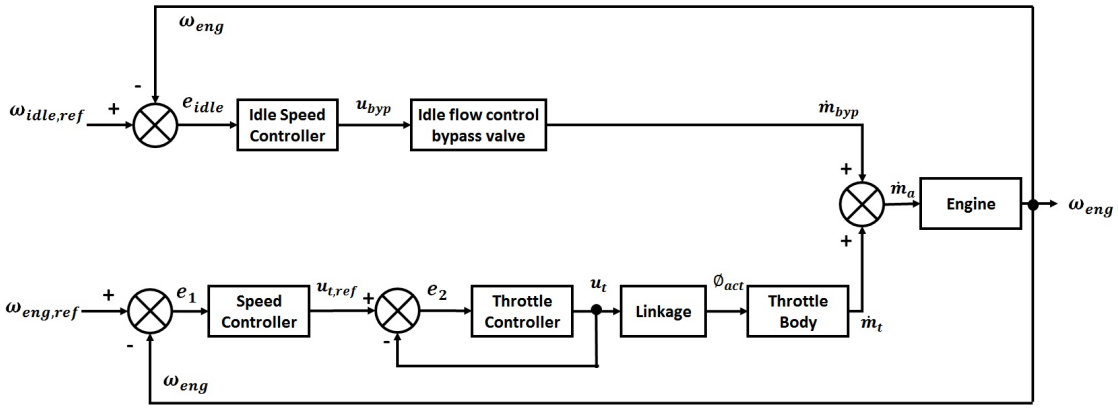

Figure 4.29. : Engine Throttle Control Block Diagram.

speed and engine reference speed respectively. e_2 is the error between the reference throttle input and commanded throttle input. u_t and $u_{t,ref}$ are the commanded and reference throttle input. u_{byp} is the input command for the bypass valve. ϕ_{act} is the actual angular throttle position. $\dot{m_{byp}}$, $\dot{m}_t$ and $\dot{m}_a$ are the mass flow rates of air from bypass valve, throttle body and total air flow rate going into the engine.

The throttle control mode gave greater flexibility in tuning the engine controller as compared to speed control mode. In this mode, the speed controller can be developed externally based on the reference speed and actual speed and the input to the actuator becomes the reference throttle position. It also gives a driving feel similar to the conventional vehicle in which accelerator pedal directly commands the actuator position instead of speed. Hence, throttle control mode was selected for implementation on the prototype.

4.5.3 Data Acquisition System

A National Instruments CompactRio (cRio) real-time controller was used for data acquisition. The controller has 8 different slots for input/ output cards that can be used for control and data acquisition. The details of the CompactRio and the data cards are mentioned in Table 4.14.

Table 4.14. : Electronic Control Unit and Data Acquisition System.

NI cRio-9074	Real-Time Controller, 400 MHz, 128 MB RAM, 256 MB Storage
NI Module 9205	± 10 V Analog Input, 32 Channel
NI Module 9264	± 10 V Analog Output, 16 channels
NI Module 9213	16 Channel Thermocouple Module
NI Module 9401	5 V Bidirectional Digital Input Output, 8 Channel deg/sec
NI Module 9474	24 V, Soursing Digital Output, 8 Channel

Veristand is the user interface from NI that was used to develop data acquisition system and the control strategies. The control strategies are developed in Matlab/Simulink and then deployed on cRio using Veristand. However, acquisition of hydraulic unit speed needed higher data acquisition frequency and hence, Field Programmable Gate Array (FPGA) was used along with Veristand. The frequency from the hall effect sensor in the units was processed using FPGA to evaluate the speed of the hydraulic units.

There are two methods for calculating the speed of the units. The first one is the pulse counting method and the second one is the pulse-timing method, (De Silva 2004). In the first method, the number of pulses for a given time period are counted and angular speed of the units is calculated using Equation (4.2). In the second method, the time interval between two pulses is calculated to determine the speed using Equation (4.3).

$$\omega_c = \frac{2\pi \cdot N}{T \cdot n} \tag{4.2}$$

where ω is the speed of the hydraulic unit in rad/s, N is the number of pulses, T is the fixed time period, n is the number of pulses in one rotation of the hydraulic unit.

$$\omega_t = \frac{2\pi}{T \cdot n} \tag{4.3}$$

where ω_t is the speed of the hydraulic unit in rad/s, N is the number of pulses, T is the time period between two pulses, n is the number of pulses in one rotation of the hydraulic unit. the value of n is 63 for unit 1 and 58 for units 2 and 3.

The percent resolution of the two methods can be calculated as $\Delta\omega_c/\omega_c$ and $\Delta\omega_t/\omega_t$. The percent resolution for the two method is plotted against the speed of operation of the units in Figure 4.30.

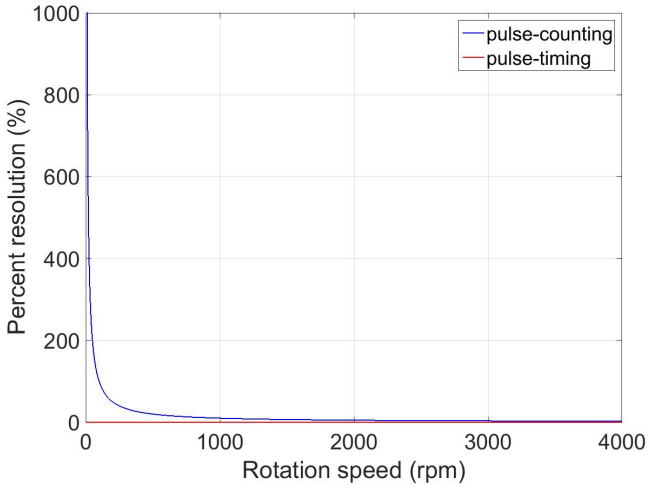

Figure 4.30. : Percent Resolution for Speed Calculation Using FPGA (n = 63, T = 0.01 sec).

Figure 4.30 clearly shows that for the range of operation of the hydraulic units, the pulse timing method has a lower percentage resolution. Hence, this strategy is selected for this application. This method helps in calculating the speed of the units even at very low speeds of rotation. The FPGA Implementation of unit 1 speed calculation is as in Figure 4.31.

Similar to the determination of speed using FPGA, the temperature signals were also processed using FPGA. Based on the table generated by the National Institute of Standards and Technology, the voltage from the k-type thermocouple was converted into temperature (^0C) using the relation $y = 24.46x$. y is the temperature and x is the thermocouple reading in mV. A cold junction compensation (CJC) was added to this value. CJC is to account for the temperature generated due to the contact between two different metals. The input at the CJC was then converted to temperature using Steinhart-Hart equations shown by Equation (4.4) and Equation (4.5).

$$R_T = \frac{10000 \cdot CJC \cdot 32}{2.5 - CJC \cdot 32} \tag{4.4}$$

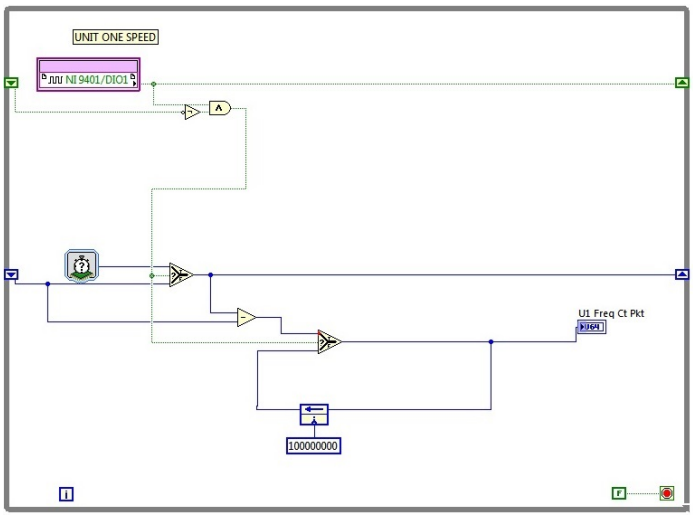

Figure 4.31. : Pulse-Timing Method implemented in FPGA.

$$T = \frac{1}{A + B \cdot ln(R_T) + C \cdot ln(R_T)^3} - 273.15 - 1 \tag{4.5}$$

This temperature was converted to voltage using $y = 0.0397x$. In this case the CJC was recorded as 27^0C which was equivalent to 1.081 mV. This value was added to the thermocouple value and the relation $y = 24.46x$ was used as described earlier to get the final temperature reading in ^0C.

4.5.4 Wiring

The controller, cRio modules, terminal blocks, relays and voltage to current converters were housed in an enclosure in the car's trunk as in Figure 4.32. The power converter and Wifi Router were installed on the opposite side of the controller chassis as shown in Figure 4.33.

Apart from these, controls were added on a front panel by removing the gear shifter and the parking brake. The front panel includes controls to switch on and off the controller and the sensors, gauges for HP and LP accumulator and a toggle switch for forward, reverse and neutral operation as in Figure 4.34.

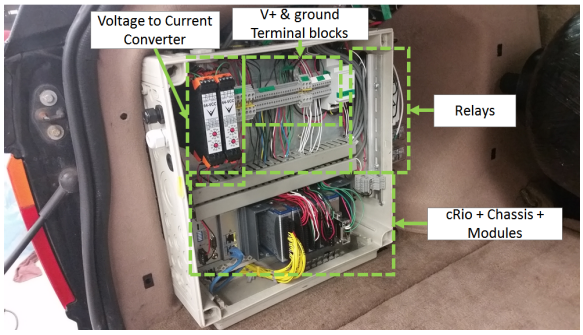

Figure 4.32. : Electrical Wiring Enclosure.

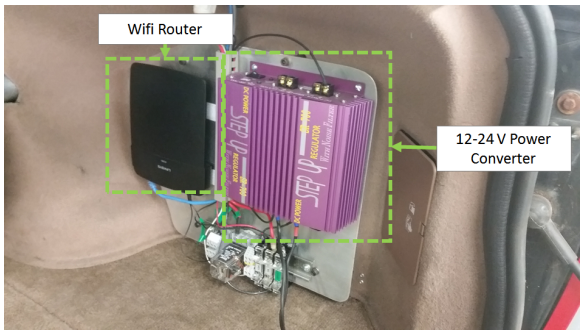

Figure 4.33. : Power Converter and Wifi Router.

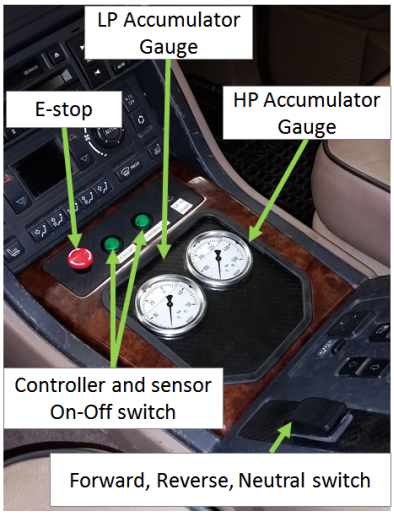

Figure 4.34. : Instrument Panel.

This chapter described the implementation of the mode-switching hybrid on an actual on highway vehicle. It is to be noted that the work on this project was done in a team and hence, the implementation of this design was a team effort.

5. MEASUREMENT RESULTS FOR SYSTEM VALIDATION

Once the vehicle prototype was manufactured, initial measurements were conducted in order to validate the system model developed for the hybrid. This allows for a close check on the accuracy of the developed system model. Validating the system is crucial for controller design and development.

5.1 Measurements on the Engine

Before testing the transmission, measurements were conducted on the engine in order to confirm the operation of the newly installed throttle actuator shown in Figure 4.27. The measurements were performed under no load condition at a constant engine speeds. Figure 5.1 shows the measurements for speed control mode of the actuator explained in Figure 4.28.

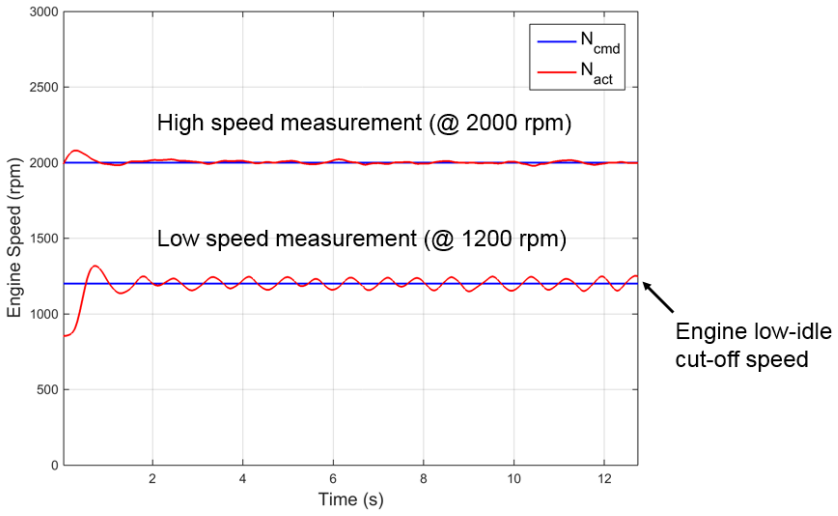

Figure 5.1. : Engine Measurement for Speed Control Mode.

Figure 5.1 clearly indicates that at high speed (2000 rpm), the speed tracking of the actuator was good. However, at low speed (1200 rpm), the engine showed an oscillatory behavior. The problem remained persistent in the speed control mode. Hence, throttle

control mode, explained in Figure 4.29, was implemented. Figure 5.2 shows the measurements for throttle control mode of the actuator. It shows the amount of throttle and the corresponding engine speed obtained.

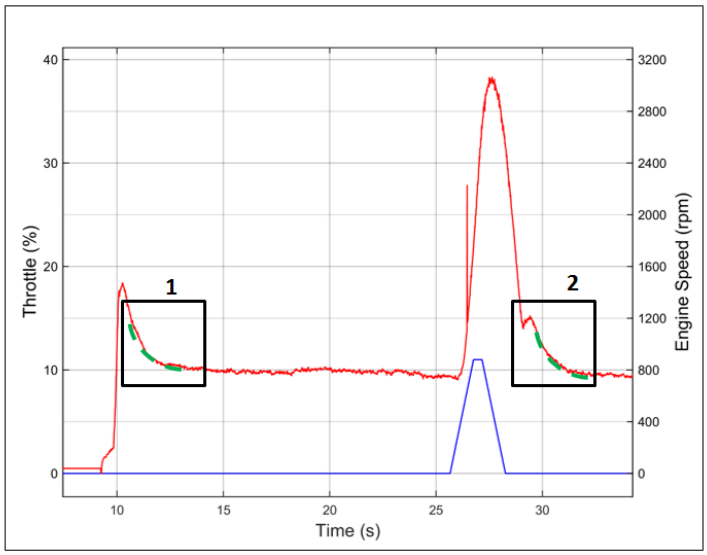

Figure 5.2. : Engine Measurement for Throttle Control Mode: Engine Behavior.

Figure 5.2 highlights the behavior of the engine during startup and when throttle command was applied to the engine. In the figure, the first peak represents the start up and the second peak shows the engine speed when throttle command was applied. When the throttle command was zero, the engine was operated at idle speed. When the engine is first started, the idle is set at a high value of 1200 rpm and once a preset temperature is reached, the idle is lowered to 750 rpm. The engine speed was steady in this case. As the throttle command was increased, the engine speed also increased. However, as the throttle was decreased and the engine speed fell below 1200 rpm, a second peak was observed and the slope of the engine speed changed as seen in the blocks (1) and (2). This clearly indicated that the bypass valve was in action when the engine speed fell below a set speed of 1200 rpm and a default air flows through it. Also, Figure 5.1 shows oscillations in engine speed at 1200 rpm when the bypass valve goes on and off. This speed was the cutoff speed for the bypass valve as mentioned in the workshop manual for the vehicle.

Thus, Figures 5.1 and Figure 5.2 show that at 1200 rpm, the bypass valve interferes with the control action of the new throttle actuator which was used to convert the engine from

torque controlled system to a speed controlled system. In order to eliminate this effect, the bypass valve was disconnected from the air intake system. The engine model as described in Chapter 3 was used to simulate the new intake system. The engine dynamics were included in the engine model using experimental data for step and ramp response and by treating the engine as a black box. Figure 5.3 shows the model of the engine without bypass valve. The results for the engine model without bypass valve for the same throttle input (as used in the case with bypass valve) is shown in Figure 5.4. However, the throttle input is modified to compensate for the lack of airflow through the bypass valve as it is eliminated from the new design. This modified throttle command is also shown in the figure. The figure makes it evident that the new actuator worked better without the bypass valve.

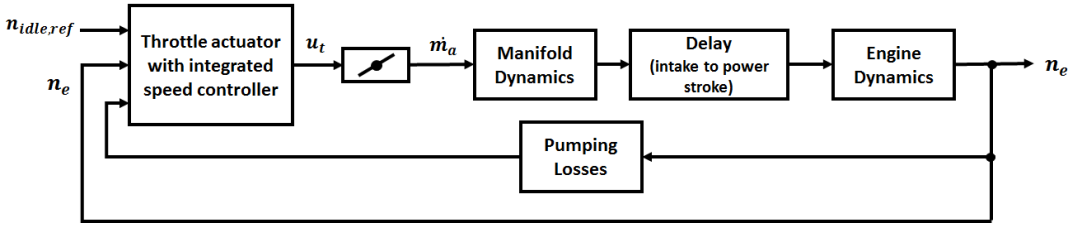

Figure 5.3. : Engine Model without Bypass Valve.

Once the engine model was validated, a controller was developed for the engine in order to perform experiments on the transmission. The aim of the controller was to maintain the required engine speed for this flow controlled hybrid. As explained earlier, a throttle actuator was installed in this system in order to control the throttle body and hence, the amount of air supplied to the engine. The actuator was operated in throttle control mode as shown in the figure 4.29. However, due to the elimination of the bypass valve, the new architecture is as in Figure 5.5. When operated in throttle control mode, the speed controller had to be developed in order to command a reference throttle position. This is sent to the actuator which has an inbuilt throttle controller which compares the reference and actual throttle position and generates input based on the error between the two.

The speed controller was developed with the aim of maintaining the feel of the conventional vehicle. Therefore, throttle actuator was directly linked to the accelerator pedal instead of commanding a reference engine speed. A polynomial was generated in order to translate the accelerator pedal position to throttle command based on the driver feel. This

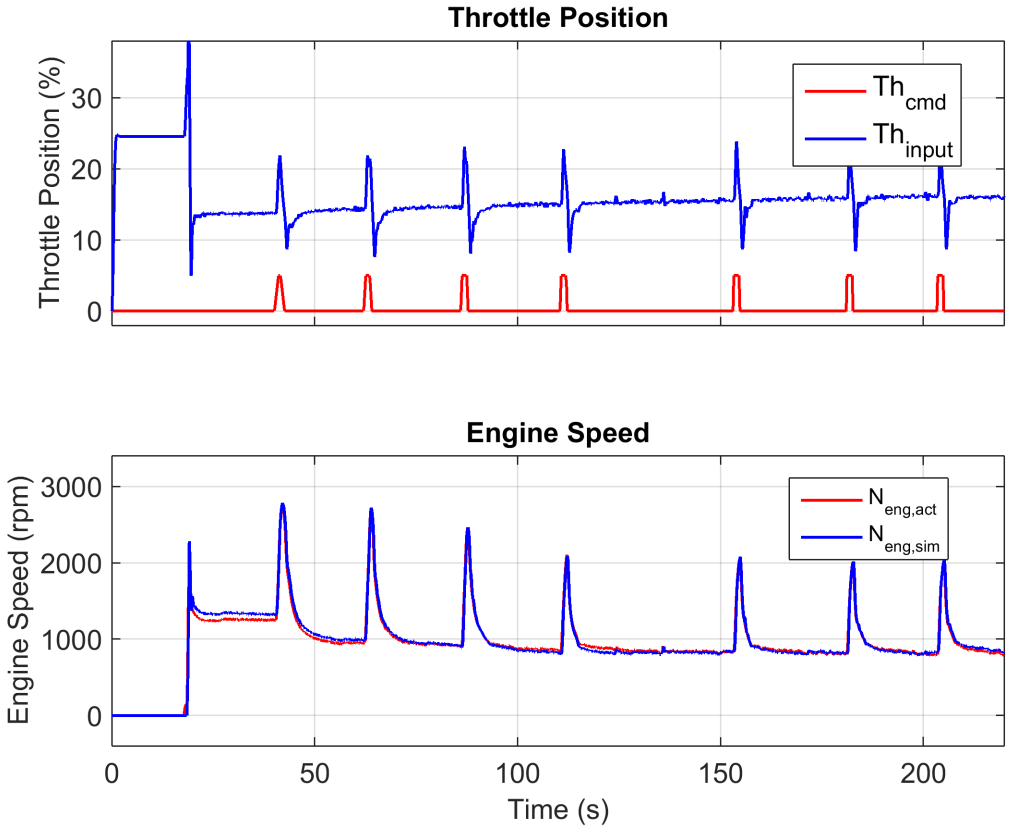

Figure 5.4. : Validation of Engine Model without Bypass Valve.

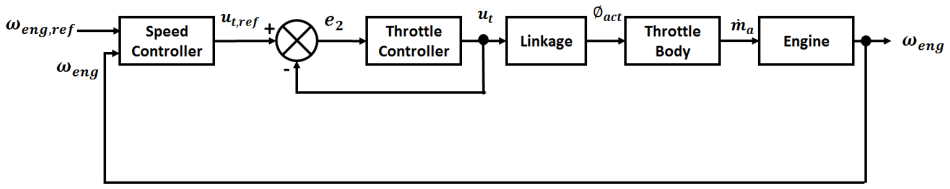

Figure 5.5. : Engine Throttle Control Block Diagram.

quantity was then added to a constant offset, K_{idle}, that incorporated in order to maintain the engine at idling speed and to compensate for the frictional loads in the system. The block diagram of the engine speed controller is shown in Figure 5.6.

This simple controller results in a driver feel like a conventional transmission and is effective for the scope of this work. Advanced controls can be developed to incorporate reference speeds at a later stage to implement power management strategies.

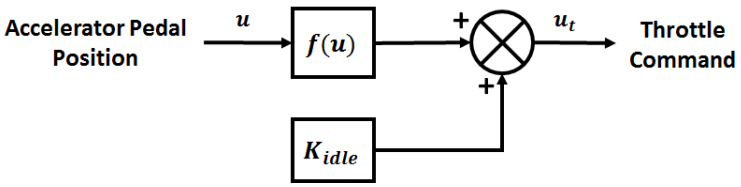

Figure 5.6. : Engine Speed Controller Block Diagram.

5.2 Measurements on the Vehicle

After conducting measurements on the engine and modifying the intake system, measurements were conducted on the vehicle. In order to perform the experiments, baseline controllers were implemented. The accelerator pedal was mapped to the displacements of the hydraulic units. To map the accelerator pedal to unit displacements, two cases were considered. Firstly, the acceleration with a variable displacement unit 1 and displacement of units 2 and 3 at 100 % and secondly, acceleration with displacement of unit 1 at 100 % and units 2 and 3 changing displacements. This is keeping in mind the sequential control strategy described in the previous chapter and as shown in Figure 5.7. The 0 - 100 % travel of the accelerator was divided to achieve both the above cases. The first 70 % of the accelerator pedal travel was linearly mapped to have a 0 - 100 % displacement of unit 1 and the next 30 % to allow 100 - 70 % displacement of units 2 and 3. Figure 5.8 shows the mapping of the accelerator pedal. Hence, increasing or decreasing accelerator pedal travel is converted to displacements of the hydraulic units.

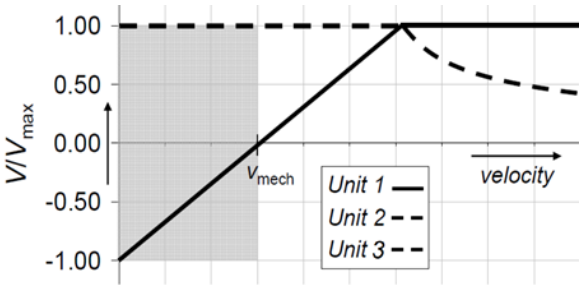

Figure 5.7. : Sequential Control Logic.

Similarly, the brake pedal was mapped to the units 2 and 3 by normalizing the brake pedal position for regenerative braking (0-35 %) to the displacements (0-100%) of the units.

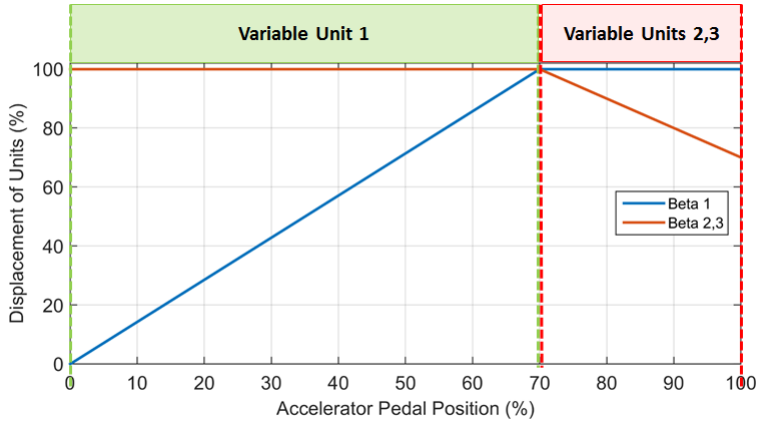

Figure 5.8. : Accelerator Pedal Mapping for Hydraulic Unit Displacements.

A factor was used to change the rate of deceleration while braking in order to ensure a good driver feel. The block diagram for the brake controller is as shown in Figure 5.9.

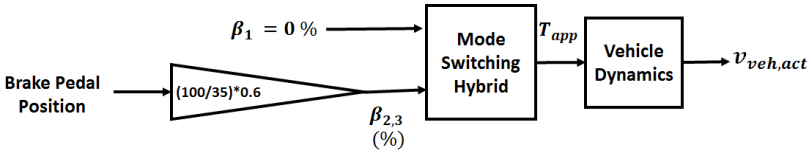

Figure 5.9. : Braking Controller

Coasting was demonstrated by setting the displacements of all the hydraulic units to zero.

The measurements were performed on the vehicle in the hydrostatic mode. The inputs were in terms of accelerator and brake pedal. These result in displacements of the units. The measured displacements of the units and also the engine speed were used as inputs for system validation. The pedal positions are shown in Figure 5.10 and the corresponding displacements of the units are shown in Figure 5.11 while the engine speed is shown in Figure 5.12.

Using the displacement of the units and engine speed as inputs to the system model, the test and the simulation results for vehicle velocity and pressure in the hydraulic lines were compared. Figure 5.13 shows the comparison of vehicle velocity, Figure 5.14 shows the pressure in line A, Figure 5.15 shows the pressure in line B and 5.16 shows the pressure in

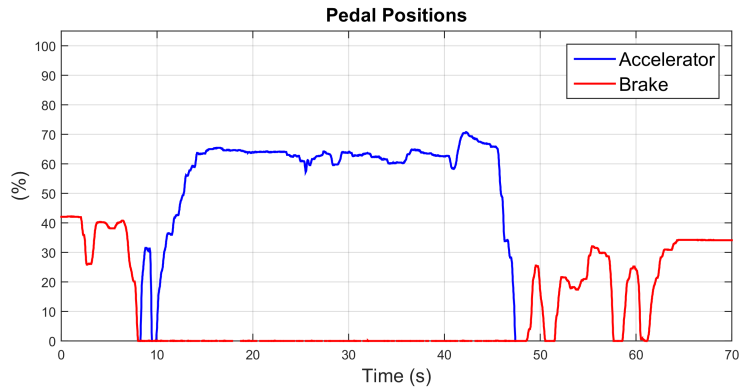

Figure 5.10. : System Validation: Input Pedal Positions.

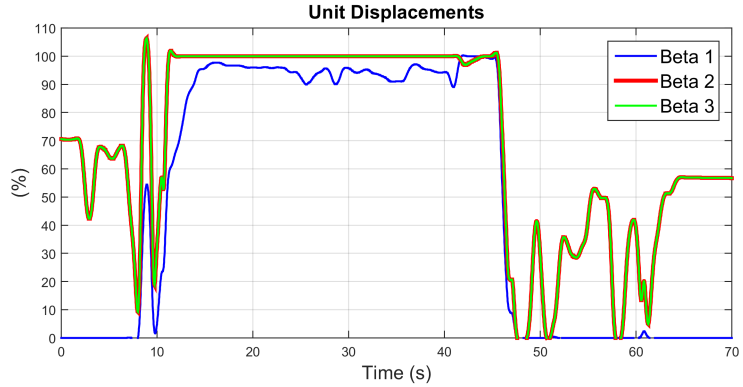

Figure 5.11. : System Validation: Displacements of the Units.

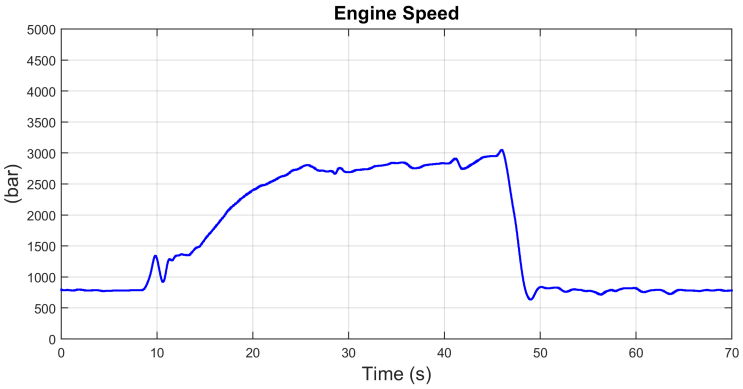

Figure 5.12. : System Validation: Engine Speed.

the HP accumulator. It is to be noted here that the accumulator was initially at 400 bar and was given as an initial condition in the system model.

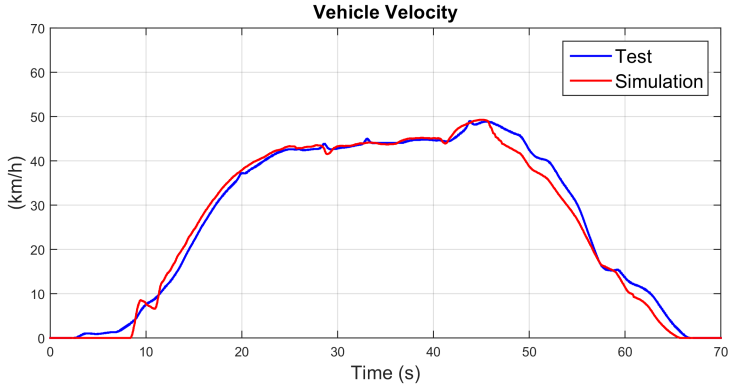

Figure 5.13. : System Validation: Vehicle Velocity.

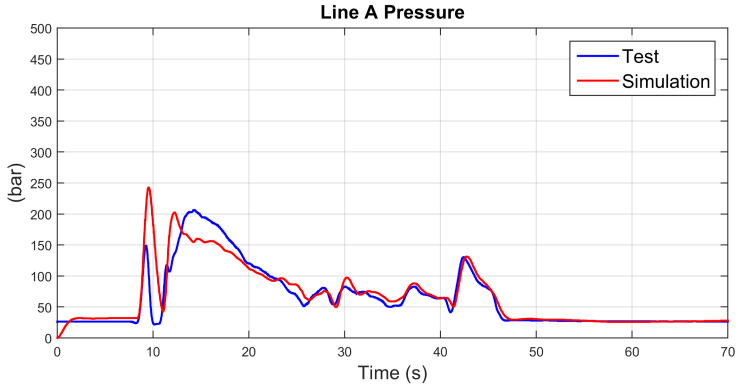

Figure 5.14. : System Validation: Pressure in Line A.

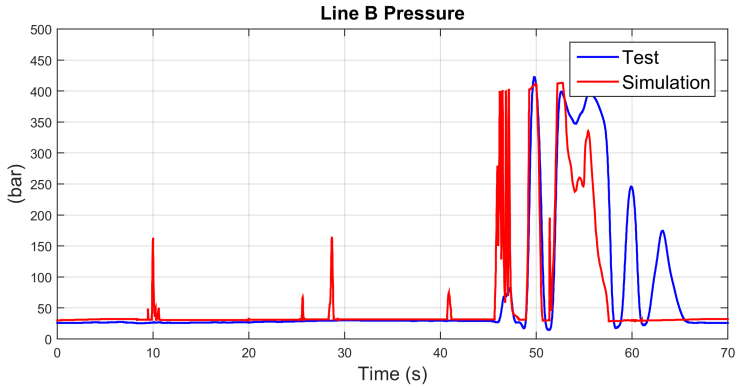

Figure 5.15. : System Validation: Pressure in Line B

As seen in the figures, initially the units are at zero displacement. As soon as the accelerator pedal is pressed as in block (1), units 2 and 3 go to full displacement and the displacement of unit 1 increases from zero to a maximum value. As the unit 1 pumps

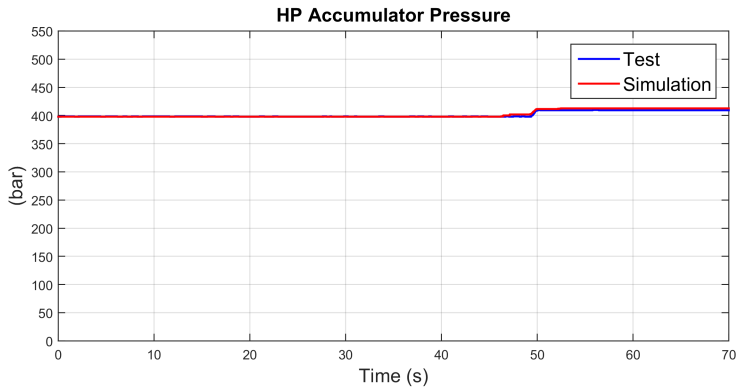

Figure 5.16. : System Validation: Pressure in HP Accumulator.

flows into line A, the pressure in the line increases. This pressure rise is based on the load on the vehicle. line B is maintained at the pressure of the low pressure system. When the accelerator and brake pedal inputs are both zero (block (2)), the vehicle coasts and decelerates due to the resistive forces. Finally, when the brakes are applied (block (3)), the displacement of unit 1 is commanded to be zero and the units 2 and 3 displacement increases. The pressure switches lines and line B pressure increases. As the pressure in the line exceeds the HP accumulator pressure, the fluid flows into to the accumulator increasing the pressure of the accumulator due to energy storage.

The measurements show that simulation closely follows the test results. This validates the system model.

6. CONTROLLER DEVELOPMENT

Once the vehicle prototype was manufactured and the system model was validated, the next step was to develop controls strategies. The mode-switching hybrid has different modes of operation like hydrostatic driving, secondary control mode, coasting and regenerative braking. These modes are dependent on user input and current state of the vehicle. The accelerator pedal and the brake pedal serve as inputs from the driver. Apart from these, several other inputs like the engine speed, wheel speed, state of charge of the high pressure accumulator are communicated from the sensors to the controller. Based on these inputs, the controller generates the control inputs like engine throttle position, displacements of the three hydraulic units and position of the enabling valve. Figure 6.1 shows a top level operation diagram for the mode-switching hybrid.

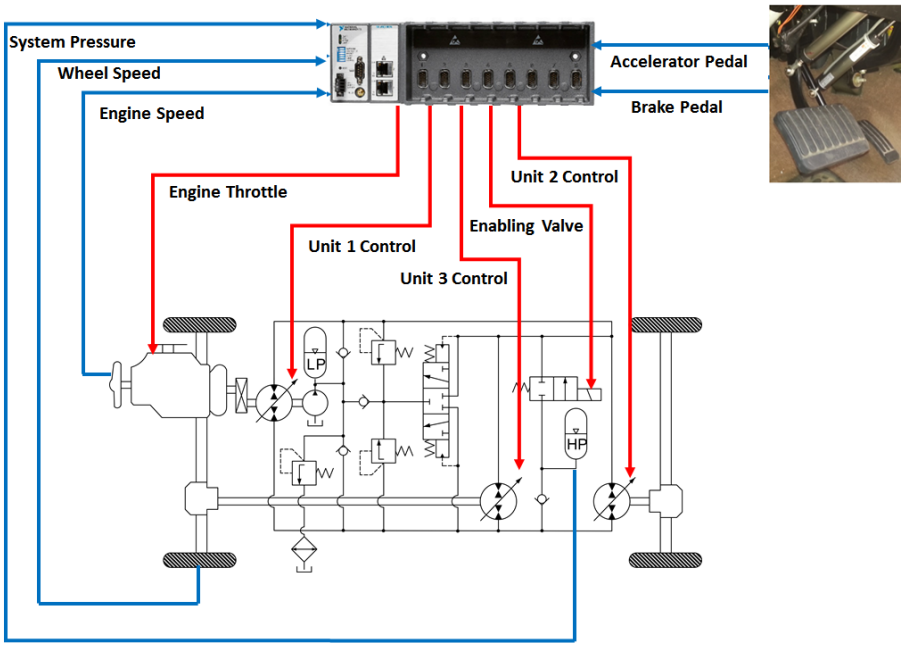

Figure 6.1. : The Mode-Switching Hybrid top level Diagram.

The engine controller was used as described previously in Chapter 5. The controls for the transmission were designed using the concept of velocity tracking. The objective of the

controller is to operate the mode-switching hybrid in different modes. This chapter gives a detailed description of the control strategies.

6.1 Velocity Tracking

In this technique, the velocity of the vehicle was calculated based on the pedal inputs from the driver and then a controller was developed to match the actual vehicle velocity with the reference. Due to complexity of the system, simplified non linear equations are used to calculate the reference velocity. There are separate models to estimate the reference velocity for accelerator pedal input, brake pedal input and no input from any of the pedals. These cases represent acceleration, braking and coasting respectively.

6.1.1 Acceleration

The driver inputs in the form of accelerator pedal was mapped to correspond to displacements of the units as shown in Figure 5.8. These displacements act as reference inputs. When the reference engine speed is a known constant for a flow controlled system, Equation (3.9) gives the flow displaced by unit 1, Q_1. This entire flow is transferred to units 2 and 3 and using Equation (6.1), the rotational speed of the wheel can be determined. Once the wheel speed is evaluated, the velocity of the vehicle can be calculated using Equation (6.4). The velocity obtained from this model becomes the reference velocity. Figure 6.2 shows the projection of the accelerator pedal into velocity.

$$\omega_{wheel} = \frac{Q_1}{\beta_2 \cdot V_{23} \cdot i_{axle}} \tag{6.1}$$

$$\alpha = \frac{d\omega_{wheel}}{dt} \tag{6.2}$$

$$a = \alpha \cdot r_{dyn} \tag{6.3}$$

$$v_{ref} = \int a dt + v_{veh,act} \tag{6.4}$$

Where V_{23} is the total volume displaced by units 2 and 3, α is the angular acceleration of the vehicle, a is the acceleration in m/s and $v_{veh,act}$ is the current vehicle velocity, v_{ref} is the reference velocity and t is the time respectively.

The accelerator pedal mapping results in reference displacements that are useful while calculating the reference velocity. But these values are fixed for a given accelerator position. However, if the accelerator pedal is released and the vehicle decelerates, the hydraulic units 2 and 3 have the capability to act as pumps as torque is transmitted from the wheels to the transmission. Hence, during coasting the units are commanded to zero displacement to allow the vehicle to follow free wheel dynamics. If the brakes are applied, the displacement of unit 1 is zero and that of units 2 and 3 is commanded by the braking controller when the units 2 and 3 act as pumps and charge the accumulator. If the accelerator pedal is pressed while the vehicle is still moving after coasting or braking, it is important that the displacements of the units are adjusted such that the vehicle accelerates from this current velocity. Hence, velocity is fed back to estimate the reference velocity in order to adjust the displacements of the units to maintain the current velocity and accelerate from that point on. Thus, the velocity feed back is the term that compensates for the displacements of the hydraulic units when the vehicle transitions between different modes while still in motion without coming to standstill in between the modes.

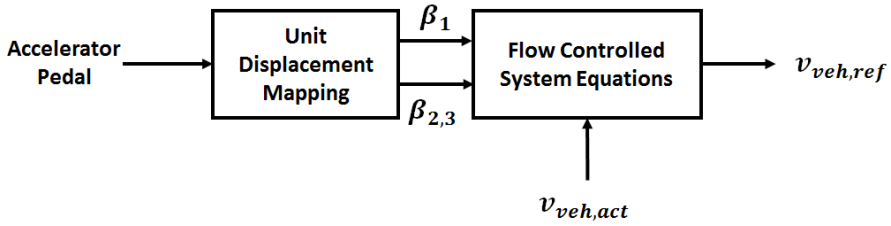

Figure 6.2. : Projection of Accelerator Pedal to Reference Velocity.

6.1.2 Braking

The braking controller was designed based on the deceleration rate that is comfortable while driving in order to achieve smoother driving feel. According to American Association of State Highway and Transportation Officials (AASHTO), the comfortable value of decel-

eration is 3.4 m/s^2. However, that was considered as the deceleration in case of extreme braking which was decided based on the rate of change of brake pedal travel. In case of braking, a deceleration of 2.0 m/s^2 was used as at this rate, a comfortable braking was observed as well as the rate resulted in generation of pressure in line B and helped in charging the accumulator. Equation (6.5) was used to calculate the velocity reference in case of a braking event.

$$v_{ref} = \int a dt + v_{veh,act} \tag{6.5}$$

Where a is the deceleration rate and $v_{veh,act}$ is the current vehicle velocity, v_{ref} is the reference velocity and t is the time respectively.

6.1.3 Coasting

Coasting is the condition when there is no input from either the accelerator pedal or the brake pedal and the vehicle is still in motion. In this case, the vehicle needs to follow free dynamics with no torque being supplied to the wheels through the transmission. However, units 2 and 3 have the capability to act as pumps during vehicle deceleration as torque is being transferred from the wheels to the transmission. This hinders the free dynamics of the vehicle. In order to prevent the units from pumping, the displacements of all the hydraulic units is commanded to be zero. In this case, the vehicle decelerates as a result of the resistive forces like aerodynamic drag and rolling resistance. Thus, it has a slow deceleration as compared to braking.

Based on the three conditions described in this section, simulations were run to estimate the velocity reference based on predefined driver inputs. Figure 6.3 shows the velocity reference. The block (1) represents acceleration. As the accelerator pedal is pressed, the displacements of the units follow the map shown in Figure 5.8 and these displacement inputs result in increase in the velocity of the vehicle. In block (2), when the brakes were applied, the velocity is a result of deceleration rate using Equation (6.5). The block (3) represents deceleration which is the result of decrease in the position of the acceleration pedal. Block (4) shows coasting when neither the accelerator nor the brake pedal inputs were applied and the velocity reduces due to the resistive forces acting on the vehicle.

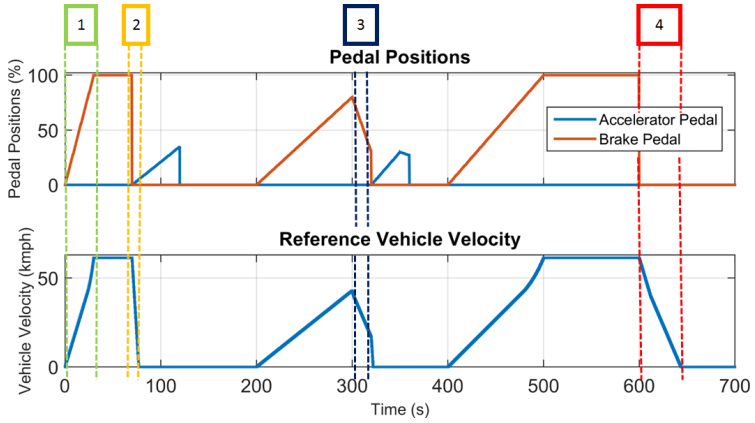

Figure 6.3. : Estimated Reference Vehicle Velocity based on Inputs from the Driver.

6.2 Control Strategy

Once the reference velocity was estimated, the feedback loop was defined around the vehicle velocity. Based on the error between the actual and reference velocity, controllers were defined for different cases. Controllers were developed for two modes during acceleration. The first mode is when the transmission acts as a pure hydrostatic one and the accumulator is not connected to the transmission. This case is in action form 0 to 70 % accelerator pedal position. The next stage is when the vehicle is accelerating further and the accumulator has stored energy. In this stage the torque at the wheels is provided from the engine as well as the accumulator. This stage is the secondary control mode and acts as power boost. A separate controller was developed for braking and coasting.

6.2.1 Hydrostatic Acceleration

6.2.1.1 Modified Sequential controller

Modified sequential control was initially proposed for the hydrostatic mode. The modified sequential control uses a PI controller to command the displacement of unit 1 based on the feedback from vehicle velocity. The displacements of units 2 and 3 are then determined based on the reciprocal of the output of the PI controller. The two units have equal displacements. Unlike traditional sequential control, this controller does not calculate the flow from unit 1 to determine the displacements of units 2 and 3. The advantage of this

method over the traditional sequential control was that the PI controller accounts for all the unaccounted losses that are neglected while estimating the flows from the units and also accounts for any other nonlinearities in the system. This made this controller more accurate. Figure 6.4 shows the control logic for this mode of operation. The displacements of the units cannot physically be outside 0 - 100 % range and hence they were saturated.

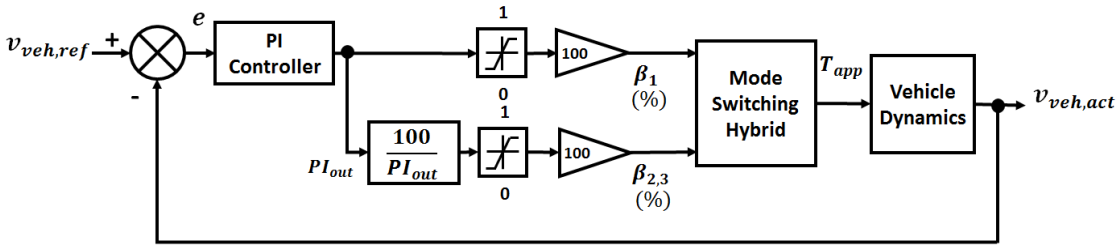

Figure 6.4. : Control Logic: Acceleration in HST Mode using Modified Sequential Control.

6.2.1.2 LQR Controller

Linear Quadratic Regulator (LQR) controller was another strategy used for the hydrostatic case in order to achieve better tracking as compared to a PI controller. It is a type of optimal control that is used to determine the input signal that will take a linear system from an initial state x_0 to final state x_f while minimizing a quadratic cost function. This is a type of state feedback controller. Given a linear time varying system as described in Equation (3.45), the cost function, J is defined as in Equation (6.6). This cost function is the summation of the deviations of the measurements from its desired state.

$$J = \int_0^{\inf} (x^T Q x + u^T R u) dt \tag{6.6}$$

where J is the cost function, x is the state, u is the input, Q is the non-negative definite matrix and R is a positive definite matrix. Q and R are the weighting matrices for the states and inputs respectively. The optimal control problem was to minimize the cost function using linear state feedback law in this case. The linear state feed back law is defined in Equation (6.7).

$$\mathbf{u}(\mathbf{t}) = -K\mathbf{x}(\mathbf{t}) \tag{6.7}$$

Where K is the gain matrix and is defined using Equation (6.8).

$$K = R^{-1}B^{T}P \tag{6.8}$$

Where P is a unique positive definite solution determined using the Algebraic Riccati Equation (ARE) given in Equation (6.9).

$$A^{T}P + PA - PBR^{-1}B^{T}P + Q = 0 \tag{6.9}$$

The weights Q and R are tuning parameters to obtain K. Q and R are as defined in the Equation (6.10). Tuning these weights is an iterative process and the results are compared with the reference values using simulations.

$$Q = \begin{pmatrix} q_1 & & & \\ & . & & \\ & & . & \\ & & & . \\ & & & & q_n \end{pmatrix}, \qquad R = \rho \begin{pmatrix} r_1 & & & \\ & . & & \\ & & . & \\ & & & . \\ & & & & r_n \end{pmatrix} \tag{6.10}$$

K can be determined using matlab code, $K = lqr(A, B, Q, R)$. Once the value of K is determined, linear state feed law as in Equation (6.7) is applied to the system. However, before applying the state feedback law it is important to check the controllability of the system. The controllability describes the ability of the system to move the internal state of the system from any initial state to a final state when an external input is applied to it. For the state feedback to work it is important that the system is completely controllable. The controllability matrix is defined as in Equation (6.11).

$$C = \begin{pmatrix} B & AB & A^2B & ... & A^{n-1}B \end{pmatrix} \tag{6.11}$$

Where C is the controllability matrix and A and B are the system and input matrices. The system is completely controllable if the controllability matrix is a full rank matrix. The

controllability matrix can be determined using Matlab code, $C = ctrb(A, B)$ and its rank using the code, $C_{rank} = rank(C)$.

The controllability only determines whether the system can be moved from one state to another. However, it does not guarantee that the system would be stable at the new state. The ability to maintain the new state is defined by stability. The stability of the system can be determined by evaluating the eigen values of the system. If the real part of the all the eigen values is less than 0 for the system matrix then the system is asymptotically state. The eigen values represent the poles of the system. The negative poles indicate that they lie in the left hand plane of the complex plane. Stability can also be determined using Matlab code, $isstable(sys)$. If the code returns a value 1, then the system is stable, else it it is unstable.

For tracking the reference value of the velocity of the vehicle, the linear model described in Chapter 3 was used. In this case, the states were Δp and ω_{wheel}. The reference values Δp_d and $\omega_{wheel,d}$ were determined using a non linear model used to calculate the reference velocity. Once the reference values were known, Equation (6.12) is used to determine the input vector to the system.

$$\mathbf{u} = K(\mathbf{x} - \mathbf{x_d}) + \mathbf{u_d} \tag{6.12}$$

where

$$\mathbf{x} = \begin{pmatrix} \Delta p \\ \omega_{wheel} \end{pmatrix}, \qquad \mathbf{x_d} = \begin{pmatrix} \Delta p_d \\ \omega_{wheel,d} \end{pmatrix}, \qquad \mathbf{u} = \begin{pmatrix} \beta_1 \\ \beta_2 \end{pmatrix}, \qquad \mathbf{x} = \begin{pmatrix} \beta_{1,d} \\ \beta_{2,d} \end{pmatrix} \tag{6.13}$$

Where $\mathbf{x_d}$ and $\mathbf{u_d}$ represent the reference values of states and inputs respectively. These desired values of inputs were obtained from the pedal mapping and the values of states from the nonlinear model of the system. Thus, this approach is based on error dynamics and the inputs to the system were commanded by the LQR controller based on the error and the value of gain, K, for the system.

While applying the LQR controller, the linear model for acceleration case was divided into two different cases. The first one was used to define the initial acceleration obtained by treating unit 1 as a variable displacement unit and units 2 and 3 as fixed displacement units

at full displacement. The second case was the one where the unit 1 reaches full displacement and is treated as fixed displacement unit whereas the acceleration was commanded by treating units 2 and 3 as variable displacement units. The reason behind this was the change in system dynamics caused due to difference in the way the units were operated. The models for the two cases were used to obtain the gain matrix K. The analysis of the system is as described next.

Case 1: Variable Displacement Unit 1 and Fixed Displacement Units 2 and 3.

The gain matrix was calculated as:

$$K = \begin{pmatrix} 0.08300 & 0.6850 \\ -0.00300 & -0.00010 \end{pmatrix} \tag{6.14}$$

The rank of the controllability matrix for the system was 2. Hence, it was completely state controllable. The poles of the system were -13.6073 and -1.4618. Both the poles were negative and were on the left hand side of the complex plane and hence, stable. The stability was also checked using the $isstable(sys)$ command which returned the value 1 indicating that the system was stable. This proved that this case was controllable as well as stable.

Case 2: Fixed Displacement Unit 1 and Variable Displacement Units 2 and 3.

The gain matrix was calculated as:

$$K = \begin{pmatrix} 0.00129 & 0.00128 \\ -0.112100 & -0.17100 \end{pmatrix} \tag{6.15}$$

The rank of the controllability matrix for the system was 2. Hence, it was completely state controllable. The poles of the system are -14.6868 and -0.3823. Both the poles were negative and were on the left hand part of the complex plane and hence, stable. The stability was also checked using the $isstable(sys)$ command which returned the value 1 indicating that the system was stable. This proved that this case was controllable as well as stable.

Hence, both the cases were completely state controllable as well as stable. Thus, the gain matrix K could be used to apply the state feedback law. The LQR Controller is as shown in Figure 6.5 and the details of the controller are in Figure 6.6.

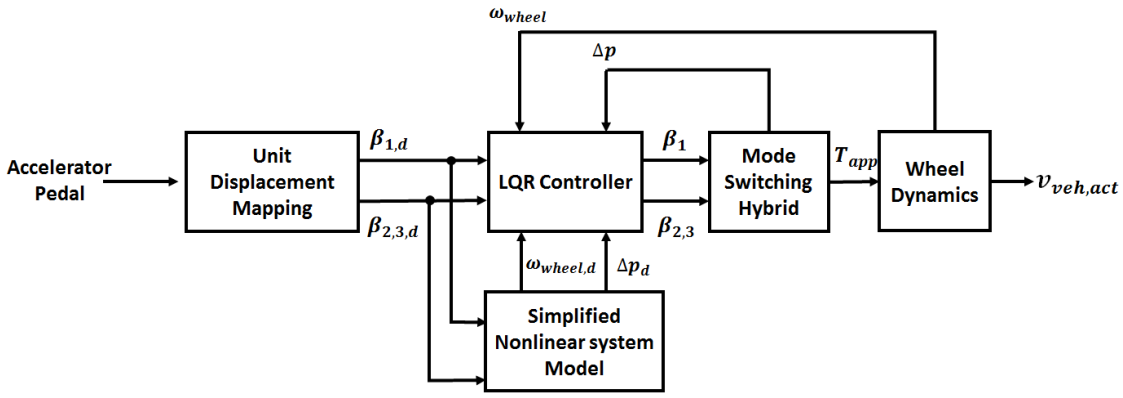

Figure 6.5. : Control Logic: Acceleration in HST Mode using LQR Controller.

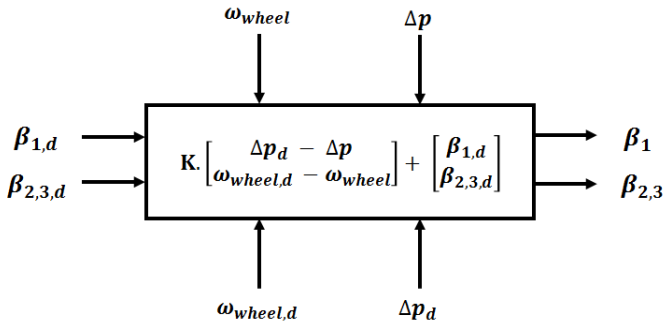

Figure 6.6. : LQR Controller .

6.2.2 Secondary Control Acceleration

When the vehicle velocity reaches 30 km/h a different strategy is used to track the reference velocity. In this case, the HP accumulator is connected to line A and its energy is utilized. However, if line A is directly exposed to the accumulator, the sudden change in pressure may result in a jerky feel to the driver. Hence, before opening the enabling valve, the pressure in line A is increased to meet the accumulator pressure in order to ensure smooth switching between the modes. Hence, the feedback from the vehicle velocity is used to control the displacement of units 2 and 3 unlike the HST controller where the displacement of unit 1 was commanded and that of units 2 and 3 were derived. Once the displacement is known, the flow required by units 2 and 3 can be calculated. The displacement of unit 1 is determined such that it is able to supply flow to raise the pressure of the line A as well as meet the demand of units 2 and 3. Once the enabling valve is opened,

accumulator energy is used to meet the torque demand at the wheels and the displacement of unit 1 is decreased. When the accumulator pressure falls, unit 1 is again used to supply the flow needed to maintain system pressure based on the load. Thus, secondary control is used to supply power boost at higher velocities by using the brake energy stored in the accumulator. Figure 6.7 shows the control logic for acceleration in secondary control mode and Figure 6.8 shows the flow based controller. p_{ref} is the reference pressure which is set at the current pressure of the HP accumulator.

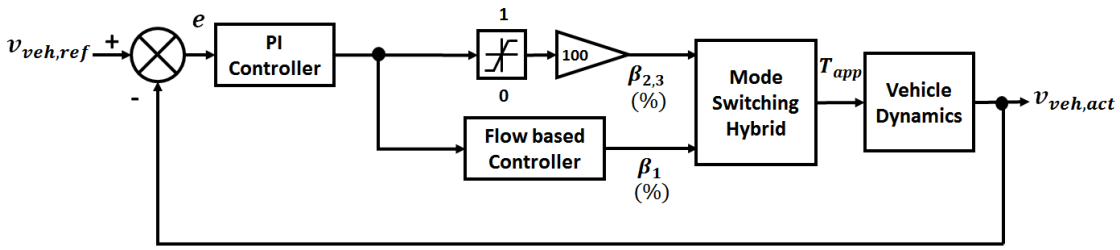

Figure 6.7. : Control Logic: Acceleration in Secondary Control Mode.

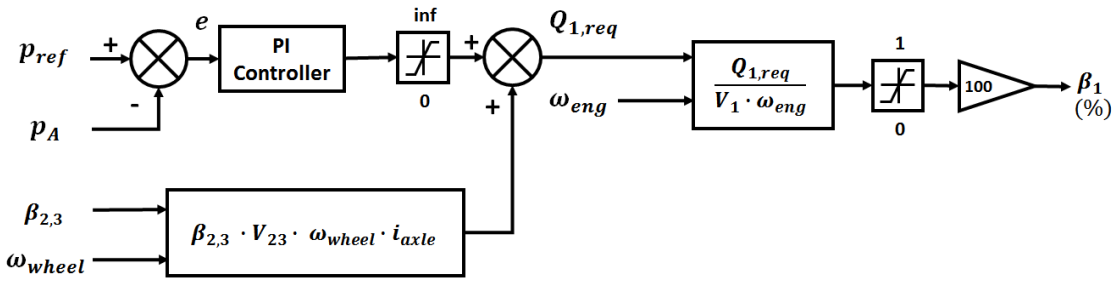

Figure 6.8. : Unit 1 displacement based on the Flow Required.

6.2.3 Braking

When brakes are applied, the reference velocity is calculated based on deceleration as discussed before. As soon as the brakes are applied, unit 1 is commanded to zero displacement. The reference velocity is then tracked using a PI controller which generates control input for the displacement of units 2 and 3. The control logic for braking is as in Figure 6.9.

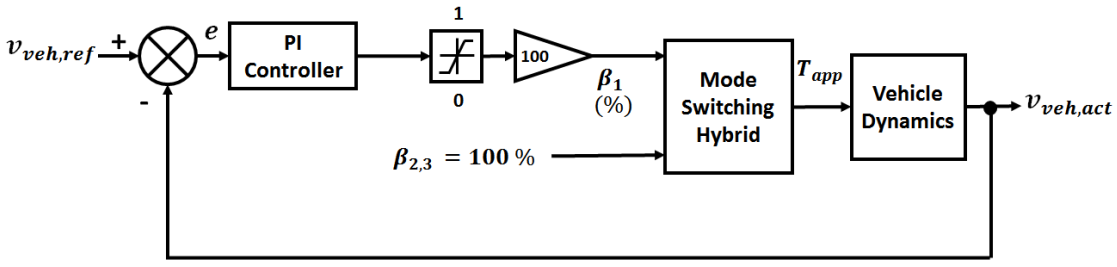

Figure 6.9. : Control logic: Braking Event.

6.2.4 Coasting

For coasting, the reference velocity is calculated based on the deceleration of the vehicle. When coasting is sensed, the displacements of all the hydraulic units are commanded to zero. The deceleration of the vehicle then occurs due to the resistive forces like aerodynamic drag, rolling resistance, friction in the components and losses in the units. The control logic for coasting is as shown in Figure 6.10.

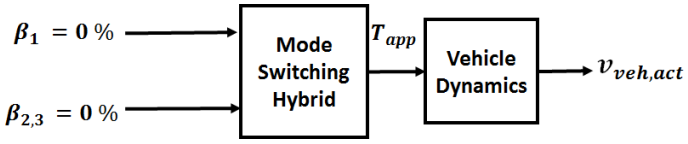

Figure 6.10. : Control logic: Coasting Event.

6.3 Results

The simulation results for the controllers to achieve different modes of operation of the mode-switching hybrid are shown in this section.

6.3.1 Forward Operation

As discussed in previous sections the mode-switching hybrid has multiple modes of operation. This section shows the simulation results for the modified sequential, LQR as well as secondary controller for a predefined accelerator and brake pedal input and a constant engine speed of 2500 rpm. During this cycle all modes of operation were realized.

6.3.1.1 Modified Sequential Controller

The modified sequential controller was simulated using a drive cycle designed to demonstrate acceleration, deceleration, braking and coating events in hydrostatic mode. The drive cycle is in the form of driver inputs in terms of accelerator and brake pedals. The inputs are shown in Figure 6.11. The inputs result in displacement of the hydraulic units based on the mapping of the pedals and generate a reference velocity. This velocity was tracked using the modified sequential controller. The controller commands the displacements of the hydraulic units as shown in Figure 6.12. The displacement of the units result in flow in the system and drive the units 2 and 3 to generate vehicle velocity. The load on the wheels result in pressure in the system. The pressures are shown in Figure 6.13 and the simulated vehicle velocity is shown in Figure 6.14.

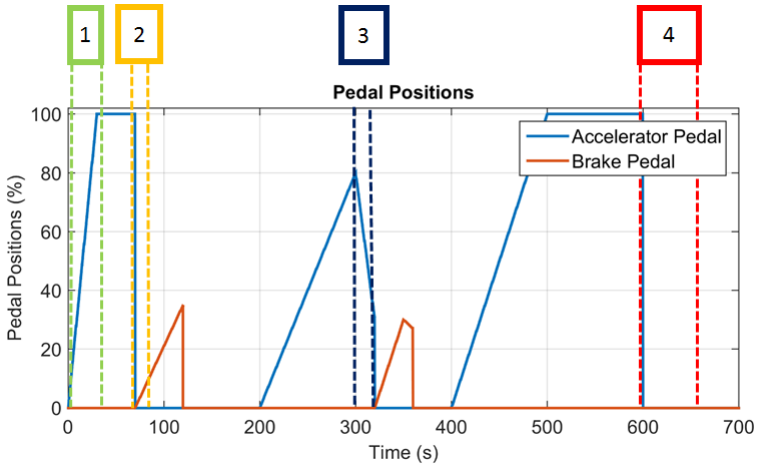

Figure 6.11. : Simulation Results for Modified Sequential Controller: Pedal Inputs.

As shown in the figures, block (1) represents acceleration, block (2) shows braking, block (3) shows deceleration and block (4) shows coasting. As the accelerator pedal was pressed, a reference velocity was evaluated and modified sequential controller commanded unit 1 displacement. The displacement of unit 2 was derived using modified sequential control logic. The pressure in the system is load dependent and increases to achieve the required velocity. While braking, the pressure switched sides and when the pressure in line B exceeded the accumulator pressure, energy was stored in the accumulator and pressure in the accumulator increased. During coasting, the commanded displacements of all the

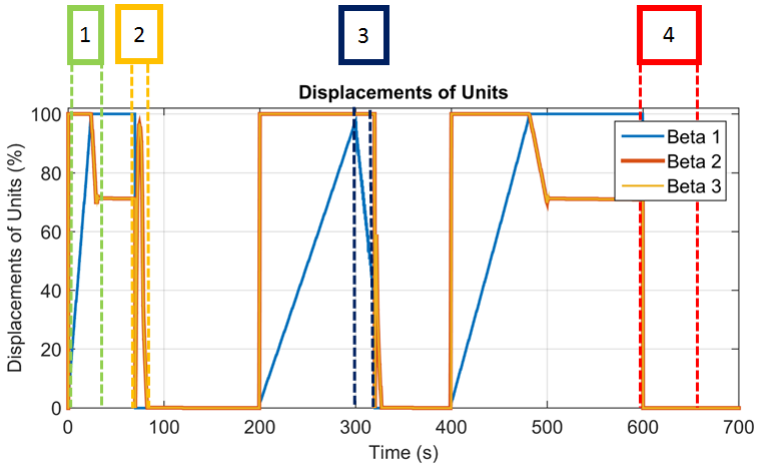

Figure 6.12. : Simulation Results for Modified Sequential Controller: Displacements of Hydraulic Units.

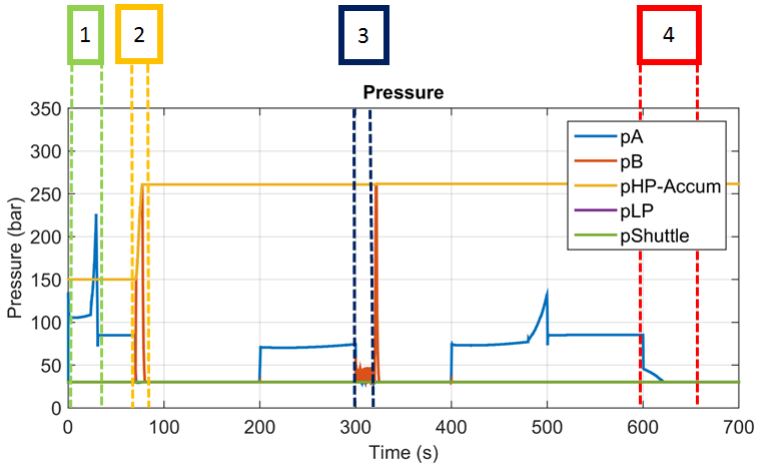

Figure 6.13. : Simulation Results for Modified Sequential Controller: Pressures.

hydraulic units changed to zero as there was non input from the driver. The decrease in the vehicle velocity was due to resistive forces. Thus, modified sequential controller performs quite well while tracking the reference velocity as shown in Figure 6.14. It is to be noted that in this case the transmission was simulated using only the modified sequential controller to demonstrate its working and hence, the accumulator energy was never used. However, in reality, the controller switches to secondary control at higher velocities in order to use the accumulator energy.

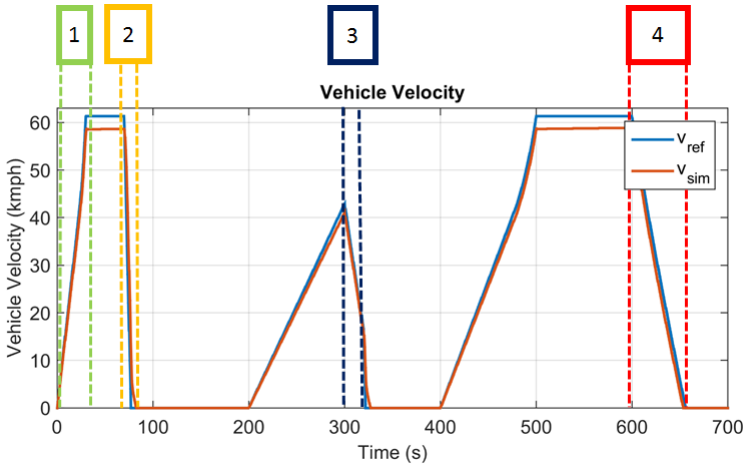

Figure 6.14. : Simulation Results for Modified Sequential Controller: Vehicle Velocity.

6.3.1.2 LQR Controller

The secondary controller was simulated using the same drive cycle designed for HST to demonstrate acceleration, deceleration, braking and coating events in hydrostatic mode. The pedal inputs are shown in Figure 6.15. The inputs resulted in displacement of the hydraulic units based on the mapping of the pedals and generated a reference velocity. This velocity was tracked using the LQR controller. The controller commanded the displacements of the hydraulic units as shown in Figure 6.16. The displacement of the units resulted in flow in the system and drove units 2 and 3 to generate vehicle velocity. The load on the wheels resulted in pressure in the system. The pressures are shown in Figure 6.17 and the simulated vehicle velocity is shown in Figure 6.18.

As shown in the figures, block (1) represents acceleration, block (2) shows braking, block (3) shows deceleration and block (4) shows coasting. As the accelerator pedal was pressed, a reference velocity was evaluated and LQR controller commanded the displacements of the units based on the current state of the vehicle and the gain matrix. The pressure in the system is load dependent and increases to achieve the required velocity. While braking, the pressure switched sides and when the pressure in line B exceeded the accumulator pressure, energy was stored in the accumulator and pressure in the accumulator increased. During coasting, the commanded displacements of units was zero but the velocity decreased due to resistive forces. Thus, LQR controller performed quite well while tracking the reference

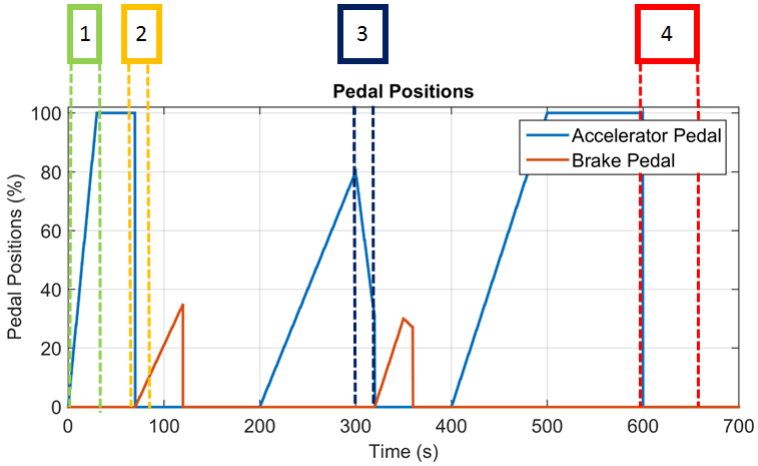

Figure 6.15. : Simulation Results for LQR Controller: Pedal Inputs.

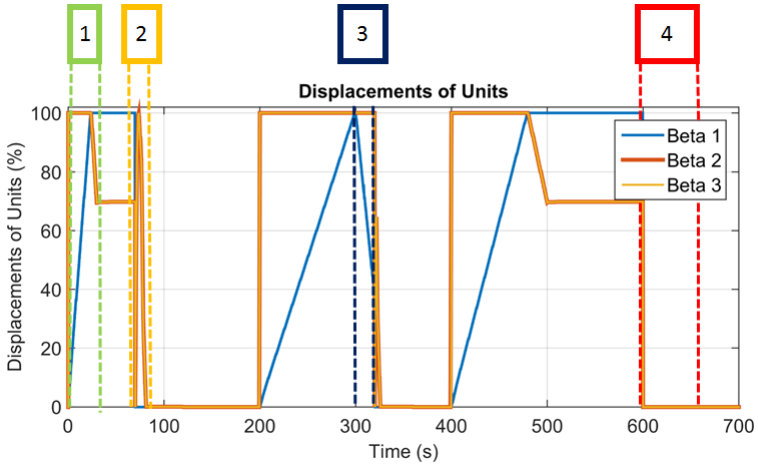

Figure 6.16. : Simulation Results for LQR Controller: Displacements of Hydraulic Units.

velocity as shown in Figure 6.18. It is to be noted that in this case the transmission was simulated using a pure LQR controller to demonstrate its working for the hydrostatic mode and hence, the accumulator energy was never used. However, in reality, the controller would switch to secondary control at higher velocities in order to use the accumulator energy.

6.3.1.3 Secondary Controller

The secondary controller was simulated using the same drive cycle designed for HST to demonstrate acceleration, deceleration, braking and coating events. The pedal inputs are shown in Figure 6.19. The inputs resulted in displacements of the hydraulic units based

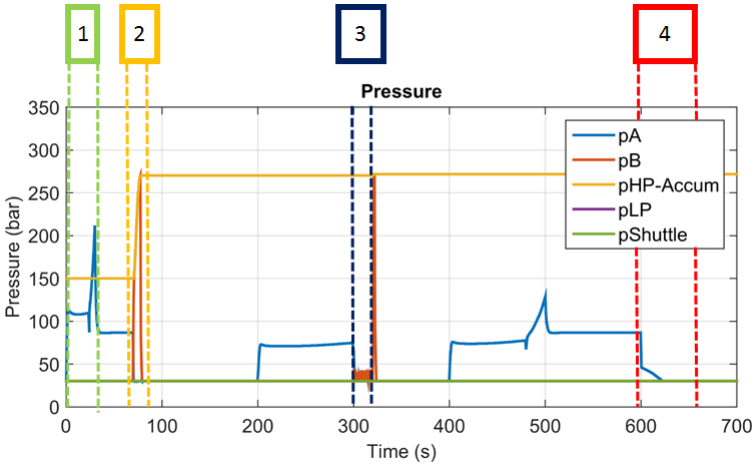

Figure 6.17. : Simulation Results for LQR Controller: Pressures.

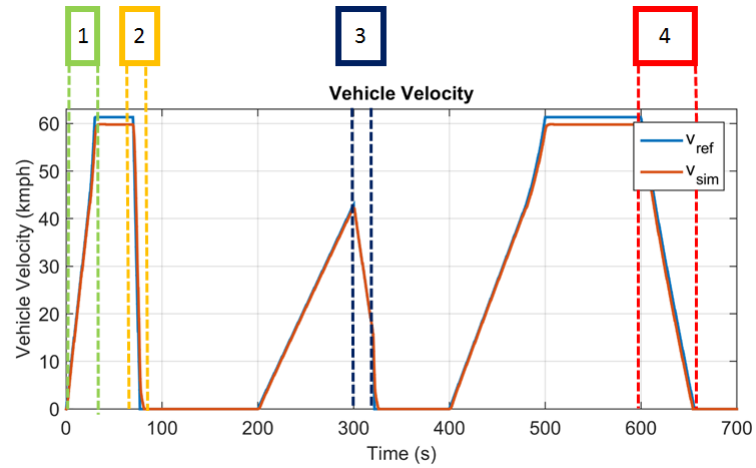

Figure 6.18. : Simulation Results for LQR Controller: Vehicle Velocity.

on the mapping of the pedals and generated a reference velocity. This velocity was tracked using the HST controller till the vehicle reached 30 km/h after which secondary control was used. The controller commanded the displacements of the hydraulic units as shown in Figure 6.20. The displacement of the units resulted in flow in the system and propelled the vehicle. The pressure in the system was governed by the accumulator after the enabling valve was opened. The pressures are shown in Figure 6.21 and the simulated vehicle velocity is shown in Figure 6.22.

As seen in block (1) of the figures, the accelerator pedal input resulted in the increase in the velocity of the vehicle based on the displacement commands determined by the HST

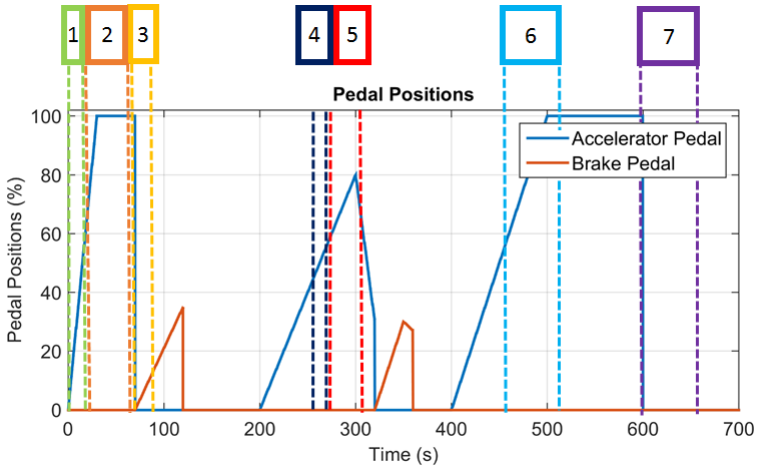

Figure 6.19. : Simulation Results for Secondary Controller: Pedal Inputs.

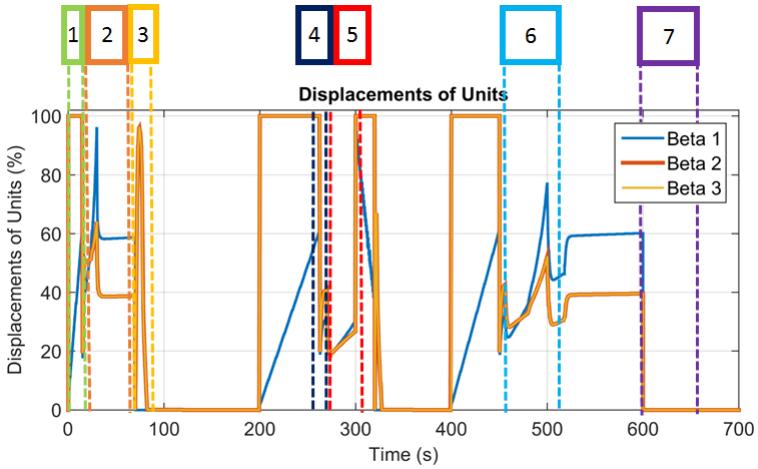

Figure 6.20. : Simulation Results for Secondary Controller: Displacements of Hydraulic Units.

controller. As the vehicle approaches 30 km/h demonstrated by block (2), the controller switched to secondary control mode. The displacements of units were controlled in such a way that the pressure in line A increases as seen in block (4). As the pressure in the line reached the minimum pressure of the accumulator, the enabling valve was opened and the accumulator energy was used to propel the vehicle. The blocks (5) and (6) show the drop in the pressure of the accumulator as the energy was used to supply the torque required at the wheels. As the energy was provided by the accumulator, the unit 1 displacement was also decreased. The HST controller is active in case of braking and coasting demonstrated in blocks (3) and (7).

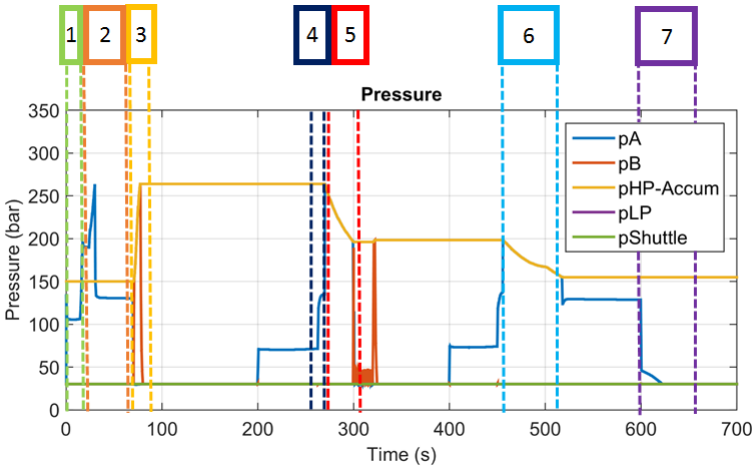

Figure 6.21. : Simulation Results for Secondary Controller: Pressures.

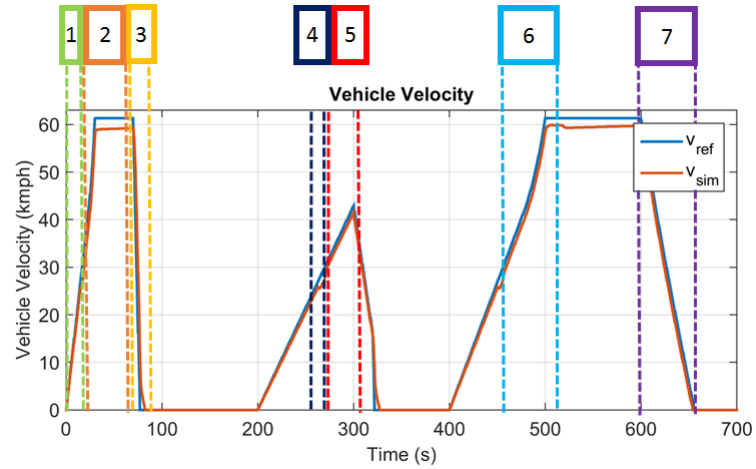

Figure 6.22. : Simulation Results for Secondary Controller: Vehicle Velocity.

6.3.2 Reverse Operation

Reverse operation was very simple in the mode-switching hybrid. Units 2 and 3 were commanded to go overcenter to provide torque in the opposite direction when the accelerator was pressed. Because of this, the pressure does not switch sides and line A acts as the high pressure line. When the brakes were applied, unit 2 and 3 displacements were commanded to get the vehicle to a standstill. Figures 6.23, 6.24, 6.25 and 6.26 show the simulation results for the pedal inputs, displacements of hydraulic units, pressures and vehicle velocity for reverse operation. Block (1) indicates acceleration and block (2) indicates braking in reverse. The velocity has a negative value just to indicate reverse operation.

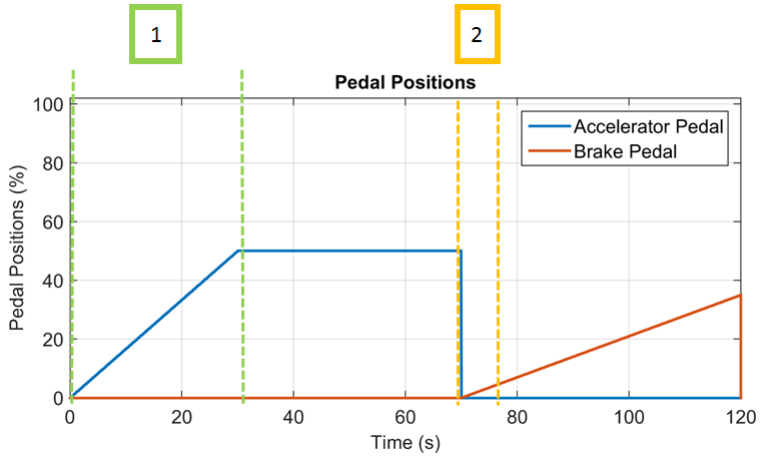

Figure 6.23. : Simulation Results for Reverse Operation: Pedal Inputs.

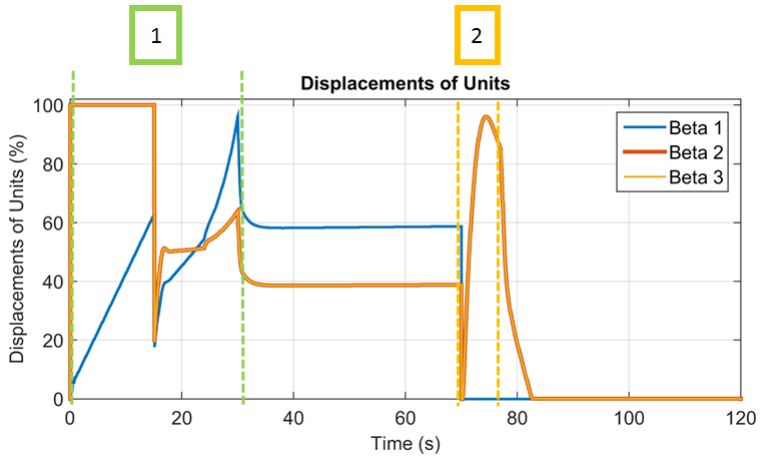

Figure 6.24. : Simulation Results for Reverse Operation: Displacements of Hydraulic Units.

This chapter outlined the control strategies and simulation results for the different modes of operation of the mode-switching hybrid. The hydrostatic controller in the form of modified sequential and LQR controller along with the secondary controller were designed for acceleration of the vehicle and then the braking and coasting were based on the hydrostatic strategy. Thus, the controllers were focused towards achieving a good driving feel as well use the regenerative braking to store energy which was used as a boost at higher velocities.

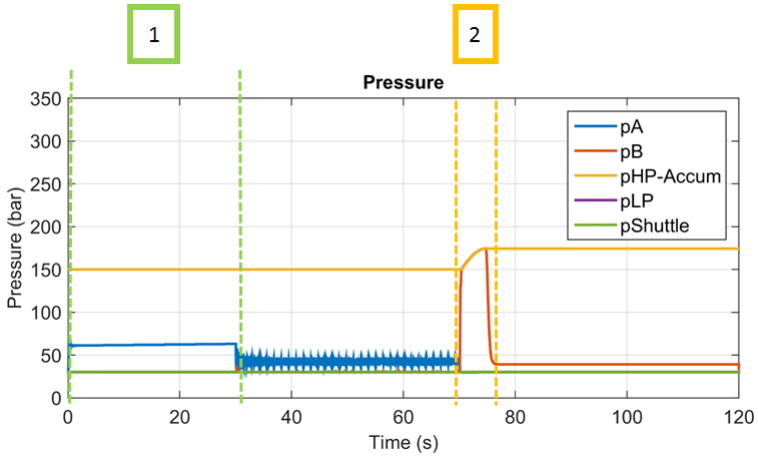

Figure 6.25. : Simulation Results for Reverse Operation: Pressures.

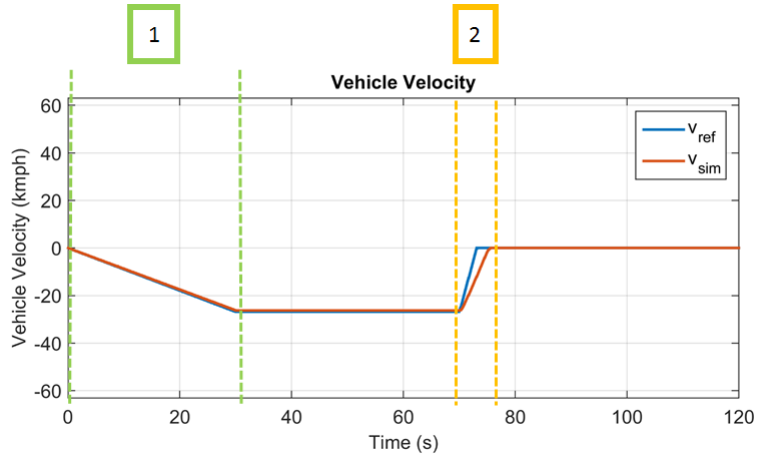

Figure 6.26. : Simulation Results for Reverse Operation: Vehicle Velocity.

7. MEASUREMENT RESULTS AND CONTROLLER VALIDATION ON PROTOTYPE VEHICLE

Measurements were conducted on the transmission to validate the working of the mode-switching hybrid on a full scale vehicle. With this goal, the different modes of operation of the hybrid were demonstrated by driving the vehicle. The performance of the control strategies for velocity tracking was also shown.

It is to be noted that while deploying the controller on the vehicle, the velocity tracking was used only for the acceleration event in the cycle for the initial set of measurements. Braking controller was maintained as the one used for system validation as shown in Figure 5.9.

The results of the initial measurements are discussed in this chapter.

7.1 Forward Operation

The results for the forward operation using three different control strategies for acceleration are discussed in this section, along with braking and coasting.

7.1.1 Modified Sequential Controller

The vehicle was operated in hydrostatic mode with velocity tracking based on modified sequential control and the results for acceleration and brake pedal positions, displacements of the hydraulic units, engine speed, pressure in the system and the vehicle velocity are shown in Figures 7.1, 7.2, 7.3, 7.4 and 7.5.

In the figures, block (1) represents acceleration, block (2) shows coasting and block (3) represents braking events. Acceleration is again divided into two cases with block (A) for variable displacement of unit 1 and units 2 and 3 at full displacement whereas block (B) for variable displacement of units 2 and 3 and unit 1 at full displacement. As the accelerator pedal was pressed, the displacements of the units were commanded by the

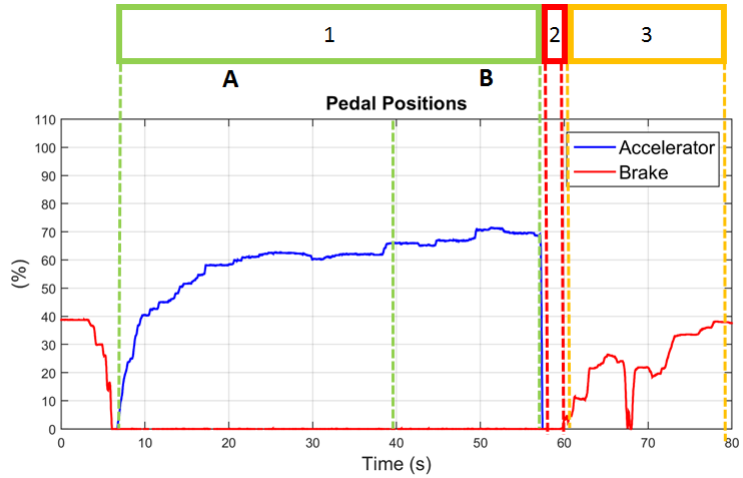

Figure 7.1. : Measurement Results for Modified Sequential Controller: Pedal Positions.

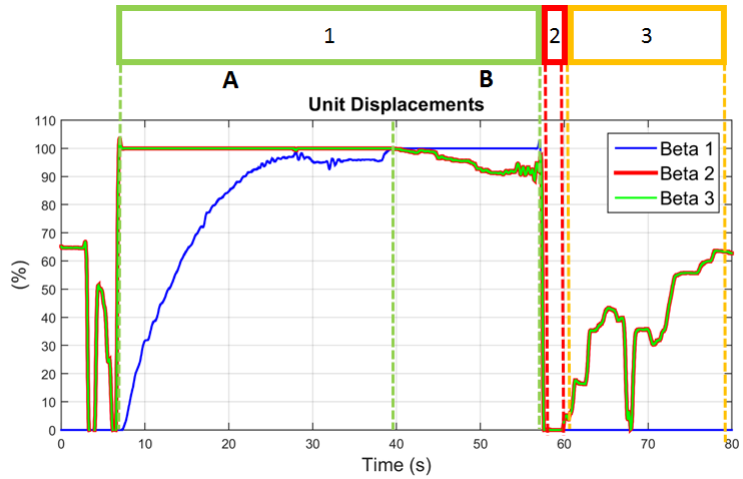

Figure 7.2. : Measurement Results for Modified Sequential Controller: Displacements of Units.

modified-sequential controller to track the reference velocity which resulted in an increases in pressure of line A based on load and hence, the vehicle velocity. Also, the engine speed iss varied based on the accelerator pedal input. The vehicle was accelerated to nearly 60 km/h for this measurement run.

During coasting, the displacements of all the hydraulic units were commanded to zero and the vehicle decelerated at a slower rate due to resistive forces acting on it.

During braking, it is seen that the displacement of units 2 and 3 was commanded based on the brake pedal position and the unit 1 was commanded to zero displacement.

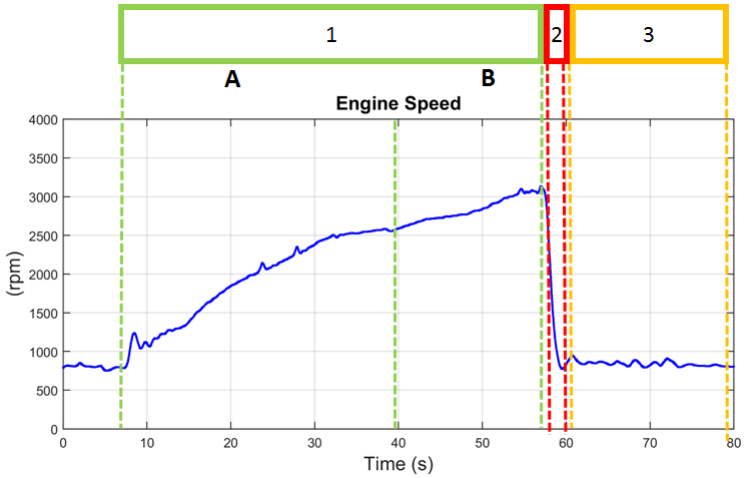

Figure 7.3. : Measurement Results for Modified Sequential Controller: Engine Speed.

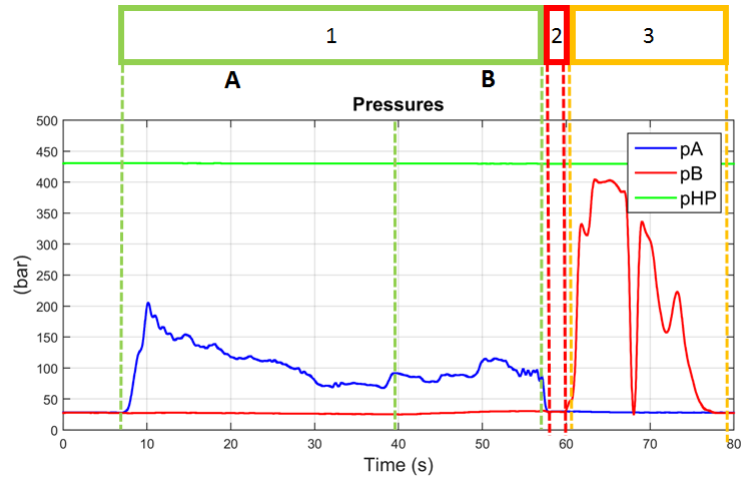

Figure 7.4. : Measurement Results for Modified Sequential Controller: Pressures.

The pressure switched lines and pressure in line B increased. When the pressure exceeds accumulator pressure, energy is stored in the accumulator. However in this case, the pressure in line B was lower than that of accumulator as the accumulator was already charged during previous testing and hence there was no flow from line B to the accumulator. The vehicle decelerated at a faster rate as compared to coasting.

The controller shows good tracking behavior. However, the driver feel is slightly compromised. Hence, LQR controller was implemented to achieve smoother acceleration.

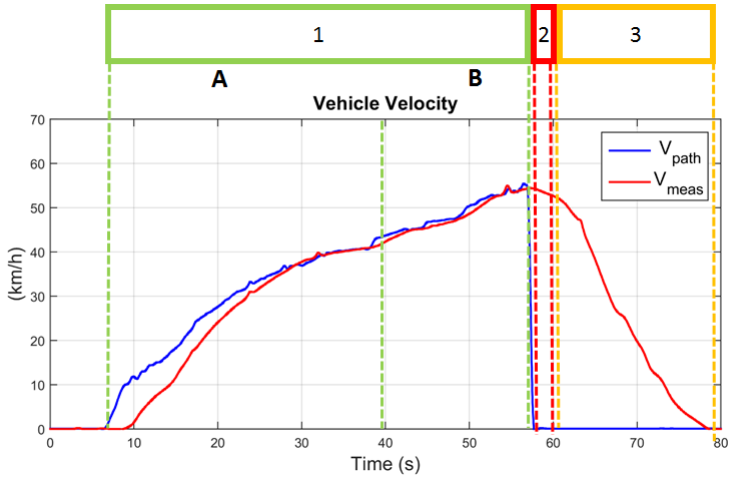

Figure 7.5. : Measurement Results for Modified Sequential Controller: Vehicle Velocity.

7.1.2 LQR Controller

The vehicle was operated in hydrostatic mode with velocity tracking using LQR control and the results for acceleration and brake pedal positions, displacements of the hydraulic units, engine speed, pressure in the system and the vehicle velocity are shown in Figures 7.6, 7.7, 7.8, 7.9 and 7.10.

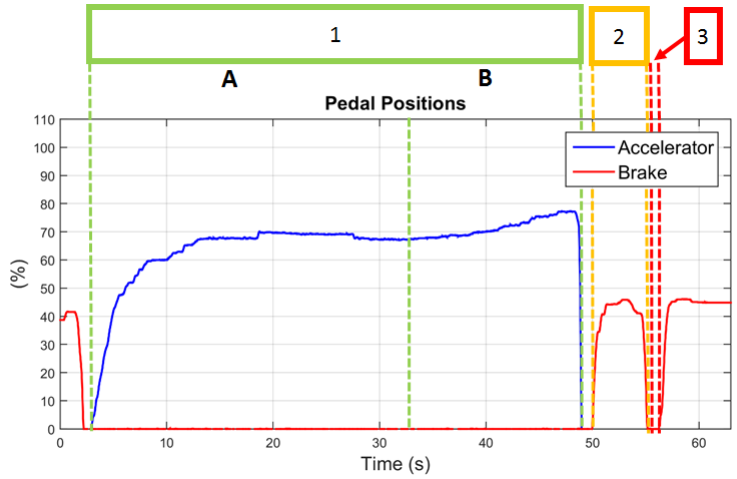

Figure 7.6. : Measurement Results for LQR Controller: Pedal Positions.

In the figures, block (1) represents acceleration, block (2) shows braking and block (3) represents coasting events. Acceleration is again divided into two cases as explained in the modified sequential controller. As the accelerator pedal was pressed, the displacements of

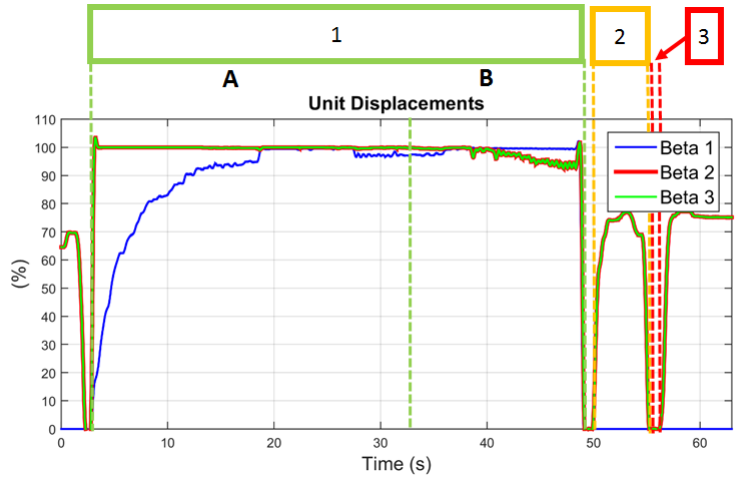

Figure 7.7. : Measurement Results for LQR Controller: Displacements of Units.

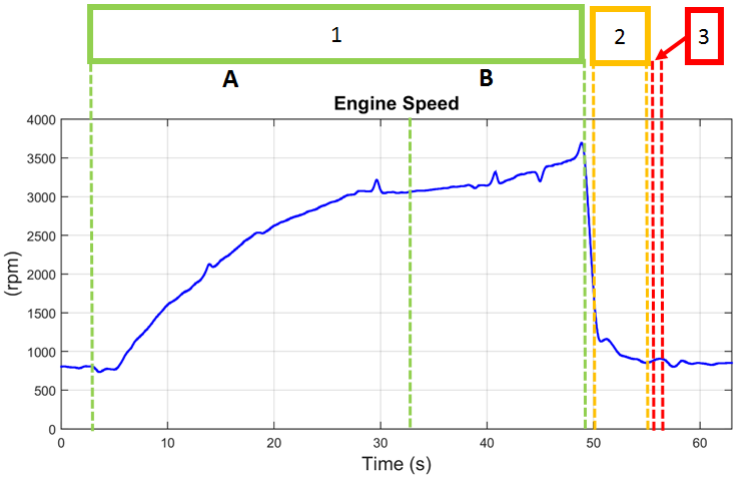

Figure 7.8. : Measurement Results for LQR Controller: Engine Speed.

the units were commanded by the LQR controller based on the current state of the system and the deviation from reference values to track the reference velocity. This results in an increase in pressure of line A based on load and hence, the vehicle velocity. Also, the engine speed is varied based on the accelerator pedal input. The vehicle was accelerated to nearly 62 km/h for this measurement. Coasting and braking occur similar to the previous case.

The controller shows good tracking behavior as well as a smoother acceleration as compared to the modified sequential control. Hence, LQR controller was chosen to be the final controller for the hydrostatic mode.

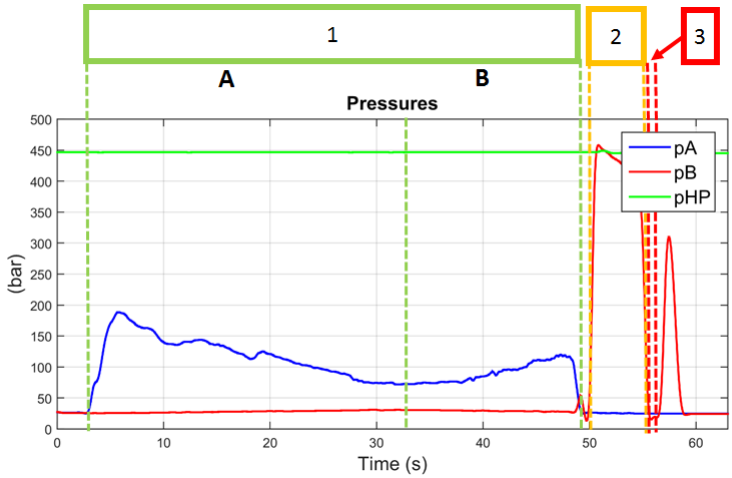

Figure 7.9. : Measurement Results for LQR Controller: Pressures.

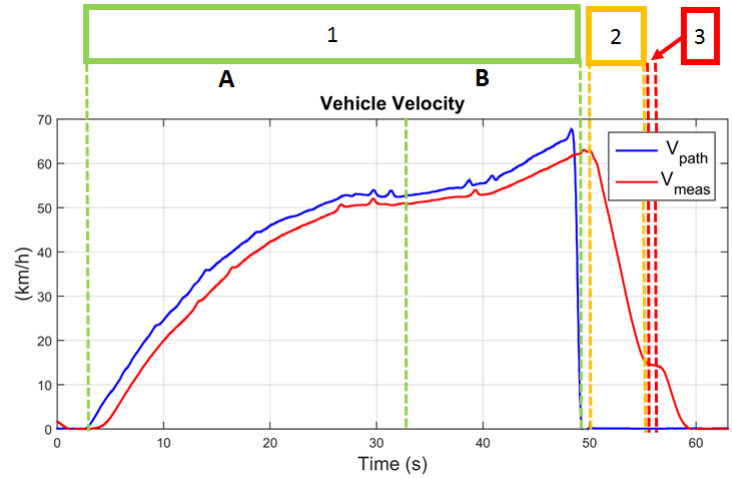

Figure 7.10. : Measurement Results for LQR Controller: Vehicle Velocity.

In order to test the controller further, measurements were performed to carry out mutliple acceleration in one test. The results of the pedal position, the displacement of the hydraulic units, engine speed, pressure and the vehicle velocity are shown in the Figures 7.11, 7.12, 7.13, 7.14 and 7.15.

As seen in the figures, block (1) represents the first acceleration event. The vehicle follows the reference velocity. After the vehicle was accelerated, the accelerator pedal was released and vehicle was allowed to coast as seen in block (2). The vehicle was again accelerated in block (3). at this point the vehicle was already at some velocity and not standstill. The path planning velocity is again tracked well as the unit displacements are

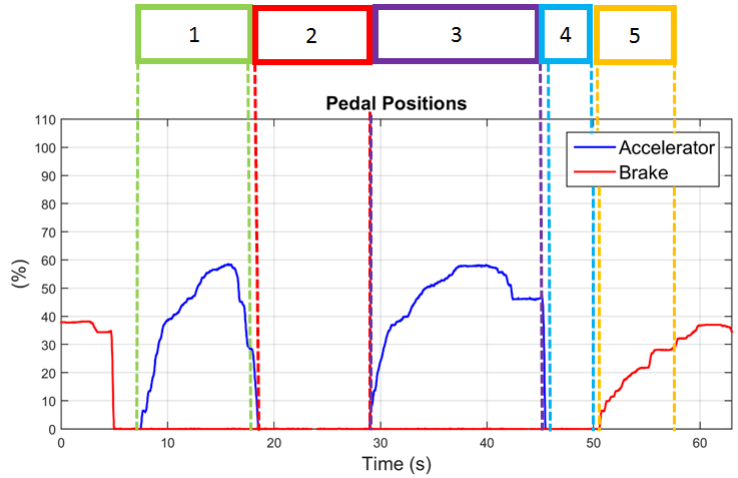

Figure 7.11. : Measurement Results for LQR Controller with Multiple Cycles: Pedal Positions.

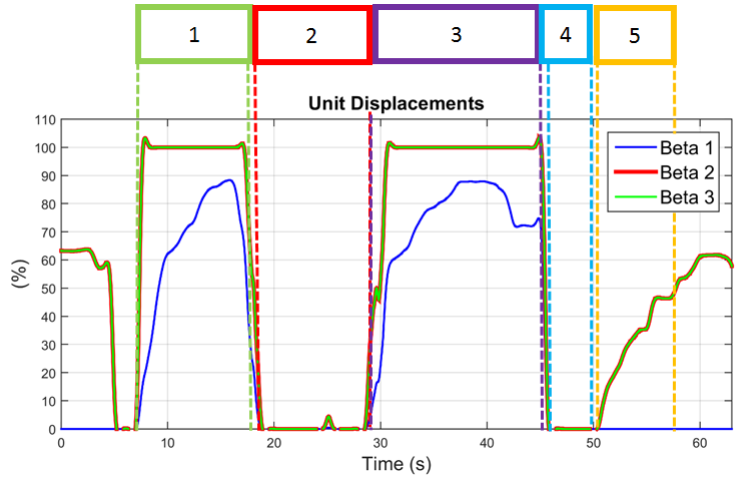

Figure 7.12. : Measurement Results for LQR Controller with Multiple Cycles: Displacements of Units.

adjusted to meet the velocity at which the vehicle was last coasting. The vehicle again tracked the reference velocity. Also, the vehicle reached a higher velocity in this case as compared to the first acceleration run even when the pedal positions are almost similar. This was the result of the compensation in the displacements of the units due to velocity feed back. The vehicle was then allowed to coast and then come to a standstill by applying brakes as shown in blocks (4) and (5). It is to be noted that the vehicle did not perform well at higher velocities in the second acceleration run due to a problem in the low pressure

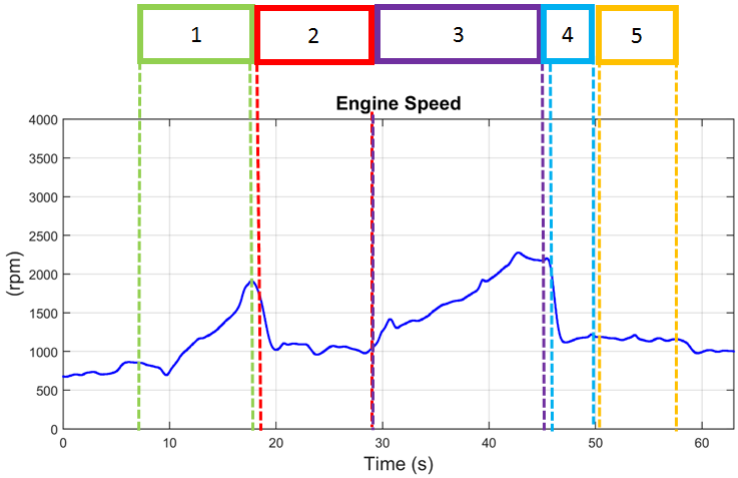

Figure 7.13. : Measurement Results for LQR Controller with Multiple Cycles: Engine Speed.

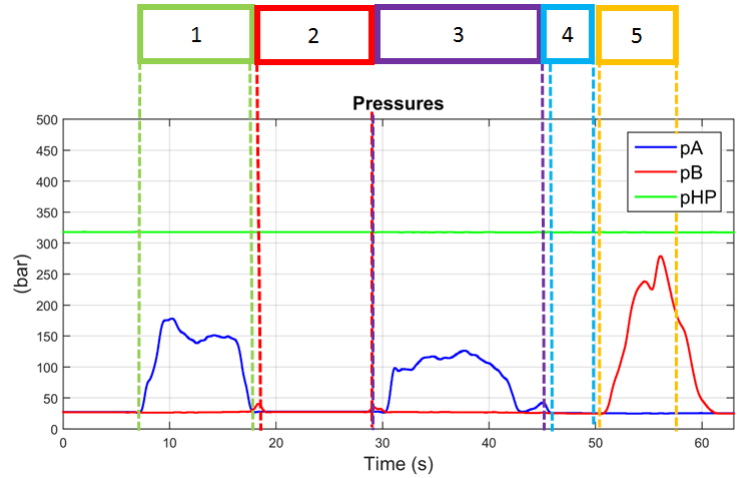

Figure 7.14. : Measurement Results for LQR Controller with Multiple Cycles: Pressures.

system as the pressure fell to a low value. The low pressure system needs to be resized to meet the requirements of the vehicle before taking further measurements.

7.1.3 Secondary Controller

The secondary controller is the mode of operation to use the energy storage in the accumulator as a power boost. The switching controller applied while testing was modified as compared to simulation in order to get a consistent transition with respect to driver feel. Instead of switching from hydrostatic to secondary control based on velocity, accelerator

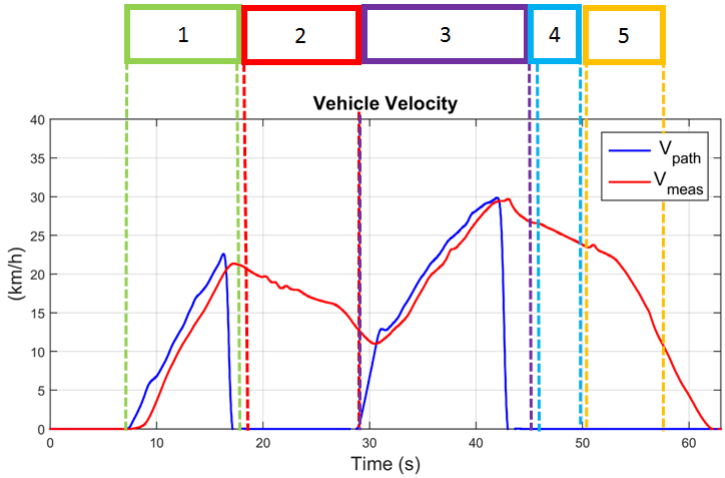

Figure 7.15. : Measurement Results for LQR Controller with Multiple Cycles: Vehicle Velocity.

pedal was used. The controller first operates in hydrostatic and then switches to secondary control when the accelerator pedal position exceeds 70 % of its maximum travel. Enabling valve is opened once the pressure in line A increases. The vehicle was operated initially in hydrostatic mode with velocity tracking using LQR controller and then in secondary control mode at higher velocity for power boost. The results for acceleration and brake pedal positions, displacements of the hydraulic units, engine speed, pressure in the system and the vehicle velocity are shown in Figures 7.16, 7.17, 7.18, 7.19 and 7.20.

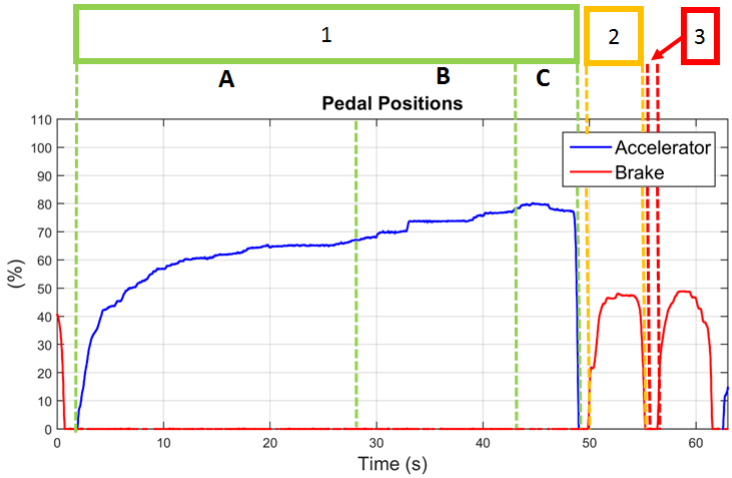

Figure 7.16. : Measurement Results for Secondary Controller: Pedal Positions.

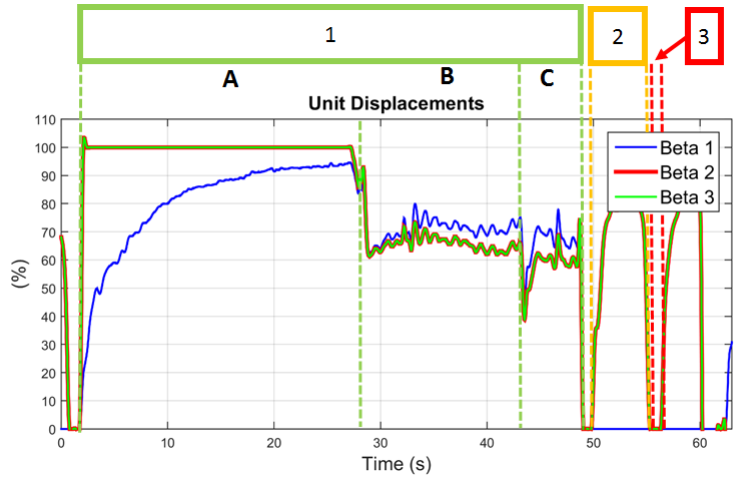

Figure 7.17. : Measurement Results for Secondary Controller: Displacements of Units.

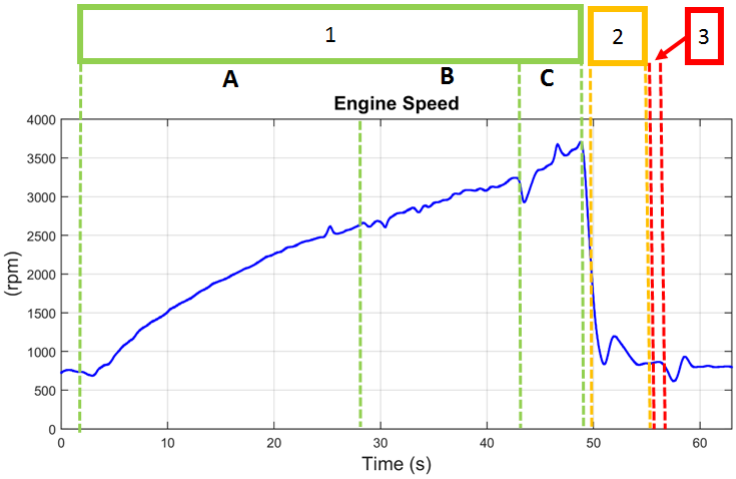

Figure 7.18. : Measurement Results for Secondary Controller: Engine Speed.

In the figures, block (1) represents acceleration, block (2) shows braking and block (3) represents coasting events. Acceleration is again divided into two cases. Initially the vehicle wass operated in hydrostatic mode and then it was switched to secondary control mode as the accelerator pedal exceeded 70 %. As the accelerator pedal was pressed, the displacements of the units were commanded by the LQR controller based on the current state of the system and the deviation from reference values to track the reference velocity as seen in block (A). When the controller switched to secondary control mode, the displacements of the hydraulic units attained lower values and the torque requirements were met by increasing the system pressure. Block (B) represents the portion of the control used to

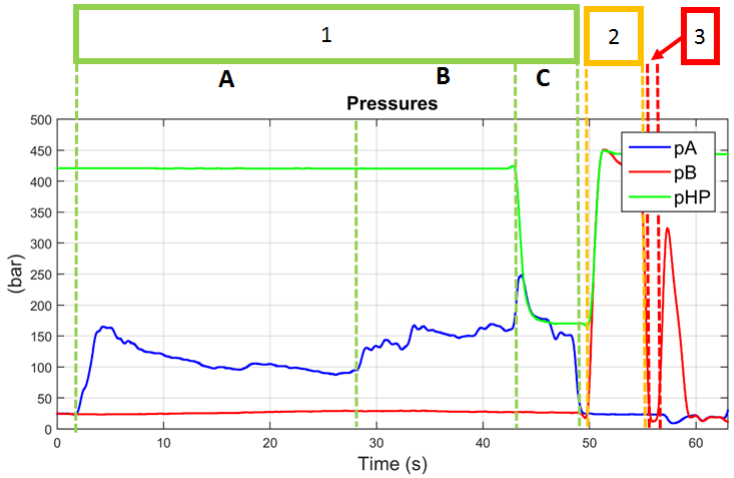

Figure 7.19. : Measurement Results for Secondary Controller: Pressures.

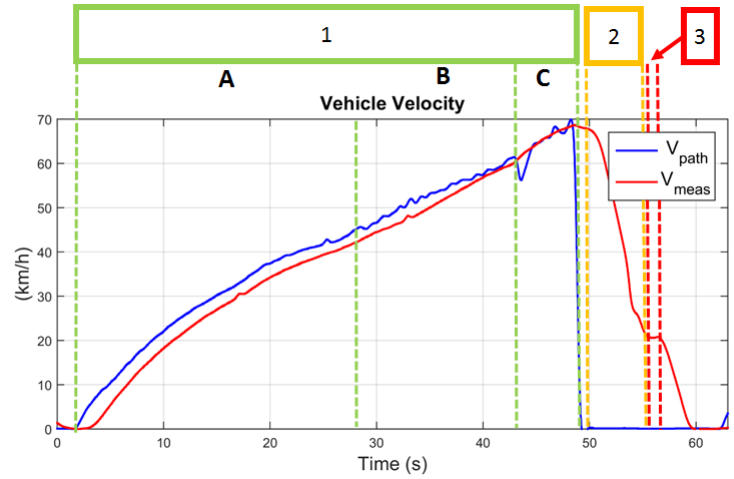

Figure 7.20. : Measurement Results for Secondary Controller: Vehicle Velocity.

increase the pressure of line A. Once the pressure increased, the enabling valve was opened and accumulator energy was used as seen in block (C). The pressure of the accumulator decreased while that of line A increased. Also, as the energy from the accumulator was used and the system operated at a higher pressure, the displacement of the units decreased. The vehicle was accelerated to nearly 68 km/h for this measurement. Coasting and braking occur similar to the previous case. During braking, it can be seen that the pressure in line B exceeded the pressure of the accumulator and resulted in charging of the accumulator. This is reflected in terms of an increase in pressure of the accumulator.

The controller shows good tracking behavior, smoother acceleration as well as smooth transition between the modes. Also, it allows the use of the braking energy stored in the accumulator.

7.2 Reverse Operation

The test results for the reverse operation are discussed in this section. The vehicle was operated in hydrostatic mode with velocity tracking based on LQR controller and the results for acceleration and brake pedal positions, displacements of the hydraulic units, engine speed, pressure in the system and the vehicle velocity are shown in Figures 7.21, 7.22, 7.23, 7.24 and 7.25.

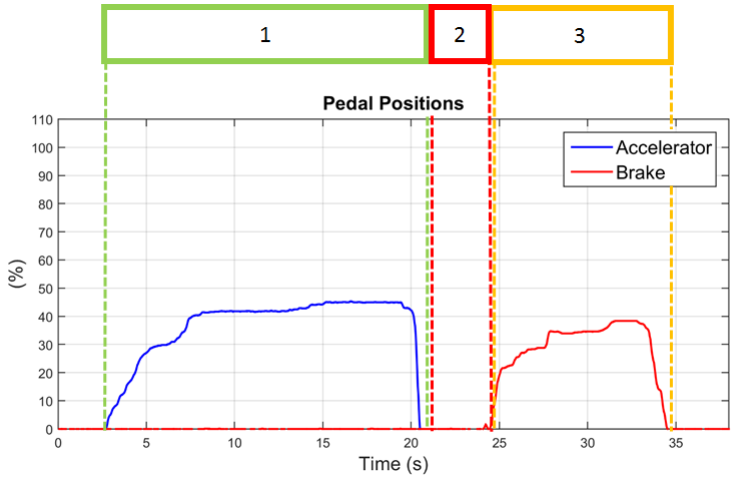

Figure 7.21. : Measurement Results for Reverse Operation: Pedal Positions.

The figures show acceleration using LQR controller in block(1), coasting in block (2) and braking in block (3) for the reverse operation of the vehicle. For this mode, the units 2 and 3 were operated in overcenter mode. As the accelerator pedal was pressed, the LQR controller commanded the displacements for the hydraulic units. The displacements of units 2 and 3 show a negative value to represent their operation in overcenter mode. These result in increase in pressure in line A and hence, acceleration of the vehicle. The coasting controller was the same as previous measurements. The braking controller operates similar to the one explained earlier except that the displacements commanded for units 2 and 3 were negative to account for the overcenter mode.

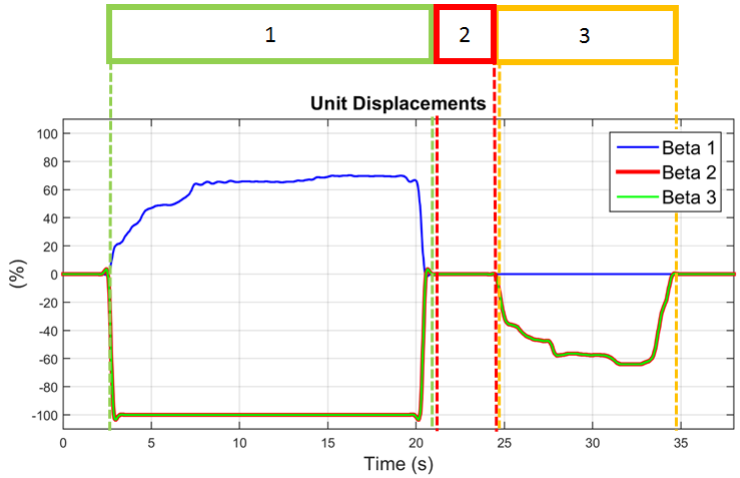

Figure 7.22. : Measurement Results for Reverse Operation: Displacements of Units.

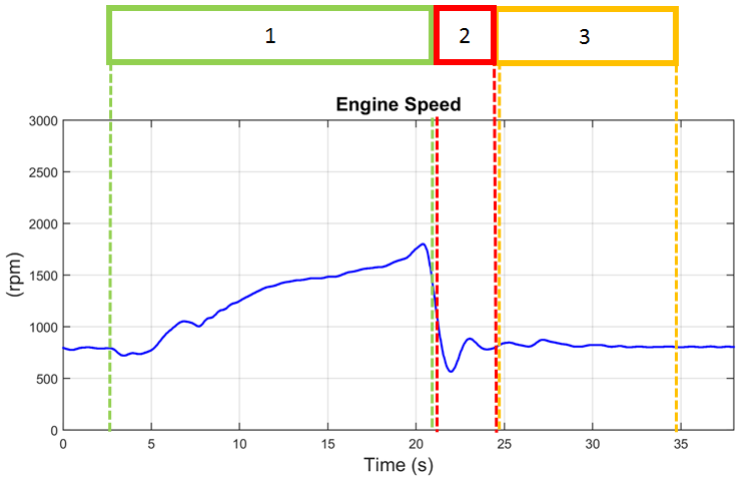

Figure 7.23. : Measurement Results for Reverse Operation: Engine Speed.

This chapter discussed the measurement results for the control strategies used to demonstrated the different modes of operation of the mode-switching hybrid. The implementation of the control strategies gave a proof of the concept of this hybrid architecture. The storage of energy into the accumulator and its usage for power boost was also demonstrated. The control strategies resulted in a smooth acceleration and transition between the different modes of operation. This resulted in a better drivability of the hybrid.

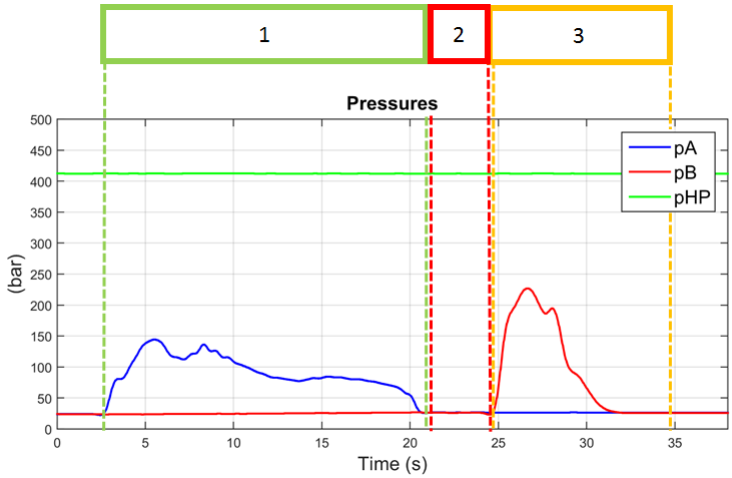

Figure 7.24. : Measurement Results for Reverse Operation: Pressures.

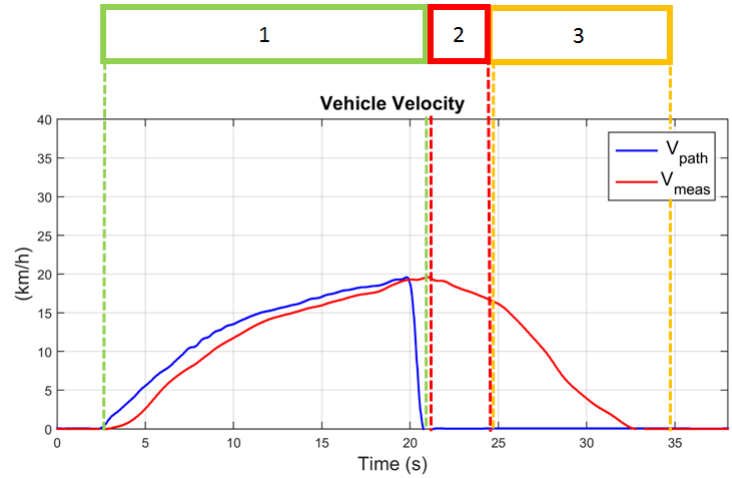

Figure 7.25. : Measurement Results for Reverse Operation: Vehicle Velocity.

8. CONCLUSIONS AND FUTURE WORK

The goal of this work was to implement a mode-switching hybrid transmission on a four wheel drive SUV. The work began with the design of the architecture such that the deficiencies of the conventional transmissions with regards to driver feel and energy storage were overcome while taking advantage of their merits. Hence, a novel mode-switching hybrid was developed as a combination of a hydrostatic transmission and a series hybrid. This architecture was analyzed initially in simulations by developing a high fidelity system model to test its feasibility.

Once the transmission was tested in simulations, the components were sized to meet the performance of the existing vehicle. The components were sized using a new methodology which involved a parameter study of different component size combinations for a UDDS cycle using dynamic programming to optimize for efficiency whereas dynamic simulation to achieve the performance better than the base vehicle. A pareto front was plotted to analyze the efficiency and the performance of each design. The results proved that a larger unit 2 and 3 help in low speed acceleration but a smaller unit is more efficient. The efficiency of unit 1 was dependent on the size of units 2 and 3 but larger the unit 1, the better is the performance of the transmission as it is capable of extracting maximum power from the engine. Though the accumulator did not show a major difference in the performance and efficiency, both the parameters were larger for a larger accumulator. However, the minimum pressure of the accumulator had a great impact on the efficiency and performance. The maximum performance was achieved with a minimum pressure that was able to fully load the engine. The simulations were conducted by Bleazard and then the post processing and data analysis was performed by the author along with Bleazard.

The main focus of this work was to implement the mode-switching hybrid transmission on an on-high way SUV. A 1999 Range Rover 4.0 SE was selected as the prototype vehicle. The sizing of the components resulted in a 100 cc/rev unit 1, 75 cc/rev units 2 and 3, a 32 liter HP accumulator with a minimum pressure of 150 bar. In order to fit all the components in the limited space available in the under body of the vehicle, a packaging architecture was

first designed in CAD by the author. Custom parts were designed and manufactured and all the components were integrated and installed in the vehicle. Also the accelerator and brake pedals were modified to create inputs for the hybrid system. The installation of parts in the prototype vehicle was a team effort.

After the installation of the components on the prototype vehicle, the braking system was redesigned to incorporate regenerative braking. The drive shafts were modified and the engine speed controller was designed to control the throttle body of the engine. The data acquisition system was designed in order to determine the current state of the system and was used to implement control strategies.

Once the prototype was completed, measurements were conducted in order to validate the system model. Control strategies were designed and implemented to demonstrate the different modes of operation of the hybrid. With this in mind, an HST controller were designed to achieve a good drivability and secondary controller was designed to utilize the brake energy stored in the accumulator as power boost at higher velocities. Simulation as well as measurement results were studied in order to validate the controller design. Two controllers were implemented for the HST mode: Modified Sequential controller and Linear Quadratic Regulator (LQR) controller. Based on the results obtained, LQR controller was selected to operate the hybrid in HST acceleration mode. Thus, the control strategies were demonstrated for acceleration in HST mode, switching the mode to secondary control, braking, coasting and reverse operations.

Though the implementation of the mode-switching hybrid on an SUV demonstrates the proof of concept of the hybrid transmission, additional work is required to make it stand in the commercial market. Firstly, the engine controller needs improvement to account for the engine speed fluctuations based on the load changes on the vehicle and make it more robust. Strategies can be developed to include engine shut on-off, traction control and cruise control. Then a supervisory controller can be developed to implement power management strategies by controlling the engine as well as unit 1 displacement using a Multi input multi output (MIMO) controller. Fuel measurements can be conducted to evaluate the improvement in the fuel economy compared to conventional transmission. Advanced control strategies can be developed using online optimization techniques for power management.

LIST OF REFERENCES

LIST OF REFERENCES

Baseley, S., Ehret, C., Greif, E. & Kliffken, M. (2007), 'Hydraulic hybrid systems for commercial vehicles', *SAE Comercial Vehcile Engineering Congress* (SAE Technical Paper 2007-01-4150).

Bleazard, T., Haria, H., Sprengel, M. & Ivantysynova, M. (2015), 'Optimal control and performance based design of the blended hydraulic hybrid', *ASME* (FPMC2015-9543).

Bleazard, T. J. (2015), Hydraulic hybrid four wheel drive sport utility vehicle - utilizing the blended hybrid architecture, Master's thesis, Purdue University.

Davis, S., Diegel, S. & Boundy, R. (2014), 'Transporation energy data book: Edition 33', (ORNL-6690).

De Silva, C. (2004), *Mechatronics: an integrated approach*, CRC press.

Dewey, C., Elder, F. & Otis, D. R. (1974), 'Accumulator-charged hydrostatic drive for cars saves energy', *Hydraulics and Pneumatics* pp. 180–183.

Dunn, H. & Wojcienchowski, P. (1972), 'High-pressure hydraulic hybrid with regenerative braking', *7th Intersociety Energy Conversion Engineering Conference* pp. 207–209.

Elder, F. & Otis, D. (1973), 'Simulation of a hydraulic hybrid vehicle powertraing', *ASME* (73-ICT-50).

Heggie, W. & Sandri, R. (1979), 'Simulation of a hydraulic hybrid vehicle powertraing', *ASME* (79-WAIDSC-15).

Heskitt, M., Smith, T. & Hopkins, J. (2012), 'Design & development of the lco-140h series hydraulic hybrid low floor transit bus', *BUSolutions Final Technical Report* .

Heywood, J. (1988), *Internal Combustion Engine Fundamentals*, McGraw-Hill, Inc.

Ho, T. & Kyoung, K. A. (2012), 'Design and control of a closed-loop hydraulic energy-regenerative system', *Automation in Construction,22* pp. 444–458.

Hugosson, C. (1993), 'Cumulo hydrostatic drive a vehicle drive with secondary control', *3rd Scandinavian International Conference on Fluid Power* .

Lammert, M., Burton, J., Sindler, P. & Duran, A. (2014), 'Hydraulic hybrid and conventional parcel delivery vehicles' measured laboratory fuel economy on targeted drive cycles', *SAE Technical Paper 2014-01-2375* .

Martini, S. (1984), 'The m.a.n. hydrobus: A drive concept with hydrostatic brake energy recovery', *International Symposium on Advanced and Hybrid Vehicles* .

Nakzawa, N., Kono, Y., Takao, E. & Takeda, N. (1987), 'Development of a braking energy regeneration system for city buses', (SAE Technical Paper 872265).

PSA-Peugeot-Citroen (2014), 'Hybrid air, an innovative full hybrid gasoline system'. [Online; accessed 02-May-2015].
URL: *www.psa-peugeot-citroen.com/en/automotive-innovation/innovation-by-psa/hybrid-air-engine-full-hybrid-gasoline*

Shiber, S. (1979), 'Automotive energy management systme', *National Conference on Fluid Power* pp. 141–147.

Shiber, S. (1980), 'Mutli-mode transmission'.

Sprengel, M., Bleazard, T., Haria, H. & Ivantysynova, M. (2015), 'Implementation of a novel hydraulic hybrid powertrain in a sports unitility vehicle', *4th IFAC Workshop on Engine and Powertrain Control, Simulation and Modeling* .

Sprengel, M. & Ivantysynova, M. (2012), 'Novel transmission configuration for hydraulic hybrid vehicles', *Proceedings of the International Sci-Tech Conference "Machine Dynamics and Vibro Acoustics"* pp. 207–209.

Sprengel, M. & Ivantysynova, M. (2013), 'Investigation and energetic analysis of a novel hydraulic hybrid architecture for on-road vehcles', *Proceedings of the 13th Scandinavian International Conference on Fluid Power* pp. 15–22.

Sprengel, M. & Ivantysynova, M. (2014*a*), 'Investigation and energetic analysis of a novel blended hydraulic hybrid power split transmission', *Proceedings of the 9th IFK International Fluid Power Conference* .

Sprengel, M. & Ivantysynova, M. (2014*b*), 'Recent developments in a novel blended hydraulic hybrid transmission', *SAE 2014 Commercial Vehicle Engineering Congress* (SAE Technical Paper 2014-01-2399).

Wargo, J., Wargo, L., Alderman, N. & Brown, D. (2006), 'The harmful effects of vehicle exhaust: A case for policy change', (-).

Wendel, G., Baseley, S., O'Briend, J., JKargul, J. & M., E. (2007), 'Hydraulic hybrid vehicle system panel', *Michigan Clean Fleet Conference.* .

Wouk, V. (1995), 'Hybrids: Then and now', *Spectrum, IEEE* pp. 16–21.

Wu, P., Luo, N., Fronczak, F. & Beachley, N. (1985), 'Fuel economy and operating characteristics of a hydropneumatic energy storage automobile', (SAE Technical Paper 851678).

APPENDICES

APPENDIX A: LINEARIZING THE EQUATIONS

```
syms b1 b2 nw pa ne v1 ip ia ch v2 m r pii dp pb k1 k2 kr kf kd

% symbolic representation

% states => dp and nw
% inputs => b1 and b2

% b1 and b2 are unit displacements
% nw is wheel speed, pa and pb are pressures in lines A and B
% dp = pa pb, v1 and v2 are the displacment volumes of the units
% ia and ip are the gear ratios between Units 2 and 3 and wheels
% ch is hydraulic capacitance of the lines
% m is the mass of the vehicle, r is the dynamic rolling radius
% pii is to represent pi as a symbol
% k1 and k2 are coefficients of pressure dependent losses in the
    units
% kr is coefficient to account for rolling resistance
% kf and kd are coefficients for friction and drag



% Linearizing for pressure dp

dp_dot = (ne*b1*v1/(ip)    2*nw*b2*v2*ia    dp*(k1+2*k2))*2/ch

f1_by_dp = diff(dp_dot,dp)
f1_by_dp = diff(dp_dot,nw)
```

```
f1_by_b1 = diff(dp_dot,b1)
f1_by_b2 = diff(dp_dot,b2)

dp_ref = solve(dp_dot==0,dp)


% Linearizing for wheel speed nw

nw_dot = (2*b2*v2*dp*ia*kr/(2*pii*m*r^2)    nw*kf*ia^2/(m*r^2)...
       nw*kd*r^2/(m*r^2))


f2_by_dp = diff(nw_dot,dp)
f2_by_nw = diff(nw_dot,nw)
f2_by_b1 = diff(nw_dot,b1)
f2_by_b2 = diff(nw_dot,b2)

nw_ref = solve(nw_dot==0,nw)

A = [f1_by_dp, f1_by_nw; ...
      f2_by_dp, f2_by_nw]

B = [f1_by_b1, f1_by_b2; ...
      f2_by_b1, f2_by_b2]

C = [1,0;...
      0,1]
```

APPENDIX B: MODE-SWITCHING HYBRID HYDRAULIC CIRCUIT FOR RANGE ROVER AND WIRING DIAGRAM

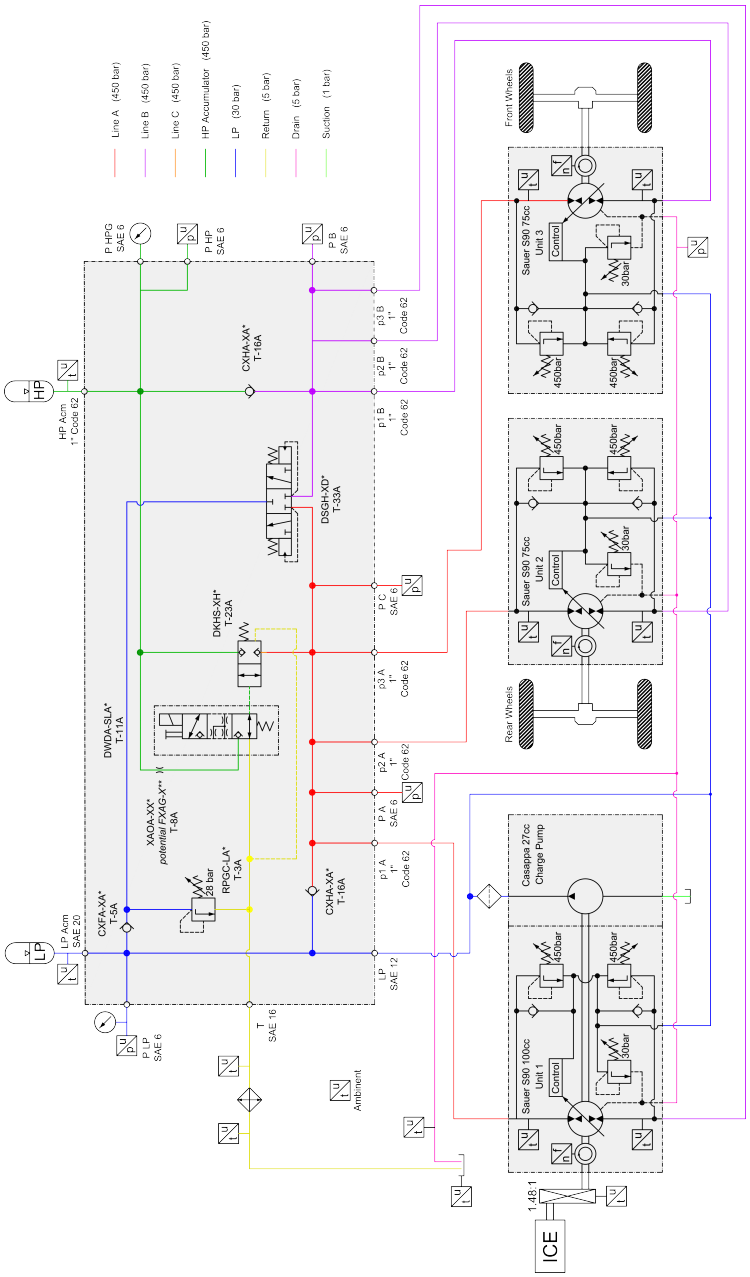

Figure B.1. : Range Rover Circuit Diagram.

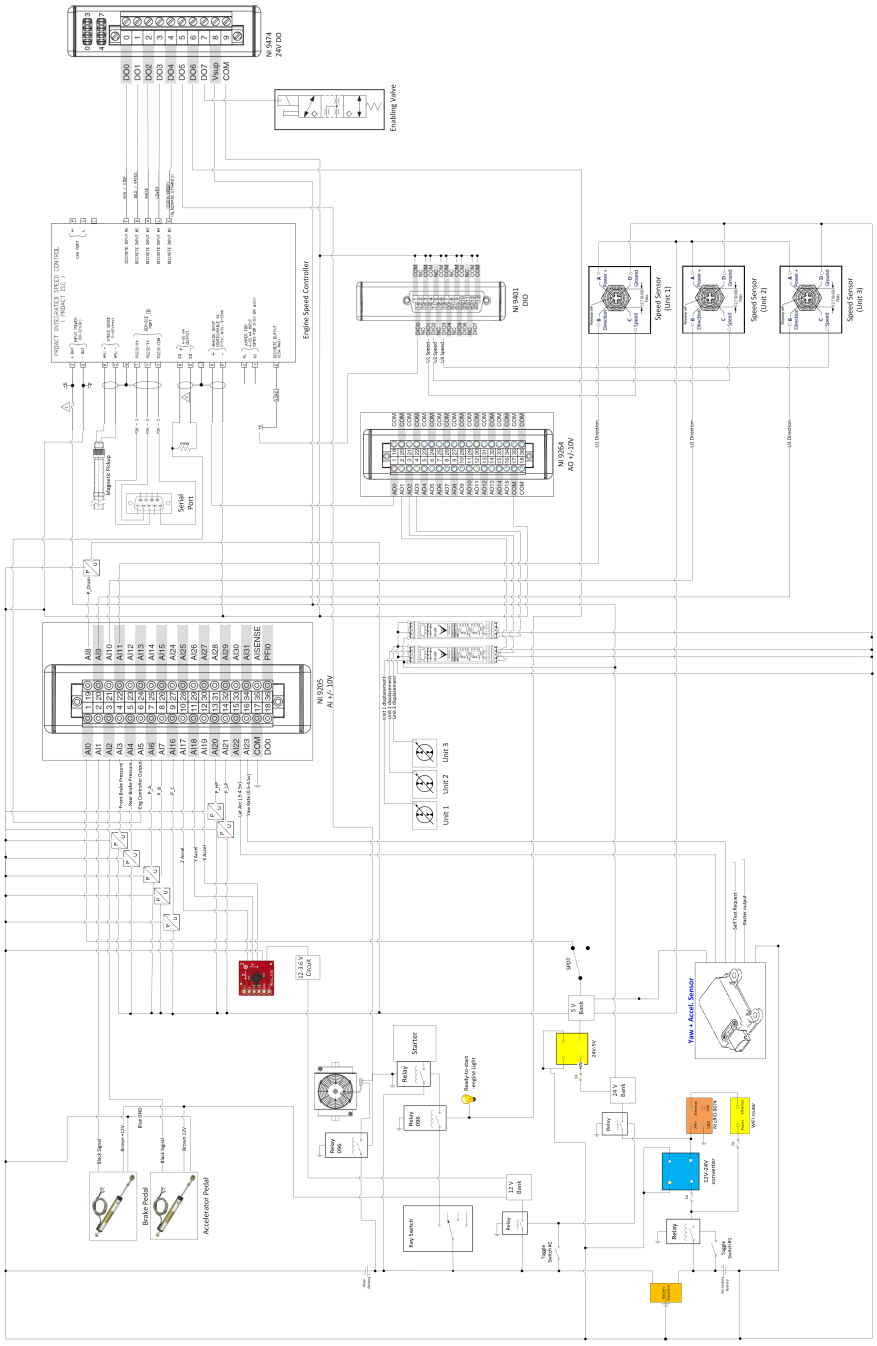

Figure B.2. : Range Rover Wiring Diagram.

VITA

VITA

B.Tech. Mechanical Engineering, May 2014

Veermata Jijabai Technological Institute, Mumbai University (Mumbai, India)

M.S. Mechanical Engineering, August 2016

Purdue University (West Lafayette, Indiana, USA)

Thesis: A Novel Mode-Switching Hydraulic Hybrid for an On-Highway Vehicle: A Study of Architecture and Control

Major Professor: Monika Ivantysynova

LIST OF PUBLICATIONS

LIST OF PUBLICATIONS

Haria, H., Ivantysynova, M. 2016. Novel Mode-Switching Hydraulic Hybrid-A Study of the Architecture and Control. SAE Technical Paper, Oct. 4-6, 2016. Rosemont, IL, USA. (Under Review)

Bleazard, T., Haria, H., Sprengel, M. and Ivantysynova, M. 2015. Optimal Control and Performance Based Design of the Blended Hydraulic Hybrid. Proceedings of the 2015 ASME/BATH Symposium on Fluid Power & Motion Control, Oct. 12-14, 2015. Chicago, IL, USA.

Sprengel, M., Bleazard, T., Haria, H. and Ivantysynova, M. 2015. Implementation of a Novel Hydraulic Hybrid Powertrain in a Sports Utility Vehicle. Proceedings of the 2015 IFAC Workshop on Engine and Powertrain Control, Simulation and Modeling, Aug. 23-26, 2015. Columbus, OH, USA.